

Recent Seismicity and Rupture Process of Some Earthquakes in the East African Rift System

By

Jima Asefa

A Thesis Submitted to

The School of Earth Sciences

Presented in Fulfillment of the Requirements for the Degree of

Doctor of Philosophy in Earth Sciences (Geophysics)

Addis Ababa University

Addis Ababa, Ethiopia

November 2020

Addis Ababa University
School of Graduate studies

This is to certify that the thesis prepared by **Jima Asefa**, entitled "**Recent Seismicity and Rupture Process of Some Earthquakes in the East African Rift System** " and submitted in fulfillment of the requirements for the Degree of Doctor of Philosophy in Earth Sciences (Geophysics) complies with the regulations of the University and meets the accepted standards with respect to originality and quality.

Dated: November 2020

Signed by the Examining committee

Supervisor:

Dr. Atalay Ayele

Readers:

Prof. Vunganai Midzi
External Examiner

Dr. Ameha Atnafu
Internal Examiner

Dr.
Chair of the Department or Graduate program Coordinator

Addis Ababa University

Date: **November 2020**

Author: **Jima Asefa**

Title: **Recent Seismicity and Rupture Process of Some Earthquakes in the East African Rift System**

Department: **School of Graduate studies**

Degree: **PhD** Convocation: **November** Year: **2020**

Signature of Author

Dedicated to my family

Table of Contents

Table of Contents v

List of Tables viii

List of Figures ix

Abstract i

Acknowledgements iv

List of Abbreviations vi

1 Introduction 1
- 1.1 Background . . . 1
- 1.2 Objectives . . . 5
  - 1.2.1 General objectives . . . 5
  - 1.2.2 Specific objectives . . . 5
- 1.3 Statement of the problem . . . 5
- 1.4 Significance of the study . . . 7
- 1.5 Thesis layout . . . 8

2 Regional Tectonic Setting and Previous Studies 10
- 2.1 Regional tectonics setting . . . 10
- 2.2 Previous studies . . . 15

3 Some Basic Theory in Seismology 21
- 3.1 Basic theory on seismic wave propagation . . . 21
- 3.2 Elastic moduli . . . 21
- 3.3 Stress tensor . . . 23
- 3.4 Strain tensor . . . 25
- 3.5 Equation of motion . . . 26
- 3.6 Earthquake source mechanisms . . . 28
  - 3.6.1 Convolution and Deconvolution modeling for linear system . . . 31
  - 3.6.2 Time-domain inversion using seismograms . . . 32
  - 3.6.3 Frequency-domain inversion for moment-time functions . . . 33
  - 3.6.4 Moment tensor decomposition . . . 37

3.7 Seismic phase picking . . . 41
3.8 Earthquakes location technique: Geiger Method . . . 41
3.9 Magnitude determination: Local and moment magnitude . . . 45

4 Seismicity of the East African Rift System for the period 2013 to 2016 47
4.1 Introduction . . . 47
4.2 Data and Methods . . . 50
4.2.1 Data . . . 50
4.2.2 Methods . . . 50
4.3 Results and Discussion . . . 52
4.3.1 Spatial and temporal distributions of earthquakes . . . 52
4.3.2 Magnitude distributions . . . 56
4.3.3 Hypocentral depths distribution . . . 57
4.3.4 Frequency magnitude distribution . . . 60
4.3.5 Seismic energy map . . . 62

5 Complex Tectonic Deformation in Circum-Tanzania Craton: East African Rift System 63
5.1 Introduction . . . 63
5.2 Tectonic setting . . . 66
5.3 Data and Methods . . . 68
5.3.1 Data . . . 68
5.3.2 Methods . . . 69
5.3.3 Earthquake location . . . 69
5.3.4 Local magnitude estimation . . . 70
5.3.5 Moment tensor inversion . . . 70
5.4 Results and Discussion . . . 72
5.4.1 The Northern Kondoa region . . . 78
5.4.2 Northern Dodoma region . . . 79
5.4.3 Kagera region . . . 83

6 Deep Rupture Process of the 3rd of April, 2017 Botswana Earthquake 87
6.1 Introduction . . . 87
6.2 Geological and tectonic setting . . . 90
6.3 Data and Method . . . 92
6.4 Results . . . 94
6.5 Discussion . . . 97

7 Conclusions and Recommendation 100

Bibliography 106

Appendix **135**
7.1 Appendix A: Full moment tensor inversion results 135
7.2 Appendix B: Global Centroid Moment Tensor (GCMT) results 135
7.3 Appendix C: Waveform modelling and depth phase analysis results 137

List of Tables

5.1 Source parameters for selected five earthquakes felt in 2014 and 2016 which are considered for the moment tensor inversion and associated aftershocks that occurred in the circum-Tanzania Craton. The symbol $*$ indicates aftershocks that are obtained in this study. 73

List of Figures

1.1 Complex tectonics regimes of the EARS. The black polygon and black rectangle show, the study areas. The magenta and blue triangles are the location of seismic stations used as shown on the legend. The red dots are the major large and destructive earthquakes that occurred in the continent (SE (Serdo), KKE (Kare Kore), LE (Langano), JE (Juba), DE (Dodoma), LTE (Lake Tanganyika), RE (Rukwa), ME (Mozambique) earthqaukes). The black and green dots are the location of some earthquakes that obtained from waveform inversions combined from previous works of (Shudofsky, 1985; Grimison and Chen, 1988a; Jackson and Blenkinsop, 1993; Foster and Jackson, 1998; Brazier et al., 2005; Yang and Chen, 2010; Craig et al., 2011) and from full moment tensor inversion (in both time and frequency domains) of this study. RS represents the Red Sea, GA the Gulf of Aden, AD the Afar depression, NP Nubian Plate, SP Somalian plate, MER the Main Ethiopian rift, WB the western branch, EB the eastern branch and SWB for the southwestern branch. 4

2.1 Different tectonic regimes of the EARS. The black and white beach balls are focal mechanisms for some earthquakes that obtained using waveform modeling combined from previous works (Shudofsky, 1985; Grimison and Chen, 1988a; Jackson and Blenkinsop, 1993; Foster and Jackson, 1998; Brazier et al., 2005; Yang and Chen, 2010; Craig et al. 2011) whereas the blue and white beach balls are from the Global Centroid Moment Tensor (GCMT). The red and white beach balls are fault plane solutions that computed in this study using full moment tensor inversion (in both time and frequency domains). RS represents Red Sea, GA Gulf of Aden, AD Afar Depression, NP Nubian Plate, SP Somalia Plate, MER the Main Ethiopian Rift, WB the Western Branch, EB Eastern Branch and SWB the Southwestern Branch. 15

2.2 Different tectonic regimes of the EARS. The red dots are locations of earthquakes from USGS. RS represents Red Sea, GA Gulf of Aden, AD Afar Depression, NP Nubian Plate, SP Somalia Plate, MER the Main Ethiopian Rift, WB the Western Branch, EB Eastern Branch and SWB the Southwestern Branch. 18

3.1 A cubic element in a continuum. The stresses of each face acting in a given direction leads to the equation of equilibrium stresses on $+X_1$, $+X_2$ and $+X_3$ faces. 24
3.2 The three types of faults: Normal fault, strike-slip and reverse faults (Fossen, 2010). 29
3.3 Examples of three-component seismograms for 2016/09/10 earthquake near Lake Victoria with magnitude Mw 5.7: a) time domain and b) frequency domain. . . . 30
3.4 As a signal goes through two linear systems in succession, the net output is the convolution of the impulse responses or the product of the transfer functions. . . 32
3.5 A seismogram can be modeled as the convolution of the source signal with operators representing the effects of the earth structure and the seismometer. A seismogram can be expressed as a convolution of source, structure and the instrument effect (Stein and Wysession, 2003). 32
3.6 An example of generated seismograms of traces from three-component seismic station in time domain for the 2017/02/24 earthquake of Mw 5.9 occurred in Congo. The red color is for data, black is for synthetics. 34
3.7 An example of generated moment-time functions in frequency domain for the 2017/02/24 event Mw 5.9 occurred in Congo. The red color is for data, black is for synthetics. 35
3.8 Nine couples of equivalent dipole forces forming the moment tensor. The system of force couples representing the components of Cartesian moment tensor. 36
3.9 Sample results obtained using full moment tensor inversion for 2016/09/10 earthquake around Lake Victoria of Mw 5.7. The moment tensor decomposition values for three components are (DC, CLVD and ISO) are also obtained. 40
3.10 A sample of miniseed data recorded at MBAR seismic station. P- and S-phases picks are also shown on the plot. Plot is for earthquake of local magnitude 3.7 recorded on January 5, 2014 at 0.295°N and 30.003°E. 41

4.1 Seismicity of the EARS for the period 2013 to 2016: (a) The spatial distribution of earthquakes compiled from the International Seismological Center (ISC) catalog with magnitudes in the range of 0.5 to 6.5, with red circles earthquake epicenters: (b) The spatial distribution of earthquakes in this study with magnitudes in the range of 1.3 to 6.2. Triangles on the inset map are seismic stations used (P. seismic stations, Permanent seismic stations and AT. seismic stations, AfricaArray and Temporary seismic stations). The current study has revealed significant difference as compared to earthquakes captured in International catalog. NP Nubain Plate, SP Somalian Plate, AD Afar Depression, RS Red Sea, GA Gulf of Aden, MER main Ethiopian rift, TD Tendaho Discontinuity, SS Southern Sudan, WB western branch, NTDZ Northern Tanzania Divergence Zone, EY Eyasi rift, MR Manyara rift and PR Pangani rift. 49

4.2 Spatio-temporal distribution of earthquakes recorded in the EARS for the period 2013 to 2016. Only events recorded by at least three seismic stations have been considered. The circles with color show the distribution of earthquakes (temporal/year) in the region as shown on legend. NP Nubian Plate, SP Somalian Plate, AD Afar Depression, SS Southern Sudan, WB western branch and EW eastern branch of the East African Rift System. 53

4.3 Distribution of earthquakes magnitude as a function of time (2013 to 2016) for the entire catalog for earthquakes distribution is shown in Figs. 4.1b and 4.2. The minimum earthquake local magnitude 1.3 and maximum earthquake local magnitude 6.2 have been observed. 56

4.4 Hypocentral depth versus Latitude of earthquakes for the time period 2013 to 2016. 58

4.5 Hypocentral depth versus Longitude of earthquakes for the time period 2013 to 2016. 59

4.6 Plot of the yearly and total number of earthquakes as a function of time. The left vertical axis is the number of events per year. The right vertical axis is the total of events. The result shows that the number of earthquakes decreases in 2014 but increase again in between 2015 to 2016. 60

4.7 Magnitude-frequency distribution of earthquakes in the study area for the catalog. The b-value estimate for the whole region is 1.01 ± 0.16 and a-value with ∼6.5. Magnitude of completeness (Mc) is the magnitude increment at which the lower end of the FMD departs from the linear trend in the log-lin plot. In this study, a visual evaluation can lead to a correct estimate of the completeness magnitude (Mc ∼3.0). Circles represent the discrete (non-cumulative) and the orange line the cumulative distributions of events. 61

4.8 Variation of seismic energy released for the period 2013 to 2016 in the EARS. Dominant energy peaks are observed in the Afar depression (AD), main Ethiopian rift (MER), Southern-Sudan (SS), Northern eastern branch (NEB), eastern branch (EB) and western branch (WB). 62

5.1 Regional tectonic map of the western and eastern branches of the East African Rift System. The magenta loop shows outline of the Tanzania Craton. The Northern Tanzania Divergence Zone (NTDZ) rift segments (Eyasi, Manyara and Pangani), and the mobile belts surrounding the Tanzania Craton. The two black boxes show the study areas and green triangles on the map are local and regional seismic stations while magenta triangles on the inset map show the distant seismic stations used in this study. Solid black lines show major faults and geological features. Major faults are from Le Gall et al., 2004. The purple dashed lines indicate the boundaries of the Victoria and Ruvuma microplates (Stamps et al., 2008). Kinematics symbols are from Saria at el., 2014; the blue arrows show predicted relative motions between plates; numbers are velocities in mm/yr. Seismicity of the western and eastern branches of EARS with body wave magnitudes in the range of Mb 1.2 to Mb 6.5 homogenized using regression analysis for the time period of 1995 to 2013 compiled from the International Seismological Center (ISC) catalogue. Different color circles (white, yellow and red) show the epicenters of earthquakes where circle size is proportional to earthquake magnitude as shown in the legend. 65

5.2 Percentage of variance reduction, double couple and source mechanism for 2014/10/31 earthquake with origin time 16:50:01.1 as a function of focal depth variations from 2 to 40 km. The optimal origin time shift is -1 s and preferred focal depth is 26 km. The size of beach ball is proportional with the value of variance reduction (VR) and percentage of double couple (DC) solution. 76

5.3 Relative misfit versus focal depths of September 10, 2016 Kagera earthquake of magnitude Mw 5.7 computed from moment tensor inversion. The best solution for focal depth of the event has been chosen at the smallest misfit. 76
5.4 These plots show values of variance reduction, double couple and depth versus origin time shift of -1 s relative to origin time for lower, middle and upper panels, respectively. The blue line shows the value of results adopted in this study (depth 26 km, Mw 4.8 and focal mechanism). 77
5.5 Moment tensor inversion result for waveform fits of the observed (red lines) and synthetic seismograms (black lines) displacement waveforms for the preferred focal mechanism deduced at 26 km source depth. The epicentral distance (km) and azimuth (degree) of each station is written above their trace. Z, R, T indicate vertical, radial and transverse components, respectively. 79
5.6 Moment tensor inversion in frequency domain for the 2016 Kagera earthquake with magnitude Mw 5.7 for spectra amplitude fit. The panel is dedicated to spectra comparison (red color is used for data, black for synthetics). Stations are sorted on the base of epicentral distances, with station name, distance, azimuth and maximal amplitudes provided on the left side. Up, RadAway, TraRight of each station is written above the fits of data and synthetics. 80
5.7 Moment tensor inversion in time domain of 2016 Kagera earthquake with magnitude Mw 5.7 for amplitude and phase fits. The panel is dedicated to waveform comparison (red color is used for data, black for synthetics). Stations are sorted on the base of epicentral distances, with station name, distance, azimuth and maximal amplitudes provided on the left side. Up, RadAway, TraRight of each station is written above the fits of data and synthetics. 81

5.8 Plots of five earthquakes fault plane solutions determined in this study and previous studies. The red and white beach balls are mechanisms of earthquakes from moment tensor inversion of this study, black and white beach balls are mechanisms from Brazier et al., (2005); Mulibo and Nyblade, (2016); Weinstein et al., (2017) and GCMT solutions, while the blue and white is mechanism of the 2002 Mb 5.5 main shock (Yang and Chen, 2010). The size of beach ball is proportional to the magnitude of earthquake. Color coded circles show the epicenters of the four earthquakes that felt in 2014 (red), the 2016 Kagera earthquake (blue) and aftershocks of Mw 5.2 and Mb 5.5 (black) sequences. The purple dashed lines indicate the boundaries of the Victoria microplate (Stamps et al., 2008). The blue vectors represent surface motion velocities in mm/yr (Saria at el., 2014). Blue stars: the two major towns of Tanzania. 84

6.1 Seismicity of the Botswana with (earthquake magnitudes in the range of 0.5 to 6.8) for the time period 2000 to 2017 compiled from the ISC catalog. The region is dominated by lower magnitude earthquakes within the range of 0.5 to 3.0 and the southern part of the study area is seismically active as compared to the other parts of the region. Different color circles (black, yellow and red) show the epicenters of earthquakes where circle size is proportional to earthquake magnitude as shown in the legend. The large blue circle is the location of the April 3, 2017 Botswana main shock. The magenta box on the map shows the study area. 89

6.2 An overview of the tectonic and geologic map of Botswana and its surroundings. The epicentral location of the April 3, 2017 Botswana earthquake of Mw 6.5 is shown by red asterisk. Black lines represent the tectonic boundaries from Fadel et al., (2018) modified after Singletary et al. (2003) and McCourt et al., (2013). Geologic map of Archean Cratons and Proterozoic Orogenic Belts in Botswana and surroundings are after Leseane et al., (2015). 92

6.3 Seismograms of the April 3, 2017 Botswana main shock recorded at SOE seismic station. a) The raw data for three-component seismograms. b) The three-component seismograms filtered at bandpass filtering range from 0.02 to 0.05 Hz (after instrument response removed) which are used in inversions. E, N, Z indicate (E-W), (N-S) and vertical components respectively. 94

6.4 Regional waveform fits of the April 3, 2017 Botswana main shock using moment tensor inversion in the time domain. The panel is dedicated to waveform comparison (the red color is for data, black is for synthetics). Stations are sorted according to epicentral distances, with station name, distance, azimuth and maximal amplitudes provided on the left side. 95
6.5 Spectra amplitude fits of the April 3, 2017 Botswana main shock using moment tensor inversion in frequency domain. The panel is dedicated to spectra comparison (the red color is for data, black is for synthetics). Stations are sorted based on epicentral distances, with station name, distance, azimuth and maximal amplitudes provided on the left side. 96
6.6 The relative misfits (illustrate how our misfit increases when we perturb one single parameter) versus Strike, Dip and Rake angles for the fault plane solution estimated using moment tensor inversion and obtained at a hypocentral depth of 38.4 km. The bold black dots represent the values at which the three angles are selected from the minimum variance. 97
6.7 Relative misfits versus hypocentral depths of the April 3, 2017 Botswana earthquake of magnitude Mw 6.5 computed from the moment tensor inversions. The best solution has been chosen at smallest misfit for the hypocentral depth (38.4 km). 97
6.8 Focal mechanism of the April 3, 2017 Botswana main shock (black and white color beach ball) and its aftershocks distribution. The white dot represents the location of main shock and magenta dots represent the epicenter location of aftershocks. The blue triangles represent the seismic stations used and the blue star is the location of historical earthquakes of the 11^{th} of September and 11^{th} of October 1952 earthquakes with magnitudes of 6.1 and 6.7 ML. The red and white beach ball is the focal mechanism for 2017 Botswana main shock from GCMT solution while pink and white are for some earthquakes from GCMT solutions. Broken red lines represent the fault system of the Okavango Rift Zone (ORZ) and Southwestern Branch, ODR represents Okavango Delta Region modified from Kinabo, (2007). Heavy black lines represent plate boundaries modified from Bird, (2003). Inset map shows the study area. 99

Abstract

This work principally deals with the recent seismicity for the period 2013 to 2016 and rupture process of some selected earthquakes across the different tectonics regimes of the East African Rift System (EARS). We analyzed phase and waveform data from temporary and permanent seismic networks which are installed along EARS and hosted by different agencies. In this investigation three different works have been conducted.

In the first part, spatial and temporal distribution of earthquakes in the East African Rift System has been investigated for the years 2013 to 2016. The spatial earthquakes distribution in the time window considered in this study has revealed that the Main Ethiopian Rift (MER) is structurally connected to the eastern branch of the East African Rift System (EARS). A relatively high level of seismicity has been obtained in this study compared to the ISC (International Seismological Centre) catalogue database for the same time period which implies the region is seismically more active than we thought. In addition to the rift floor, the rift margins and the surroundings plateaus are found to be seismically active. The western and eastern branches of the EARS are found to be more active than the others rift segments for the time period considered. The frequency-magnitude distribution of earthquakes during this study period provided an average b- and a -values of $\sim$1.01 and $\sim$6.5, respectively. The b-value result is implying relatively high stress with tectonic origin of earthquakes occurrence dominating the region. On the other hand, threshold magnitude completeness of Mc 3.0 is obtained which is the minimum value that has never been observed previously for such large area. The seismic energy map of the region has been systematically investigated and peaks energy-release is observed at Afar depression, eastern and western branches of the EARS during this study period. The energy mapping shows that the MER is structurally connected to the eastern branch of the EARS which is consistent with seismicity distribution. The overall depth of occurrence of earthquakes in the eastern and the western branches of the EARS are relatively deeper than the one found for Afar and MER. This implies that the seismogenic thickness increases in EARS when we go from north to south which is in agreement with rift age, magmatism and influence of the African Super plume on the crust and upper mantle deformation in EARS.

In the second part, complex tectonic deformation of the circum-Tanzania Craton has been investigated. The reliable earthquakes source parameters and the current deformation in relationship with the dynamic change of Victoria plate rotation are generally poorly understood owing to the lack of the proper techniques used in the region. Here, moment tensor inversion is made from broadband seismic data for five earthquakes that occurred in the region in the years 2014 and 2016 with magnitude ranging from Mw 4.1 to 5.7. The 2014 sequence comprises four earthquakes where two of them occurred north of Kondoa with purely normal faulting mechanisms following the N−S oriented rift structure. The other two earthquakes from the 2014 group occurred north of Dodoma and are found to be normal faulting with significant strike-slip component with dextral sense of motion trending in the NW−SE direction which seems to agree with fault structure and aftershock distribution. On the other hand, focal mechanism of the 2016 earthquake in Kagera region with magnitude Mw 5.7 shows dominantly normal faulting trending WNW−ESE with strike-slip component and dextral sense of motion. We therefore find that the observed normal, strike-slip and oblique slip deformation seems to be influenced by the extensional stress regime of the EARS and the anti-clockwise rotation of the Victorian plate. On the other hand, it is not uncommon to observe deactivation of the NW−SE oriented weak zones in the EARS which seems to agree with our fault mechanism results. In addition, the waveform inverted depths of the studied earthquakes vary from 12 to 26 km in the circum-Tanzania Craton is implying relatively larger effective elastic thickness compared to the northern part of the EARS in the Afar region.

In the third part, a deep rupture process of the April 3, 2017 Mw 6.5 Botswana main shock has been investigated. The event has occurred in Botswana in a region where there was no recent tectonic activity and where present-day deformation is believed to be negligible. The event was followed by several aftershocks distributed along NW−SE direction with NE−SW extension direction. We focused on the determination of reliable source parameters for the Mw 6.5 main shock using a moment tensor inversion, both in time and frequency domains from regional, broadband waveform data. We retrieve the source depth at 38.4 km, deeper than other studies in the region. The estimated hypocentral depth of this earthquake is roughly about the Moho depth beneath the region, reflecting a deep source that is relatively rare in stable continental regions. The result may suggest that the seismogenic depth is as deep as the average global Moho thickness indicating the upper mantle lower crust region is actively deforming due to a reactivation of the pre-existing fault that may oriented in the NW−SE direction. The resulted focal mechanism of the event shows normal faulting with NE−SW extension.

In a summary, the findings of this work will provide useful information for geodynamic modeling of earthquakes occurred at plate boundaries and along the rift floor of the EARS. In Addition,

the result of this study is intriguing and exciting which will provide useful information about the future seismicity in a stable continental region where rare large magnitude and a relatively deep earthquake occurred in the past.

Key words: b-value, Catalog, East African Rift System, Magnitude, Moment Tensor Inversion, Northern Tanzania Divergence Zone, Okavango Delta Region, Okavango Rift Zone, Seismicity.

Acknowledgements

Above all, I would like to start by thanking my GOD, for his help during this thesis work as a part of his generous help. Foremost, I kindly acknowledge my advisor Dr. Atalay Ayele for coaching me in handling real-life problems. His overall patience, motivation, guidance, constant advice, constructive criticism, tireless and considerate efforts, enthusiasm, and immense knowledge throughout this thesis work. His invaluable advice, and support encouraged me to pursue my study smoothly and made my stay at the university considerably relaxed which otherwise would have been difficult. I have learned a lot from his personality aspects, which would benefit me tremendously for the rest of my life. I thank you so much, Dr. Atalay Ayele!!!

I would like to express my deepest appreciation and special thanks for the School of Earth Sciences Graduate Studies Dissertation committee: Prof. Tilahun Mammo, Prof. Tigistu Haile, Dr. Abera Alemu and Dr. Tarun Kumar for generously offering their helpful, support, guidance, constructive comments and advice during proposal presentation and all the progress presentations.

I feel honored to thank GFZ, Germany for provided me a chance to participate the summer school on International Training Course which I benefited from it a lot. I would like to thank the experts of the GFZ members, especially, Dr. Simone Cesca for unwavering help and discussions we made on a moment tensor inversion during and after training. Thank you the organizer of the training Dr. Clause. I am thankful to the International Centre for Theoretical Physics (ICTP) for my summer school visit for two weeks at Triesty, in which I got some experiences from the discussions I made with several scientists who came from different countries on the world. Thank you Prof. Abdelkrim Aoudia for giving me such golden opportunity. My especial thanks go to Dr. Brain Baptie, Prof. Richard Lucket and Dr. Andrew Bell, from British

Geological Survey and the University of Edinburgh for the training that you have given to me at AAU, IGSSA. Thank you very much Dr. Andrew Bell for detail discussions we made during and after the training through E-mail on Python and Jupyter Notebook code which I have used for seismicity analysis in this thesis work.

I appreciate much the help of my friend Sisay Alemayehu, who is a Ph.D candidate and staff of IGSSA, at Addis Ababa University for uncountable contributions during my stay at Addis Ababa University. I appreciate for his constant help on computational part, material support and encouragement, as well as for taking his time to be with me during this thesis work. I am also thankful to all staff of IGSSA of AAU for fruitful time we had. I thank Mr. Worku Taye who is the staff of School of Earth Sciences at AAU, for his help during the thesis work in one way or other ways.

Finally, I owe my deepest gratitude to all my family and relatives for encouraging me in all of my pursuits and inspiring me to follow my hope. I would like to express my deepest appreciation to my brothers Tesfaye Asefa, Tolosse Asefa, and my sisters Tadelech Asefa, Berkinesh Asefa, and my wife Almaz Kebede who helped me in one way or other ways, who have made my stay here better. Lastly, but not least, I appreciate much the help of my friend Dr. Minisha Alemu, who is the Wolkite University Physics department staff.

List of Abbreviations

AD – Afar Depression

AF – AfricaArray

CLVD – Compensated Linear Vector Dipole

DMC – Data Management Center

DEV – Deviatoric

DE – Dodoma Earthquake

DC – Double Couple

EAF – East African Network

EARS – East African Rift System

EB – Eestern Branch

ESSN – Ethiopian Seismic Station Networks

FMD – Frequency-Magnitude Distribution

GFZ – German Research Centre for Geosciences

GCMT – Global Centroid Moment Tensor

GDSN – Global Digital Seismograph Network

GPS – Global Positioning System

GA – Gulf of Aden

IRIS – Incorporated Research Institutions for Seismology

IGSSA – Institute of Geophysics, Space Science and Astronomy

ICTP – International Centre for Theoretical Physics

IDC – International Data Centre

ISC – International Seismological Centre

InSAR – Interferometry Synthetic Aperture Radar

ISO – Isotropic

JE − Juba Earthquake

KKE − Kare Kore Earthquake

LTE − Lake Tanganyika Earthquake

LE − Langano Earthquake

ML − Local Magnitude

Mc − Magnitude of Completeness

MER − Main Ethiopian Rift

Mw − Moment Magnitude

ME − Mozambique Earthqauke

NEIC − National Earthquake Information Centre

NDTZ − Northern Divergence Tanzania Zone

NP − Nubian Plate

ODR − Okavango Delta Region

ORZ − Okavango Rift Zone

RS − Red Sea

RE − Rukwa Earthquake

SE − Serdo Earthquake

SP − Somalia plate

SWB − Southwestern Branch

UN − United Nations

UNDAC − United Nations Disaster Assessment and Coordination

USGS − United States Geological Survey

VR − Variance Reduction

WB − Western Branch

CHAPTER 1

Introduction

1.1 Background

The East African Rift System (EARS) is one of the most outstanding and significant rift systems. It extends from the Afar triple junction in at the north where rifting is the most advanced places and where the Arabian plate moves away from Nubian plate (Manighetti et al., 1997) and pulling away from Somalia plate (Manighetti et al., 1998) propagates to Malawi basin to the south. Rifting within the EARS began at the Afar triple junction approximately 25-40 million years ago and has since propagated southward (Lay and Wallace, 1995) through the main Ethiopian rift and has a structural connection with the eastern branch to the south (e.g., Mohr, 1983; Rosendahl, 1987; Braile et al., 1995; Chorowicz, 2005). Near Lake Turkana the EARS splits into two distinct rift segments: a volcanically active eastern branch and less volcanically active western branch (Albaric et al., 2010). Furthermore, the third arm of the EARS (the southwestern branch) propagates into the northern Botswana, towards Okavango Rift Zone (ORZ) (Fig. 1; Modisi, 2000; Corti, 2009) where spreading is at the most juvenile stage. The EARS is virtually the only places in the world where the oceanic rifting is subaerially exposed and the rift is dotted with shield different volcanoes (Keir et al., 2006).

Currently, active deformation and magmatic activity, including offshore of the Indian Ocean which are found in the Eastern Africa are parts of the of EARS (Ebinger et al., 2017). An active continental rift is a region that is accompanied by seismicity and volcanic activity. Thus, seismically active regions are primarily located at the rift zones (Shudofsky, 1985; Nyblade et al., 1996; Lindenfeld and R*ü*mpker, 2011), along the boundary between several microplates plates,

that are embedded within the EARS (e.g., Mulibo and Nyblade, 2016) and also in the regions with active magmatism (e.g., Albaric et al., 2010, 2014). The northern part of the EARS is also surrounded by western and eastern Ethiopian plateaus.

The EARS has been a target of many studies as it encompasses the various stages in geodynamic settings with structures that accompanied a significant active deformation which may relate to seismic activity. An investigation of seismic activity of the EARS continually draws an interest because the region is one of the most known areas of ongoing tectonic deformation experiencing small to large earthquakes (Zhao et al., 1997; Meghraoui and Pondrelli, 2012). The major active faults of the region may generate destructive earthquakes. Some of the large earthquakes may occur in densely populated regions causing severe damage and significant economic losses in the region.

Thus, the EARS has been the site of numerous large and destructive earthquakes which are still poorly understood. The most recent events being the August 25, 1906 Langano earthquake (Ayele and Kulhánek, 2000) with Mw 6.5 in which shaking was felt in Addis Ababa and its surroundings. In December 13, 1910, an earthquake of magnitude 7.4 struck in the Rukwa region with little damage (Ambraseys, 2007), might be due to less development of Urban and modern houses at a time. In May 19, 1961, an earthquake of magnitude greater than 6.4 was felt near Kara Kore and completely destroyed the town of Majete. In the central Afar depression, the 1969 Serdo sequences of the main shock of magnitude Mb 5.9 completely destroyed Serdo town. In 1990, an earthquake of magnitude 7.0 struck Juba in Southern Sudan. On November 4, 2002 an earthquake of magnitude Mb 5.5 struck Dodoma, the capital city of Tanzania, causing cracks in the Parliament building (Macheyeki et al., 2008). On December 5, 2005 an earthquake of Mw 6.8 rocked Lake Tanganyika region, causing damage in Congo (Moussa, 2008). Furthermore, in February, 2006, one of the largest earthquakes to occur in the EARS, took place in Mozambique with a magnitude of ∼Mw 7.0. The event was widely felt in the region (Yang and Chen, 2008). Intra-plate earthquakes in stable continental regions are infrequent and occur in regions with low strain rates (Calais et al., 2006). Despite their rare occurrence, earthquakes with larger

magnitudes, affect several continents (Calais et al., 2016). Most of the present-day intra-plate earthquakes are followed by an intense aftershock sequences (Boyd et al., 2015). Thus, the April 3, 2017 Botswana main shock is an example of the intra-plate earthquake that exhibits hundreds of aftershock sequences and occurred in the region with low seismicity.

Damage from earthquakes has become a subject of importance in today′s world because earthquakes lead to human casualties and major structural damage. Ground shaking resulting from earthquakes may collapse buildings and destroy infrastructure. Recent devastating earthquakes and induced seismicity near infrastructures must become the centerpiece of analysis in reducing risk and increasing resilience. These are very important in the EARS which contains many developing countries where population size, urbanization and the development of mega projects are rapidly growing. Existing towns are expanding in size with the number of large buildings increasing.

Information required to study active deformation and seismic activity of the EARS may depend on the number of seismic stations used. However, sparsely distributed seismic stations available in the EARS previously resulted in challenges in effectively studying the seismicity of the region. We computed source parameters such as earthquake location and focal mechanisms from a reasonable amount of seismic data to improve our knowledge of faulting and potentially seismic areas, which may help in seismic hazard assessments. Earthquake distributions, their magnitudes, focal mechanisms, the tectonic parameters and energy released by earthquakes are the most important aspects of seismic activity of the EARS. Therefore, updating the regional earthquake catalog and the seismotectonics of the EARS are very crucial to quantify the risks posed by earthquakes.

This thesis principally deals with the recent seismicity of the EARS, including earthquakes distribution, b-value, energy mapping and rupture process of some selected earthquakes with detailed interpretations. Thus the main aim of this study is to provide useful information on earthquakes in the region. We assessed seismicity of the EARS (10°S to 15°N) and (24°E to 45°E) for the time period 2013 to 2016. In addition, the rupture processes of the 2017 Botswana

main shock has been investigated.

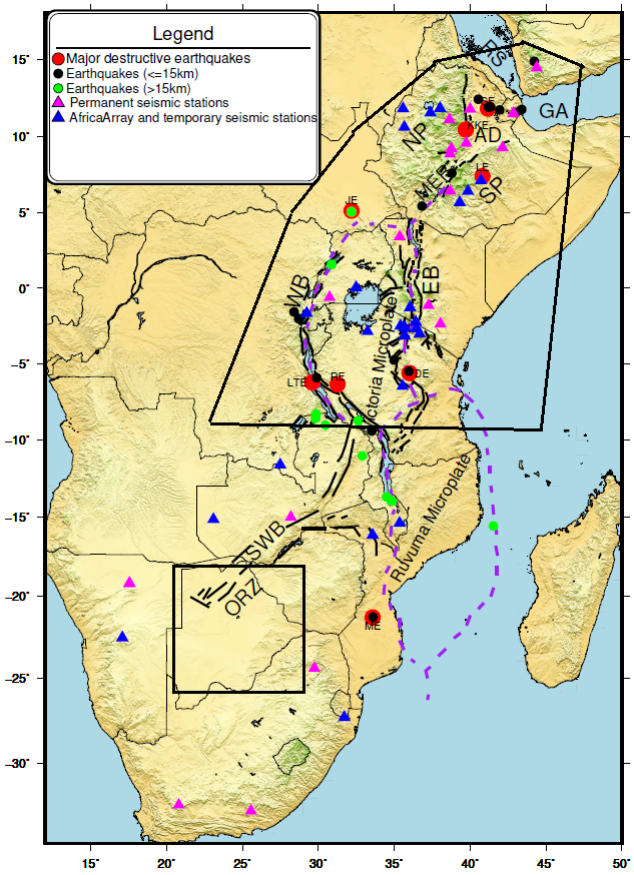


Figure 1.1: Complex tectonics regimes of the EARS. The black polygon and black rectangle show, the study areas. The magenta and blue triangles are the location of seismic stations used as shown on the legend. The red dots are the major large and destructive earthquakes that occurred in the continent (SE (Serdo), KKE (Kare Kore), LE (Langano), JE (Juba), DE (Dodoma), LTE (Lake Tanganyika), RE (Rukwa), ME (Mozambique) earthqaukes). The black and green dots are the location of some earthquakes that obtained from waveform inversions combined from previous works of (Shudofsky, 1985; Grimison and Chen, 1988a; Jackson and Blenkinsop, 1993; Foster and Jackson, 1998; Brazier et al., 2005; Yang and Chen, 2010; Craig et al., 2011) and from full moment tensor inversion (in both time and frequency domains) of this study. RS represents the Red Sea, GA the Gulf of Aden, AD the Afar depression, NP Nubian Plate, SP Somalian plate, MER the Main Ethiopian rift, WB the western branch, EB the eastern branch and SWB for the southwestern branch.

1.2 Objectives

1.2.1 General objectives

The study of seismicity of the EARS, which plays a vital role in understanding the detailed seismic activities of the region, was carried out. Therefore, the general objective of this study was to study the recent seismic activity of the region for the time period 2013 to 2016 due to available earthquake data from permanent and temporary seismic stations and to investigate the rupture processes of some selected earthquakes.

1.2.2 Specific objectives

The specific objectives are:

- Developing an earthquake catalog of the region for the period 2013 to 2016.
- Estimating a and b-values of the region.
- Producing the recent earthquake's energy map of the region.
- Estimating the source parameters of earthquakes using a moment tensor inversion.
- Computing and interpreting the focal mechanisms resulted from a moment tensor inversion.

1.3 Statement of the problem

The EARS is a region of complex tectonic settings with active faults. Therefore, studying the associated seismicity of the region is very important. The study of earthquakes would provide insight to the seismogenic process of the region and may reveal the present picture of the seismic activity in the EARS. The seismic monitoring of earthquakes in the region was carried out using both permanent and temporary seismic stations. Therefore, seismicity of the region is monitored by several International agencies and by Eastern and Southern Africa Seismic Working Group from different institutions for long periods. However, a gap in the database is

observed for earthquakes of small magnitude due to lack of reasonably dense seismic network. Even the available seismic data is neither comprehensively done by observatories in the region nor available for analysis by International Seismological Centre (ISC), National Earthquake Information Centre (NEIC), East African Network (EAF) and many other international data centres.

In addition, several events location is reported to ISC by different agencies which are not revised by ISC. Some of the reported events were not systematically analysed since a single station was used for an event location. The estimated magnitude from a single station are likely to have high errors, while some of the events did not even have a magnitude value estimated. The ISC, aims to produce earthquake source parameters like latitude, longitude and depth but an earthquake depth is usually the most uncertain parameter that is often required to be fixed (Bolton et al., 2006). In many areas around the world, the approximated earthquake depth in average is 10 km, however, this assumption is not valid for all earthquakes and for all regions.

Therefore, an improvement of earthquake depth estimation in the database is also an important in addition. Furthermore, different reports of magnitude values of earthquakes from different agencies may be due to differences in methodology and inherent uncertainties in data used. Agencies can use magnitude estimation procedures designated to meet the agency′s specific needs and monitoring capabilities. Therefore, different values of the estimated magnitudes of earthquakes have been observed in the database among agencies that may arise due to the different magnitude estimation models, data availability and data processing procedures used. In this study, in order to estimate relatively good earthquake magnitude values, we use a local magnitude estimation formula which was developed for the specific part of EARS (Keir et al., 2006).

A lot of studies have been already done on investigation of seismicity of the EARS (Kebede and Kulhánek, 1994; Ayele and Kulhánek, 1997; Hofstetter and Beyth, 2003) and many others. However, most of the previous studies were mainly based on teleseismic and regional earthquake data from International catalogs. With the establishment of local seismic networks in the EARS,

the volume of good quality data has increased sharply in recent years. Thus, combining and analysing waveform data from seismic stations, which are found within the region can refine earthquakes database. Therefore, revising the database to improve earthquakes catalog of the EARS and to come up with clear geometric nature of the seismicity of the EARS are very crucial. Furthermore, source parameters and focal mechanisms for some regional earthquakes are not well determined and not interpreted in line with the tectonic setting of the region. Thus, computing the source parameters of earthquakes using good techniques such as moment tensor inversion and interpreting the source parameters are well important.

1.4 Significance of the study

An earthquake catalog has information about recorded earthquakes that occurred within the area of interest which may help in quantifying the present and future seismic hazards. This is particularly true for the EARS where the causative mechanisms and the occurrence of small to large earthquakes are generally poorly understood. The updated earthquake catalog of this study, can be used to characterize the present seismicity and occurrence of future earthquakes in the region. Therefore, the catalog in this study may be used for statistical analysis of seismicity of the region. In addition, the estimated source parameters of earthquakes using moment tensor inversion method and the computed focal mechanisms of earthquakes are very important for characterization of the past and future hazard analysis of the EARS. The present study has great significance in many aspects as it is carried out based on the data available at permanent and temporary seismic stations. This study presents a clear picture of earthquake distribution in space and time during the study period. In addition, it will reveal the reliable source parameters and focal mechanisms of earthquakes. In general, this study signifies the present seismicity of the EARS and it will solve relatively some of the limitations mentioned in the international database and enlarge the scope of a research topic of seismicity.

1.5 Thesis layout

This dissertation had a compilation of results that emanated from studies made on the topic Recent Seismicity for the period 2013 to 2016 covering an area of latitude 10°S to 15°N and longitude 24°E to 45°E and Rupture Process of Some selected Earthquakes in the EARS. The whole dissertation is presented in seven chapters. Starting from chapter four, the organization of the thesis is based on a number of papers published and under review in peer reviewed international journals.

Chapter 1: In this chapter we have introduced the topic of work and the study area. This chapter also covers the basic terminologies related to the topic, objectives of the study, the statement of the problem, and the significance of the study.

Chapter 2: In this chapter we introduced the highlights of the regional tectonic setting of the EARS that may relate with the seismicity of the region. In addition, we have incorporated some of the previous work done in the region in perspectives of the current study (earthquake catalog analysis, seismicity distribution and a general aspect of focal mechanisms).

Chapter 3: This chapter introduces some of the important background of basic seismic theory in seismology: basic concepts of source parameters and the focal mechanisms of earthquakes. Furthermore, basic methods (theories) that have been used under this study (phase picking, earthquake location and magnitude estimation) were introduced.

Chapter 4: This chapter provides the general recent seismicity of the EARS for the time period 2013 to 2016. A comparison of the results of this study to the international catalog (International Seismological Centre (ISC)) has been made. Furthermore, a- and b-values and energy mapping of the region have been described. The manuscript of this chapter is submitted and under review in international journal.

Chapter 5: This chapter assesses the complex tectonic deformation in the circum-Tanzania Craton within the EARS using moment tensor inversion. Source parameters of some selected earthquakes that occurred in 2014 and 2016 have been computed. In addition, hypocentral

depth and focal mechanisms of events have been interpreted with respect to the tectonic setting of the area and with respect to the rotation of microplate embedded in the EARS relative to the major plates found in the continent. The results of this chapter have been submitted and published in peer reviewed international journal.

Chapter 6: The work presented in this chapter focuses on the deep rupture process of the April 3, 2017 Botswana main shock. The event is different from the traditional occurrence of earthquakes in EARS. The source parameters of the earthquake are computed from a mixed moment tensor inversion approach and relatively deep hypocentral depth has been obtained. The results of this chapter have been submitted for publication and the article is currently undergoing peer review in an international journal.

Chapter 7: Under this chapter we have provided a general summary of the dissertation based upon the results, presented in chapter four to chapter six. Finally, we concluded this chapter by making general recommendations for future work.

CHAPTER 2

Regional Tectonic Setting and Previous Studies

Discribed in this chapter is a succinct overview of the regional tectonics setting and previous seismotectonics studies of the EARS. The EARS comprises several rift segments which are at different stages of development with some of them are at advanced stage such as the Afar depression which is at oceanic stage. The lithospheric structure of the EARS encompasses different tectonics that play a key role in the occurrence of seismicity in the region. The current study region covers the Afar region and the MER in the north as well as the western and eastern branches of the EARS are in the south. Furthermore, the southwestern branch of the EARS that propagates towards Botswana region was included in chapter six of this thesis under section on geologic and tectonic setting.

The region exhibits strong variation in lithospheric structure from the thinnest at rift to thickest at cratonic areas. In different rift segments of the EARS, the cratons, Microplates and mobile belts that developed through rifting process play a key role in the occurrences of seismic activity of the region. Rifting is evident from topographic expression, geology, volcanism, seismicity, and gravity (Mohr, 1967; Moore and Davidson, 1978; Davidson and Rex, 1980). In the following sections, the regional tectonics will be described briefly. Next to that, an overview of the previous seismotectonics studies of the region will be given.

2.1 Regional tectonics setting

Rifting is defined as the splitting apart of a single tectonic plate into two or more tectonic plates. Thus, it is a fundamental process by which the continent has separated into pieces of tectonic plates. For example the extension of the world′s largest continental rift structures of the EARS

(Ebinger, 1989; Bendick et al., 2006; Chorowicz, 2005) separates the African continent into the Nubian and the Somalian plates. The EARS is one of place where the earth′s tectonic forces are presently trying to create new plates by splitting apart (Corti, 2009).

The extensional development of the EARS has begun around the Miocene, 22-25 million years ago (Ebinger, 2005) whereas the peak extensional rifting has begun in the Cenozoic era. It has been continued extending into the late Tertiary keeps on going in recent times (Ghebreab, 1998). The EARS meets the two Oceanic ridges at triple junction in Afar depression (Makris and Ginzburg, 1987).

The tectonic stress might be drive lithospheric or crustal extension. Some of the physical parameters may accelerate the lithospheric deformation within the EARS within the rift structure: the rate of extension (England, 1983; Prez-Gussiny et al., 2006), geothermal gradient (Buck, 1991), the rheological of the lithosphere (Ricard and Froidevaux, 1986; Huismans and Beaumont, 2011), variation in crust and lithospheric mantle thikness (Hopper and Buck, 1996), and the magmatic intrusions (White and McKenzie, 1989). The African continent sits above a major mantle upwelling thus, rifting is developed beneath the EARS. The African Supers well is breaking apart the EARS (Bagley and Nyblade, 2013).

The Cenozoic active continental rifting of the EARS geodynamic process is currentily leading to a rupture of the continent and the birth of new seafloor spreading in the Afar Depression (Buck, 1991). In general, it gets younger and younger from the Afar to the Okavango delta. Deformation is preferentially localized along a large-scale of the tectonic boundaries (Nyblade and Brazier, 2002; Corti et al., 2007). The EARS is bounded on one or both sides by large offset border faults (Ebinger et al., 1984; Bosworth, 1985). Basically the region is dominanted by normal faulting and by lithospheric attenuation in both the crust and mantle.

The Afar depression is one of unique geophysical region where three major tectonics rift namely the Red Sea, the Gulf of Aden and the MER (Figs. 1.1 and 2.1) are interacting. The movements of the Nubian, Arabian and Somalian plates have created several structures across the region (e.g. Hofstetter and Beyth, 2003; Beyene and Abdelsalam, 2005).

In the Afar region active faulting is concentrated within the center of wider rift zone and the strength of the lithosphere is decreasing with increasing strain rates and magmatism (Hayward and Ebinger, 1996). Active faults also occur on the western margin, outside of the rift centre (e.g., Zwaan et al., 2010). The region has evolved continental rifting with the thinnest crust except for the Northern Afar that would be a transition zone between a continental and oceanic crust with volcanic contributions (Hayward and Ebinger, 1996). High angle border rifts were developed during the Oligo-Miocene (29-26 Ma) at the initial stage, but later on a sea-floor spreading was developed within the center of the rift with strain accommodated by dyke injection (Wolfenden et al., 2005). The dike intrusion is accommodating strain that cause extension by a brittle deformation and ductile mostly in the crust (Ebinger and Casey, 2001; Ebinger, 2005). For example, the Quaternary extension is accompanied by magmatism which has been formed the NW-SE trending axial volcanic ranges of fissure basalts and shield volcanoes. The geology of central Afar is dominated by volcanic ranges and volcanic shield complexes (Beyene and Abdelsalam, 2005). The region is almost completely circumscribed by continental crustal blocks, and lacks a narrow, oceanic-type spreading zone except in the extreme north (Mohr, 1971). The southern Afar is bound by the Somalian escarpment in the south and by transfer fault zones in the western direction (Hayward and Ebinger, 1996).

The MER is located in the northern part of the EARS, south of the Afar rift (e.g. Makris and Ginzburg, 1987; Ebinger and Casey, 2001; Bastow and Keir, 2011). The flood basaltic and the separation of Arabian plate from Africa continent were widely observed in the time from the opening of the MER. The MER is an extensional rift from the Afar where rifting began around $\sim$11 Ma and at 18 Ma, in the northern and southern MER (Hendrie et al., 1994; Woldegabriel et al., 2000; Tesfaye and Harding, 2004; Wolfenden et al., 2004) respectively. The MER is composed of several complex structural segments of: the northern, central and southern segments (Bonini et al., 2005b). The rift segments are characterized with different level of magmatic activity and seismicity distributions. The initial opening in the central MER has commenced about 15 Ma (Ebinger et al., 2000; WoldeGabriel et al., 1990) which is the youngest of the

three sectors of MER (Bonini et al., 2005). Along the MER, Quaternary-Recent volcanism is dominated by rhyolites, and subordinate basalts (Peccerillo et al., 2003; Rooney et al., 2012c; Giordano et al., 2014). The rift is bordered by Miocene aged normal faults (Pizzi et al., 2006). The extensional activities of the region are focused along a 20 km wide and 60 km long faulted magmatic segments (Casey et al., 2006).

The major border faults of the MER were developed during Oligo-Miocene, however the rift extension is migrated towards the tectono-magmatic segments (Ebinger and Casey, 2001; Mammo, 2013). Majority of the magmatic segments are concentrated in the rift axis of the MER. The main tectonic structures of the rifts are dominated by north-northeast-south-southwest direction (Mohr, 1962b) and the expansions of the rifts would have induced the linking of different segments (WoldeGabriel et al., 1990).

The uplift of the Ethiopian plateaus have begun in between 20 and 30 Ma (Marty and Carignan, 2003) where the MER bisects the country into the western and eastern plateau, which are also called Nubian and Somalia plateaus respectively. The northwestern and southeastern plateaus are separated by Oligocene-Miocene border faults of the MER (Corti et al., 2013). The southeastern plateau is characterized with limited recent volcanism as compared to western plateau which has been relatively featured by localized volcanoes (Chambers et al., 2019). For example the Choke and Guguftu shield volcanoes are found in the northwestern plateau (Kieffer et al., 2004). An ongoing tectonic deformation (e.g., Biggs et al., 2011; Pagli et al., 2014) in particular and geophysical data results suggest a partial melt beneath the northwestern plateau (Keir et al., 2009) might be accommodating an extensional strain outside the MER (Kogan el at., 2012).

A complex structure near the southern main Ethiopia rift-Southern-Sudan-Kenya border impresses Mesozoic to Palaeogene rifts (Hendrie et al., 1994). The region is poorly understood since seismic activity of the region is more diffuse and faults are small (Saria et al., 2014). The region is found at the southern part of South-Sudan where seismic activity of the region is related to the movements of the fault bounded basins in the area probably related to the Cenozoic volcanism in Jebel Merra and Bayuda volcanic fields (Babikeret al., 2015).

Near the Lake Turkana, the EARS splits into the western and eastern branches of the EARS (Fig. 2.1). The development of the western rift is attributed to resistance of the Tanzanian craton to tectonic stress regimes. The western branch is developed in Paleo and Mesoproterozoic orogenic belts and is structurally connected to the Malawi Rift via the Rukwa Rift (Delvaux and Macheyeki, 2012). The western branch has a distinct rift segments that developed since the Miocene (circa 12 -10 Ma) (Ebinger, 1989; Corti et al., 2007). The western branch is poor in magma (Roberts et al., 2012) as compared to the eastern branch of the EARS.

The eastern branch of the EARS is extending from the MER through Kenya (Lake Turkana in northern Kenya). It encloses the Tanzania Craton which is surrounded by several Proterozoic mobile belts (Nyblade and Brazier, 2002). The volcanism that began in the southern rift segment of the Ethiopian rift has propagated to the Kenya and Tanzania (Ebinger et al., 1993). It contains the Cenozoic northern Tanzania that is tangental to the southeastern frank of the Kenya dome, which is covering a major feature of the region with different tectonics that reflect the nature of faulting, volcanism, geothermal activity and seismicity (Fairhead, 1980). Volcanism of the region was initiated at about 25 Ma (Furman, 2007) and the region is marked by abundant geothermal features.

The evolution of the rift is structurally exploiting the weak collisional zone at the contact between the Archean Tanzania craton and Proterozoic orogenic belts (Smith and Mosley, 1993). Rifting has characterized by a localized deformation and volcanism in the Kenya rift to a wider deformation in the Northern Tanzania Divergence Zone (Dawson, 1992; Le Gall et al., 2008). Active deformation and volcanism are distributed across a >300-km-wide rift (Isola et al., 2014) in the region.

The EARS is subjected to different activities. For example the lithospheric thinning within the Afar is due to plume activity (e.g. Ebinger and Sleep, 1998; Manighetti et al., 1998). The MER is also subjected to the magma assisted faults and tectonic faults (Pizzi et al., 2006) whereas the contribution of magmatism, tectonics and fault-block motion contribution are very significant in the southern of EARS.

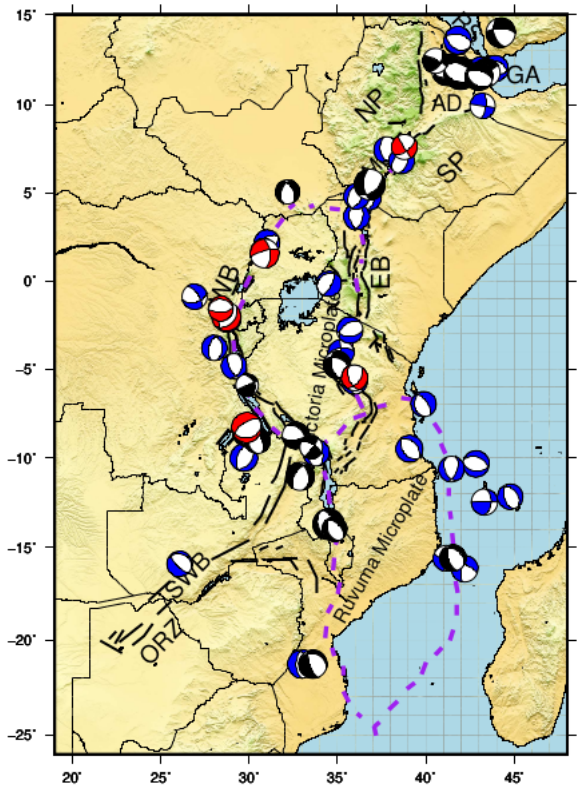


Figure 2.1: Different tectonic regimes of the EARS. The black and white beach balls are focal mechanisms for some earthquakes that obtained using waveform modeling combined from previous works (Shudofsky, 1985; Grimison and Chen, 1988a; Jackson and Blenkinsop, 1993; Foster and Jackson, 1998; Brazier et al., 2005; Yang and Chen, 2010; Craig et al. 2011) whereas the blue and white beach balls are from the Global Centroid Moment Tensor (GCMT). The red and white beach balls are fault plane solutions that computed in this study using full moment tensor inversion (in both time and frequency domains). RS represents Red Sea, GA Gulf of Aden, AD Afar Depression, NP Nubian Plate, SP Somalia Plate, MER the Main Ethiopian Rift, WB the Western Branch, EB Eastern Branch and SWB the Southwestern Branch.

2.2 Previous studies

Several studies have been conducted in the EARS to study seismic activity of the region (Kebede and Kulhánek, 1994; Ayele and Kulhánek, 1997; Lindenfeld et al., 2012). Seismic activities of the region are believed to be associated to the rift development for a long time. Some of the previous studies have been focused in large areas of the EARS while some of studies have been focused on specific areas of the region. Within the EARS, the historical earthquakes records

show sparsely distributed earthquakes, with significant variations in magnitudes of completeness at different time as a result of the sparsely distributed networks.

So far, earthquakes catalogues of the region have been compiled from the global and regional databases that recorded teleseismic and regional earthquakes. For details investigation, the well documented earthquakes records are very crucial. Accordingly, earthquakes observations for over 500 years (in Ethiopia) were collected and compiled from various sources by Gouin, (1979). Seismic activities are mainly concentrated in the Afar and at the margin of the northern MER. Numerous publications have been focused on earthquakes catalogue that compiled from the International catalogue. For example an earthquake catalogue of the Horn of Africa has been compiled by Ayele, (1995) for the period 1960 to 1993 with a threshold magnitude of 4.5 (mb) with a relatively high seismicity that focused on the northern part of EARS and the northern part of the western branch. For the period 1960 to 2000 earthquakes data are compiled and revealed earthquakes distribution that correlated with active faults in the Afar and the surroundings (Hofstetter and Beyth, 2003). On the other hand, Kebede and Kulhánek, (1991) has compiled earthquakes data for the time period 1963 to 1989 for the whole EARS and southern Red Sea and suggested the structural connection between the MER and the western branch of the EARS. Furthermore, the compiled earthquakes data in the eastern branch for the period 1954-1988 revealed a correlation of seismic activities with the major rift structure and tectonic features (Iranga, 1992).

Moreover, few years ago a considerable progress has been made towards a good understanding of the tectonic and geophysical properties of b-values (that determine the relative number of earthquakes of magnitude) in the EARS at different time for a part or all of the region (Tongue et al., 1992; Ayele and Kulhánek, 1997; Lindenfeld et al., 2012). Accordingly, varies b-values have been obtained within the region might be due to different earthquakes data used. For example, a 0.87 of b-value has obtained for the period 1954 to 1967 by considering earthquake magnitude >4 for the whole EARS (Kaila and Narian, 1971). Kebede and Kulhánek, (1994) has compiled earthquakes for magnitude of completeness of 4.6 and computed an average b-values

with in the range of 0.5 to 1.5 for the whole EARS and relatively low b-values range 0.5 to 0.8 for Afar depression and northern western branch. This observation implies that the southern part of the EARS is characterized with high b-values implies relatively low stress levels than the northern part. For the Horn of Africa region b-values varies from 0.55± 0.12 to 1.31± 0.29 have been observed by Ayele and Kulhánek, (1997). Wohlenberg, (1969) has computed the b-values of 0.65 and 0.79 from earthquake data of regional networks for western and eastern branches of the EARS respectively. On the other hand, Lindenfeld et al., (2012) computed a b-value 1.1 that is consistent with the hypothesis of magmatic processes within the crust for Rwenzori Mountains in the EARS due to more smaller events.

Different results have been obtained for the magnitude of completeness from several previous studies. Ayele, (1995) obtined a body magnitude completeness above 4.5 for the Horn of Africa whereas Hofstetter and Beyth, (2003) has obtained body magnitude of completeness above 4.6 from the compiled earthquakes catalogue in Afar depression. For the period 1954 to 1988, Iranga, (1992) has analysed for earthquake catalog that is complete down to magnitude 4.5 in the eastern branch.

Earthquakes distributions are mainly confined within the rift floor (Nyblade et al., 1996; Langston et al., 2002), at rift margins and at the boundary of microplates (Fig. 2.2; Mulibo and Nyblade, 2016) within the EARS. In addition to, a region of active faults and volcanism, significant amounts of earthquakes are observed beneath the plateaus (Ayele and Kulhánek, 1997; Keir et al., 2006, 2009). The western branch of the EARS is seismically very active and characterized with larger magnitude than the eastern branch (Twesigomwe, 1997).

Majority of earthquakes in the EARS are related to faults that are visible along the surface of the earth but some faults have no surface expressions which are in the crust below the surface. Earthquakes depths distribution of the EARS is at shallow depths (Ayele et al., 2007; Wilks et al., 2017) in which majority of earthquakes have depths in the range of $10-25$ km. Earthquakes with deeper hypocentral depth are found in the southern part of the EARS than the northern part. The earthquakes depth extent may have a relationship with a deformation of continental

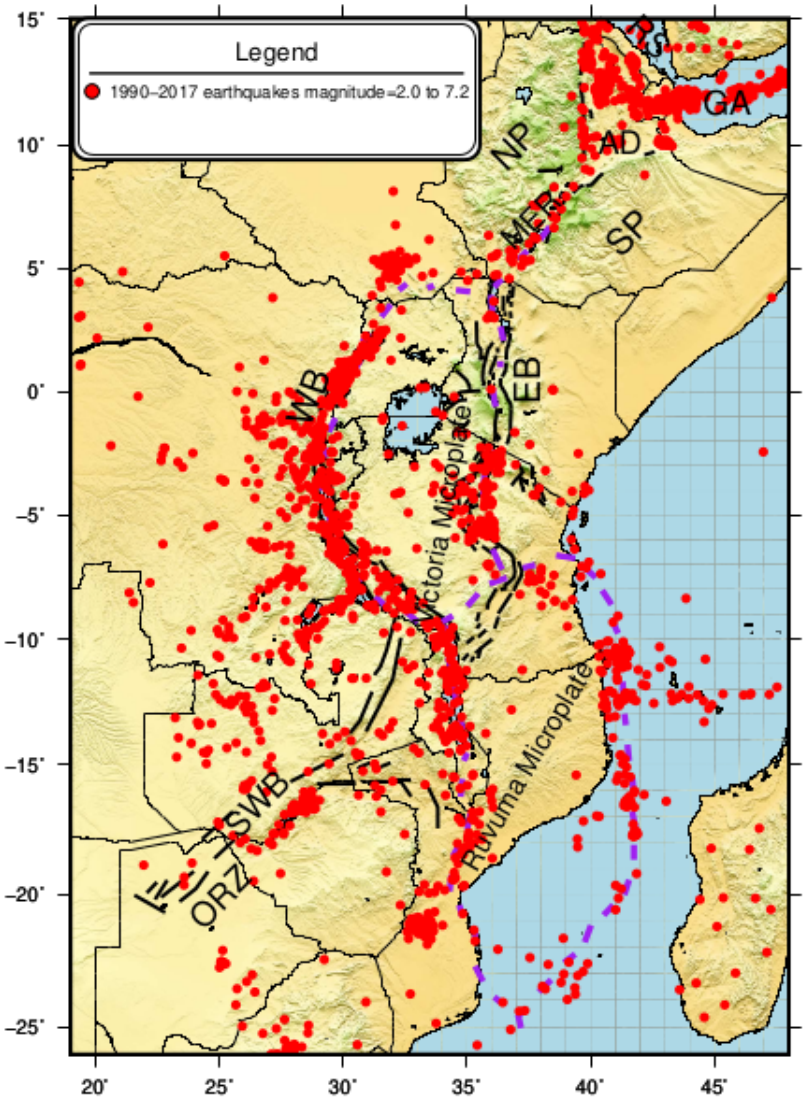


Figure 2.2: Different tectonic regimes of the EARS. The red dots are locations of earthquakes from USGS. RS represents Red Sea, GA Gulf of Aden, AD Afar Depression, NP Nubian Plate, SP Somalia Plate, MER the Main Ethiopian Rift, WB the Western Branch, EB Eastern Branch and SWB the Southwestern Branch.

lithosphere, and magmatic processes of several rift segments of the EARS. Varies ranges of the hypocentral depths have been reported from some of the previous works. Earthquakes with hypocentral depths from the upper and lower crust have been reported (Bungum and Nnko, 1984; Foster and Jackson, 1998) within the EARS. However, unexpected results of hypocentral depths extent down to ∼35 km in the deep lower crust have been reported (Nyblade et al., 1996; Yang and Chen, 2010). Moreover, except in Afar and main Ethiopian rift some earthquakes seem to reach relatively unusual depths extending a maximum depths down to 40 km (Camelbeeck and Iranga, 1996; Albaric et al., 2009; Mulibo and Nyblade, 2009; Craig et al., 2011). Earthquakes depths between 53 and 60 km (Lindenfeldet al., 2012) have been reported for a few events that occurred in the EARS.

Earthquakes focal mechanisms have been computed in several studies to determine fault orientation within the EARS. The solution is available for larger events from Harvard CMT but focal mechanisms of earthquakes down to lower magnitude are not available as needed. Therefore, in some previous studies focal mechanisms were computed and compiled for a number of earthquakes that occurred within the EARS (Kebede et al., 1989; Kebede and Kulhánek, 1989; Ayele and Arvidsson, 1998; Ayele, 2000; Fig. 2.1). Foster and Jackson, (1998) and Hofstetter and Beyth, (2003) determined focal mechanisms of earthquakes in connection with the seismotectonic setting of the region and many others. Normal faulting is dominating (Kebede et al., 1989; Kebede and Kulhánek, 1989; Ayele et al., 2007) within the EARS.

However, the tectonic setting of the EARS is not simple as we believed hence focal mechanisms of some earthquakes are found to be a non-normal faulting or a mixture. The strike- slip mechanism in an extensional continental crust of the EARS (Asfaw, 1990; Doser and Yarwood, 1991; Gaulon et al., 1992) has been obtained. Recently some studies revealed normal faulting with significant strike-slip components (e.g., Ayele, 2000; Asefa and Ayele, 2020) and a combination of normal and strike slip faulting with some sinistral motion (Mulibo and Nyblade, 2016). A complicated stress pattern with possible dextral strike-slip motion on some faults but oblique motion on others is also observed in western branch (Brazier et al., 2005). From the stress

orientation, several previous studies have suggested different trendings of the EARS (Bungum and Nnko, 1984; Macheyeki et al., 2008; Yang and Chen, 2010) from fualt plane solutions of earthquakes. The extensional direction of the EARS has been suggested either E−W, (Delvaux and Barth, 2010; Fairhead and Stuart, 2011) or NW− SE trending (Strecker et al., 1990) for the eastern branch. GPS and plate kinematic studies also show that, MER is opening in NE-SW direction.

CHAPTER 3

Some Basic Theory in Seismology

3.1 Basic theory on seismic wave propagation

Seismology is the study of earthquakes, seismic wave propagation and recording of elastic waves in the Earth and also the study of earthquakes sources. Body and surface waves are the two main types of seismic waves. Body waves can travel through the Earth′s inner layers while surface waves travel along free surface. Body waves can be categorized into P-wave or compressional wave which is the fastest kind of seismic waves, and S-wave is the second wave we feel in an earthquake shaking. S-wave is slower than P-wave and only moves through solid rock, not through any liquid medium.

On the other hand, surface waves have lower frequency than body waves and arrive at a seismic station after body waves. Surface waves are almost entirely responsible for the damage and destruction associated with earthquakes. Surface waves are resulted from the interaction of P and S -waves with boundary condition on the body with no shear stress. The surface waves can be categorized into two. The Love wave is the fastest surface wave and moves the ground from side-to-side. Rayleigh wave is the second kind of surface wave that rolls along the ground and moves the ground up and down and side-to-side in the same direction as a wave is moving. Most of the shaking felt from an earthquake is due to the Rayleigh wave, which can be much larger and destructive than the other kind of waves.

3.2 Elastic moduli

In seismology, elastic seismic waves that travel through the Earth can be generated by earthquakes, volcanic eruptions, magma movement, large landslides and large man-made explosions. Location and nature of the source information of an earthquake can be obtained by processing the elastic waves recorded on seismic stations. If the origin time is known when the waves left the source, their arrival times at the receiver give the travel time required to pass through the medium. Earthquakes can be natural or man-made based on the sources of deformational energy that generate the seismic waves. The highest resolution of the internal Earth structure can be obtained from the study of seismic waves which is very difficult from other geophysical methods. Based on the mode of generation, earthquake can be categorized into three. The first kind of the earthquake is tectonic earthquake produced by rocks fracture due to various geological forces. This kind of earthquake is very important to study the structure and interior of the Earth, and much social significance as it pose greatest hazard. The second kind of earthquake is volcanic earthquake that occurs due to volcanic activity. It may occur before an eruption with minor seismic activity increases in the vicinity of the volcano and may occur when fault rupture precedes the motion of magma and eruption of lava. The third kind of the earthquake is induced earthquake produced by human activity. It can be Reservoir induced seismicity, nuclear explosion, Rock burst and fluid injection.

Earthquakes may further classified into three types depending on the distance from source to seismic station. The first type is teleseismic earthquakes which are recorded by a seismic station at a greater distance. In convention the epicentral distances more than 1000 km for a teleseismic earthquakes (Lay and Wallace, 1995) while earthquakes that occur beyond say 500 km but within 1000 km epicentral distance is called regional earthquakes. On the other hand, earthquakes that occur within a distance of few hundred km from a seismic station are called local earthquakes.

The elastic waves can propagate away from the source region by elastic deformation of the rocks through which they travel. By the pressure front expanding from an underground explosion, or by an earthquake shear rupture, the surrounding Earth material is subjected to stress

(compression, tension and/or shearing). As a consequence, it undergoes strain, i.e., it changes volume and/or distorts shape. The forces that cause deformation are referred to as stresses. The mathematical relationship between the forces applied and the resulting deformation that used to describe the elastic properties of a medium is provided from the theory of elasticity. It can be generalized in the form of Hooke′s law as follow:

$$\sigma_{ij} = C_{ijkl}\varepsilon_{kl}, \tag{3.2.1}$$

where σ_{ij}, is the stress tensor, C_{ijkl} is the constants of proportionality known as elastic moduli and ε_{kl} is the strain tensor.

3.3 Stress tensor

A tensor is a multi-dimensional array of numerical values that can be used to describe the physical state of a material. A stress tensor is an example of geophysical tensor like pressure as force per unit area. In order to explain the stress tensor in seismology, consider the following figure of a unit cube of material with forces acting on it in three dimensions. The stresses acting on the material can be decomposed into nine components, thus the nine terms of surface forces have the tensor components as shown in Figure 3.1.

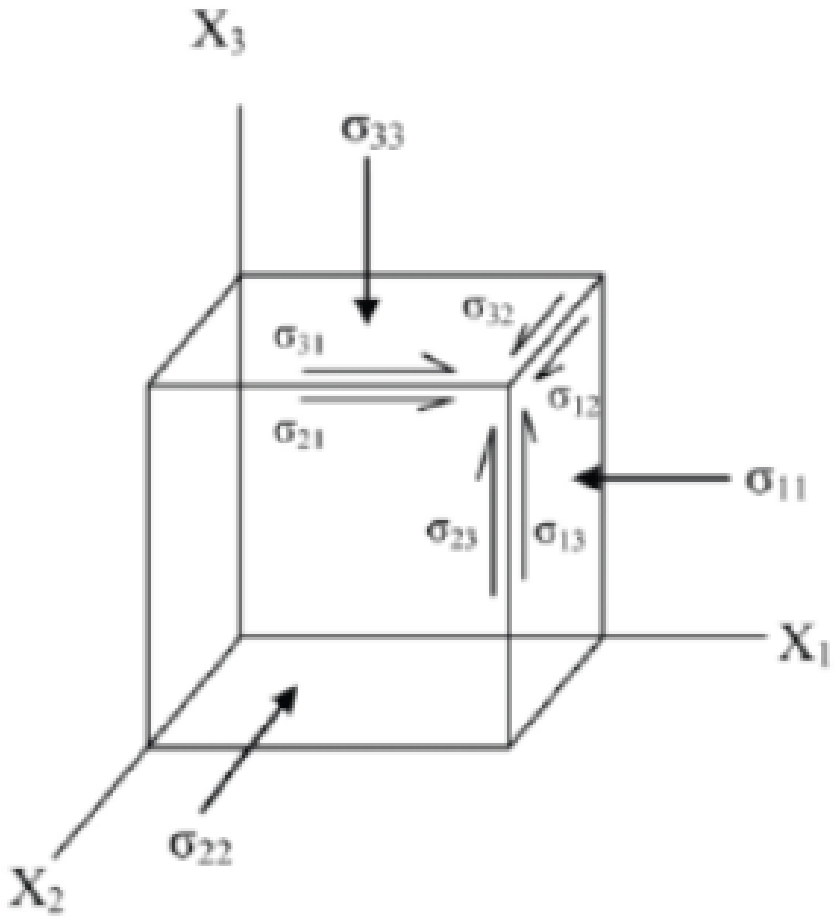


Figure 3.1: A cubic element in a continuum. The stresses of each face acting in a given direction leads to the equation of equilibrium stresses on $+X_1$, $+X_2$ and $+X_3$ faces.

From (Fig. 3.1), we can write the stress tensor as follow:

$$\left[\sigma_{ij}\right] = \begin{bmatrix} \sigma_{11} & \sigma_{12} & \sigma_{13} \\ \sigma_{21} & \sigma_{22} & \sigma_{23} \\ \sigma_{31} & \sigma_{32} & \sigma_{33} \end{bmatrix} \tag{3.3.1}$$

From (Fig. 3.1 and equation 3.3.1) we can define the two types of stresses as normal and shearing stresses due to the force acted normal to the surface and forces tangential to the surface respectively. Normal stresses are σ_{11}, σ_{22} and σ_{33}, while shear stresses are σ_{12}, σ_{13}, σ_{21}, σ_{23}, σ_{31} and σ_{32}.

3.4 Strain tensor

Strain is defined as a relative changes in the position of points within a body that has undergone deformation. For a three-dimensional coordinate system, the three normal strains describe length changes in the coordinate directions whereas the six shear strain components give angular changes of each coordinate direction with respect to the other two directions. The strain displacement relationship for a displacement vector $\mathbf{u}(\mathbf{x,\ t})$ is derived by Lay and Wallace, (1995). We can use the components of infinitesimal strain tensor in terms of displacements defined by Aki and Richards, (1980); Lay and Wallace, (1995) as follow:

$$\varepsilon_{ij} = \begin{bmatrix} \frac{\partial u_1}{\partial x_1} & \frac{1}{2}(\frac{\partial u_2}{\partial x_1} + \frac{\partial u_1}{\partial x_2}) & \frac{1}{2}(\frac{\partial u_1}{\partial x_3} + \frac{\partial u_3}{\partial x_1}) \\ \frac{1}{2}(\frac{\partial u_2}{\partial x_1} + \frac{\partial u_1}{\partial x_2}) & \frac{\partial u_2}{\partial x_2} & \frac{1}{2}(\frac{\partial u_2}{\partial x_3} + \frac{\partial u_3}{\partial x_2}) \\ \frac{1}{2}(\frac{\partial u_1}{\partial x_3} + \frac{\partial u_3}{\partial x_1}) & \frac{1}{2}(\frac{\partial u_2}{\partial x_3} + \frac{\partial u_3}{\partial x_2}) & \frac{\partial u_3}{\partial x_3} \end{bmatrix}, \tag{3.4.1}$$

where diagonals are normal strains and off-diagonals are shear strains.

Let us define $u_{i,j} = \frac{\partial u_i}{\partial x_j}$, then we can write the strain tensor in compact notation as:

$$\varepsilon_{ij} = \frac{1}{2}(u_{i,j} + u_{j,i}). \tag{3.4.2}$$

The constant of proportionality (elastic moduli) term in equation (3.2.1) has 81 terms for the general form by relating the nine elements of the strain tensor to the stress tensor. Applying the symmetric natures of the stress and strain tensors and further assuming homogenous, isotropic and linearly elastic medium, the number of elastic constants can be reduced to only two constants known as the *Lame constants* μ and λ. The two constants are related to C_{ijkl} as follow:

$$C_{ijkl} = \mu(\delta_{ik}\delta_{jl} + \delta_{il}\delta_{jk}) + \lambda\delta_{ijkl}, \tag{3.4.3}$$

where δ is the Kronecker delta function.

Now by using equation (3.4.3) into equation (3.2.1), we obtained,

$$\sigma_{ij} = \lambda\theta\delta_{ij} + 2\mu\varepsilon_{ij}. \tag{3.4.4}$$

Where $\theta = \frac{\partial u_1}{\partial x_1} + \frac{\partial u_2}{\partial x_2} + \frac{\partial u_3}{\partial x_3}$ and the Kronecker delta function is given as,

$$\delta_{ij} = \begin{cases} 1, & \text{if } i = j \\ 0, & \text{if } i \neq j. \end{cases} \quad i, j = 1, 2, 3 \tag{3.4.5}$$

3.5 Equation of motion

The elastic wave disturbance in medium can be resulted from a combination of contact and body forces with the generalized form of Hook′s law. By combining the contributions of body forces with Newton's law to a medium, the general form of equation of motion is given (Lay and Wallace, 1995) as:

$$(\frac{\partial \sigma_{ij}}{\partial x_j} + f_i)dv = m\frac{\partial^2 u_i}{\partial t^2},$$

$$(\frac{\partial \sigma_{ij}}{\partial x_j} + f_i)dv = \rho\frac{\partial^2 u_i}{\partial t^2}dv, \tag{3.5.1}$$

where ρ is density of the material and f_i is the body force per unit volume.

Dividing equation (3.5.1) through by dv gives the equation of motion for continuous media:

$$\frac{\partial \sigma_{ij}}{\partial x_j} + f_i = \rho\frac{\partial^2 u_i}{\partial t^2}. \tag{3.5.2}$$

Equation (3.5.2) is the equation of motion for a continuum that contains the right hand side inertial terms related to the density-weighted accelerations to body forces and stress gradients in the medium. Assume that the body force to be zero, then the above equation is reduced to:

$$\rho\frac{\partial^2 u_i}{\partial t^2} = \frac{\partial \sigma_{ij}}{\partial x_j}. \tag{3.5.3}$$

The homogeneous equation of motion, Hooke′s law and the strain-displacement relation are combined for an isotropic linear elastic medium with no body forces for the case i=1, 2 and 3 terms are:

$$\rho\frac{\partial^2 u_1}{\partial t^2} = \frac{\partial \sigma_{11}}{\partial x_1} + \frac{\partial \sigma_{12}}{\partial x_2} + \frac{\partial \sigma_{13}}{\partial x_3},$$

$$\rho\frac{\partial^2 u_2}{\partial t^2} = \frac{\partial \sigma_{21}}{\partial x_1} + \frac{\partial \sigma_{22}}{\partial x_2} + \frac{\partial \sigma_{23}}{\partial x_3},$$

and

$$\rho\frac{\partial^2 u_3}{\partial t^2} = \frac{\partial \sigma_{31}}{\partial x_1} + \frac{\partial \sigma_{32}}{\partial x_2} + \frac{\partial \sigma_{33}}{\partial x_3}.$$

Using equations (3.4.2 and 3.4.4), equation (3.5.3) can be written in the equivalent vector form of:

$$\rho\,\vec{\ddot{u}} = (\mu + \lambda)\vec{\nabla}(\vec{\nabla}.\vec{u}) + \mu\vec{\nabla}^2 u. \tag{3.5.4}$$

Where ∇ is the del operator and ∇^2 is the Laplacian operator. Using a vector calculus identity for the vector Laplacian,

$$\overrightarrow{\nabla}^2\overrightarrow{u} = \overrightarrow{\nabla}(\overrightarrow{\nabla}.\overrightarrow{u}) - \overrightarrow{\nabla} \times \overrightarrow{\nabla} \times \overrightarrow{u},$$

gives

$$\overrightarrow{\nabla}^2\overrightarrow{u} = (2\mu + \lambda)\overrightarrow{\nabla}(\overrightarrow{\nabla}.\overrightarrow{u}) - (\mu\overrightarrow{\nabla} \times \overrightarrow{\nabla} \times \overrightarrow{u}). \tag{3.5.5}$$

Equation (3.5.5) is a particle displacement for a general deformation through a homogeneous, isotropic, linearly elastic medium, based on the assumptions of infinitesimal strain of no body forces.

To make a sense of this complicated looking expression we make decomposition (using Helmholtz′ Theorem) where we write the displacement field as a sum of potential and the curl of a vector displacement potential (Aki and Richards, 1980; Lay and Wallace, 1995).

$$\overrightarrow{u} = \overrightarrow{\nabla}\varphi + \overrightarrow{\nabla} \times \overrightarrow{\psi}. \tag{3.5.6}$$

We separate the displacement into two parts and the second term of equation (3.5.6) will have zero divergences, as:

$$\overrightarrow{\nabla}.(\overrightarrow{\nabla} \times \overrightarrow{\psi}) = 0. \tag{3.5.7}$$

For any vector field $\overrightarrow{\psi}$, and the first part of equation (3.5.6) will have zero curl, as:

$$\overrightarrow{\nabla} \times (\overrightarrow{\nabla}\varphi) = 0, \tag{3.5.8}$$

for any scalar field φ. Substituting the Helmholtz′ potentials into the equation of motion, equation (3.5.5) gives:

$$\rho\frac{\partial^2(\overrightarrow{\nabla}\varphi+\overrightarrow{\nabla}\times\overrightarrow{\psi})}{\partial t^2} = (2\mu + \lambda)\overrightarrow{\nabla}(\overrightarrow{\nabla}.(\overrightarrow{\nabla}\varphi + \overrightarrow{\nabla} \times \overrightarrow{\psi})) - \mu\overrightarrow{\nabla} \times (\overrightarrow{\nabla} \times (\overrightarrow{\nabla}\varphi + \overrightarrow{\nabla} \times \overrightarrow{\psi})),$$

$$\rho\frac{\partial^2(\overrightarrow{\nabla}\varphi + \overrightarrow{\nabla} \times \overrightarrow{\psi})}{\partial t^2} = (2\mu + \lambda)\overrightarrow{\nabla}(\overrightarrow{\nabla}.(\overrightarrow{\nabla}\varphi) - \mu\overrightarrow{\nabla} \times (\overrightarrow{\nabla} \times \overrightarrow{\nabla} \times \overrightarrow{\psi})). \tag{3.5.9}$$

We can simplify equation (3.5.9) by noting that:

$$-\overrightarrow{\nabla} \times (\overrightarrow{\nabla} \times \overrightarrow{\nabla} \times \overrightarrow{\psi}) = \overrightarrow{\nabla}^2(\overrightarrow{\nabla} \times \overrightarrow{\psi}), \text{ and}$$
$$\overrightarrow{\nabla}.(\overrightarrow{\nabla}\varphi) = \overrightarrow{\nabla}^2\varphi,$$

So that,

$$\rho\frac{\partial^2(\overrightarrow{\nabla}\varphi + \overrightarrow{\nabla} \times \overrightarrow{\psi})}{\partial t^2} = (2\mu + \lambda)\overrightarrow{\nabla}(\overrightarrow{\nabla}^2\varphi) + \mu\overrightarrow{\nabla}^2(\overrightarrow{\nabla} \times \overrightarrow{\psi}). \tag{3.5.10}$$

Furthermore, equation (3.5.10) can be written as,

$$\overrightarrow{\nabla}\{(2\mu + \lambda)\overrightarrow{\nabla}^2\varphi - \rho\frac{\partial^2\varphi}{\partial t^2}\} + \overrightarrow{\nabla} \times \{\mu\overrightarrow{\nabla}^2\overrightarrow{\psi} - \rho\frac{\partial^2\overrightarrow{\psi}}{\partial t^2}\} = 0. \tag{3.5.11}$$

The equation of motion for an isotropic medium of equation (3.5.11) hold true (Lay and Wallace, 1995) when each term in the brackets goes to zero independently as;

$$\frac{\partial^2\varphi}{\partial t^2} = \alpha^2\overrightarrow{\nabla}^2\varphi. \tag{3.5.12}$$

And

$$\frac{\partial^2\overrightarrow{\psi}}{\partial t^2} = \beta^2\overrightarrow{\nabla}^2\overrightarrow{\psi}, \tag{3.5.13}$$

where

$$\alpha = \sqrt{\frac{\lambda + 2\mu}{\rho}}, \tag{3.5.14}$$

and

$$\beta = \sqrt{\frac{\mu}{\rho}}. \tag{3.5.15}$$

We can see that the P-and S-waves velocities are proportional to the square of the moduli and inversely proportional to the square of the density respectively. Equations (3.5.14 and 3.5.15) show the displacement field created by a stress imbalance accounted for propagating P- and S-waves. The two equations are equation of motions for P- and S-waves respectively.

3.6 Earthquake source mechanisms

Evidences that connect earthquakes with faulting come from a field of observation and from processing seismic waves. Most of natural earthquakes are caused by sudden slippage along a fault. When an earthquake is happening, the rock on one side of the fault suddenly slips with

respect to the other.

Faults can be divided into three types based on a direction of relative displacement. For any inclined fault plane we may define a block above the fault as a hanging wall block and the block below the fault as a footwall block. Normal faults are faults that resulted from horizontal extensional stresses in brittle rocks and where the hanging-wall block has moved down relative to the footwall block. Reverse faults are faults from horizontal compressional stresses in brittle rocks, where the hanging-wall block has moved up relative to the footwall block. Faults which move horizontally are called as strike-slip. The three types of faults are shown in Figure 3.2.

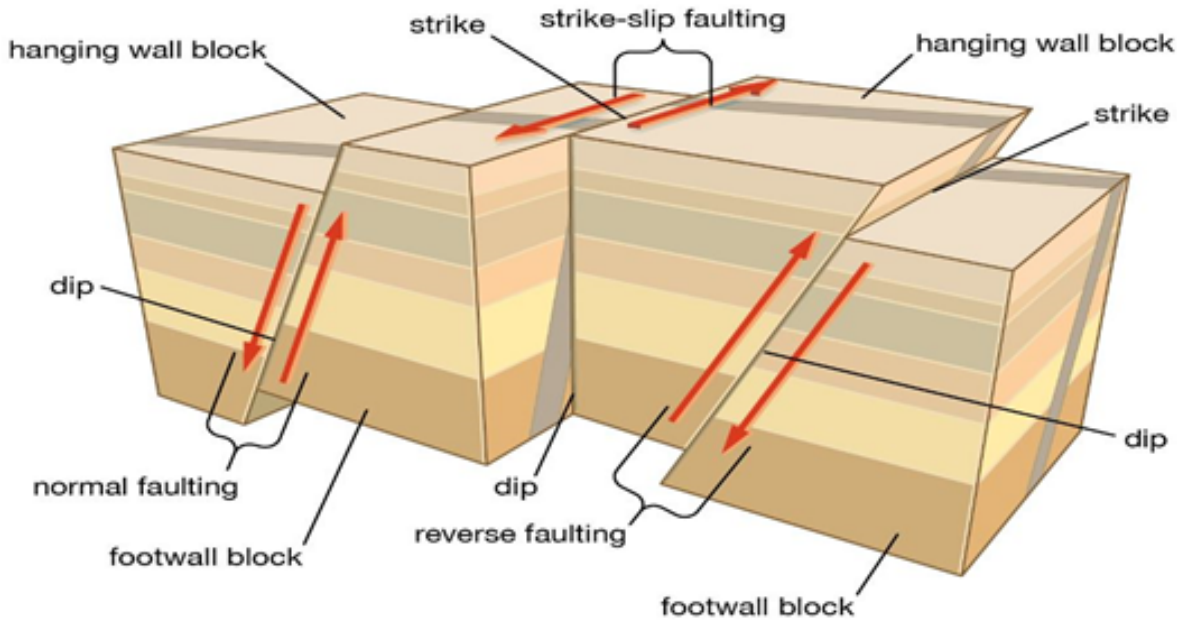


Figure 3.2: The three types of faults: Normal fault, strike-slip and reverse faults (Fossen, 2010).

Majority of earthquakes sources are either shallow or too deep to observe directly. Therefore, the source characteristics of earthquakes can be determined from the recorded seismic waves on receiver (e.g., Fig. 3.3). The type of deformation in the source region that generates the seismic waves can be identified from focal mechanism of earthquakes which is determined by processing the recorded earthquake waveform. It may often determine from first polarity reading of body waves. The polarities of the first P-waves arrival are up when the first motion is compression

(material near the fault moves towards the station) and down when it is dilatational (material motion is away from the station). P-waves first-reading often cannot constrain the focal mechanisms of earthquakes accurately. Currently, moment tensor inversion technique has become so widely accepted which have been treated almost as a fundamental law by many seismologists to obtain source mechanisms of earthquakes in which the solution is estimated from waveforms. Information about the source parameter can be determined by comparing observed with synthetic waveforms and adjusting until a suitable fit is obtained to get a reliable source parameters. This can be done using a forward and inverse approaches. This technique also gives additional information on earthquake which may not obtained from first-polarity reading.

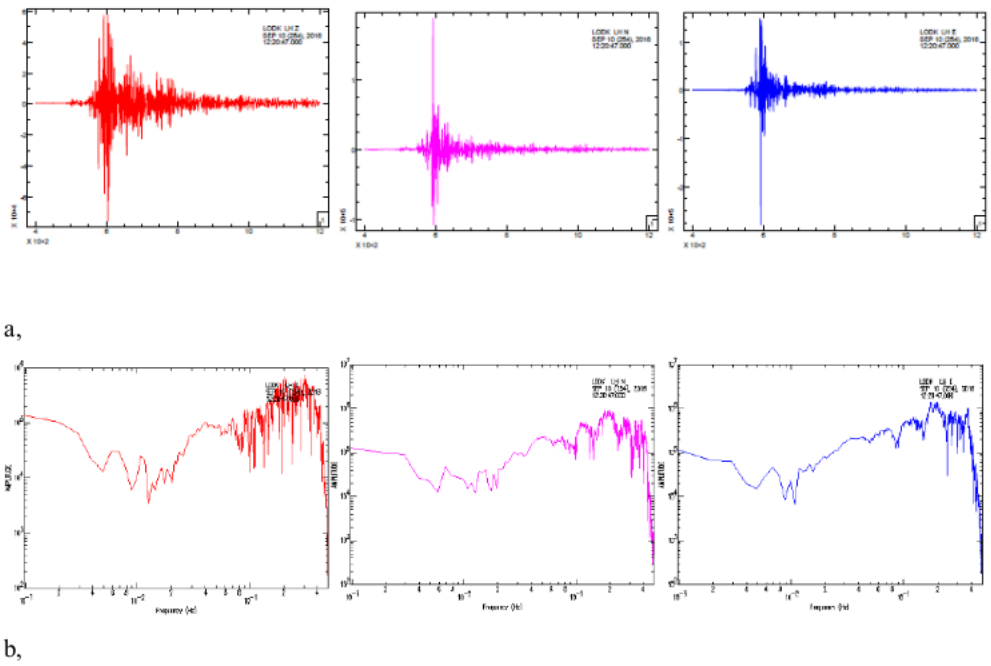


Figure 3.3: Examples of three-component seismograms for 2016/09/10 earthquake near Lake Victoria with magnitude Mw 5.7: a) time domain and b) frequency domain.

In the field of earthquake seismology, the source parameters of earthquakes can be obtained by generating synthetic seismograms and match to observed seismograms. A synthetic seismogram is the result of forward modeling of an input earth model, that defined in terms of 1D, 2D or 3D velocity model. Synthetic seismogram which is often generated in time and frequency domain

can used in investigation of Earth′s structure and in the determination of earthquake source parameters.

Moment tensor inversion is a basic tool for quantifying earthquake sources which is more robust and yields more stable results than traditional approaches of the polarity reading. It can be computed in time domain (Fig. 3.6; Dreger and Woods, 2002; Zahradnik et al., 2005, 2008; Sokos and Zahradnik, 2008; Adamova et al., 2009; Hingee et al., 2011) or in the frequency domain (Fig. 3.7; Cesca and Dahm, 2008; Vavryuk, 2011). The moment tensor can be computed as full inversion (Dziewonski et al., 1981; Sipkin, 1986; Kikuchi and Kanamori, 1991) or Deviatoric moment tensor inversion (Ichinose et al., 2014; Asefa and Ayele, 2020). The full moment tensor inversion considers the isotropic component whereas the deviatoric moment tensor assumes there is no volume change. The full moment tensor inversion is the widely used approach that applicable for large magnitude earthquakes. In this thesis we have applied the two types of the inversion techniques.

For brief explanation let us consider the seismogram $u(t)$ in time domain and its Fourier transform $U(\omega)$ as:

$$u(t) = \frac{1}{2\pi} \int_{-\infty}^{+\infty} U(\omega) e^{i\omega t} d\omega, \tag{3.6.1}$$

$$U(\omega) = \frac{1}{2\pi} \int_{-\infty}^{+\infty} u(t) e^{-i\omega t} dt. \tag{3.6.2}$$

Equations (3.6.1 and 3.6.2) help us to transform seismograms from the time domain into the frequency domain or from the frequency domain to time domain.

3.6.1 Convolution and Deconvolution modeling for linear system

If a signal $x(t)$ goes through two linear systems, with impulse responses $f(t)$ and $g(t)$, the net output is a convolution of the impulse responses in the time domain (Stein and Wysession, 2003),

$$y(t) = x(t) * f(t) * g(t). \tag{3.6.3}$$

In the frequency domain, the product of the transfer functions,

$$Y(\omega) = X(\omega)F(\omega)G(\omega). \tag{3.6.4}$$

Equations (3.6.3 and 3.6.4), can explained in Figure 3.4:

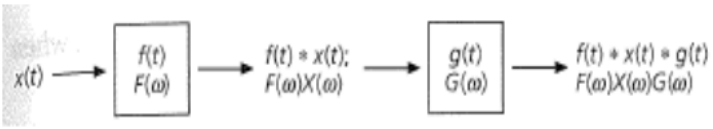


Figure 3.4: As a signal goes through two linear systems in succession, the net output is the convolution of the impulse responses or the product of the transfer functions.

A seismogram is assumed to be an output resulting from sending source signal through a set of linear systems, it can be written in terms of three basic effects (Equation 3.6.5), which are illustrated in Figure 3.5.

$$u(t) = x(t) * g(t) * i(t). \tag{3.6.5}$$

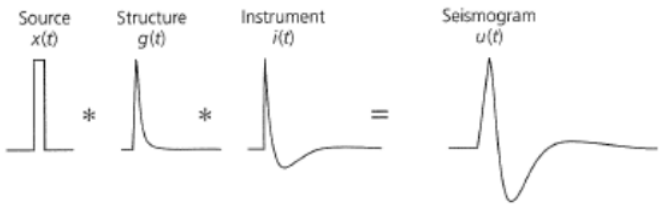


Figure 3.5: A seismogram can be modeled as the convolution of the source signal with operators representing the effects of the earth structure and the seismometer. A seismogram can be expressed as a convolution of source, structure and the instrument effect (Stein and Wysession, 2003).

3.6.2 Time-domain inversion using seismograms

Time domain seismic point source can be defined (Aki and Richards, 2002) as:

$$u_i(x,t) = M_{nk}(t) * G_{in,k}(x,k). \tag{3.6.6}$$

Where $u_i(x,t)$ is the displacement, $M_{nk}(t)$ is seismic moment tensor and $G_{in,k}(x,t)$ is the spatial derivatives of the Green′s function.

The seismograms and their spatial derivatives of the Green′s function defined as:

$$S_{in,k}(x,t) = S(t) * G_{in}(x,t), \tag{3.6.7}$$

is the time convolution of the Green′s functions and the source time function.

Displacement in equation (3.6.6) can be defined as:

$$u_i(x,t) = M_{nk} S_{in,k}(x,t). \tag{3.6.8}$$

The seismic moment tensor is inverted in the time domain using the generalized inversion:

$$m = S^{-g} d, \tag{3.6.9}$$

where m is no longer a function of frequency or time. It can be solved using the least squares method.

3.6.3 Frequency-domain inversion for moment-time functions

In the frequency domain, seismic point source is the transform of (3.6.6) and defined as:

$$u_i(x,\omega) = M_{nk}(\omega) G_{in,k}(x,\omega). \tag{3.6.10}$$

This can be expressed in matrix notation:

$$Gm = d \tag{3.6.11}$$

G is the matrix of the Green′s function derivatives, m is the vector containing the moment components and d is the vector of displacement observed at stations 1 to N.

The vector **m** of moment-time functions is computed from the generalized inversion (Menke, 1989).

$$m = G^{-g} d, \tag{3.6.12}$$

$$G^{-g} = [G^T G]^{-1} G^T. \tag{3.6.13}$$

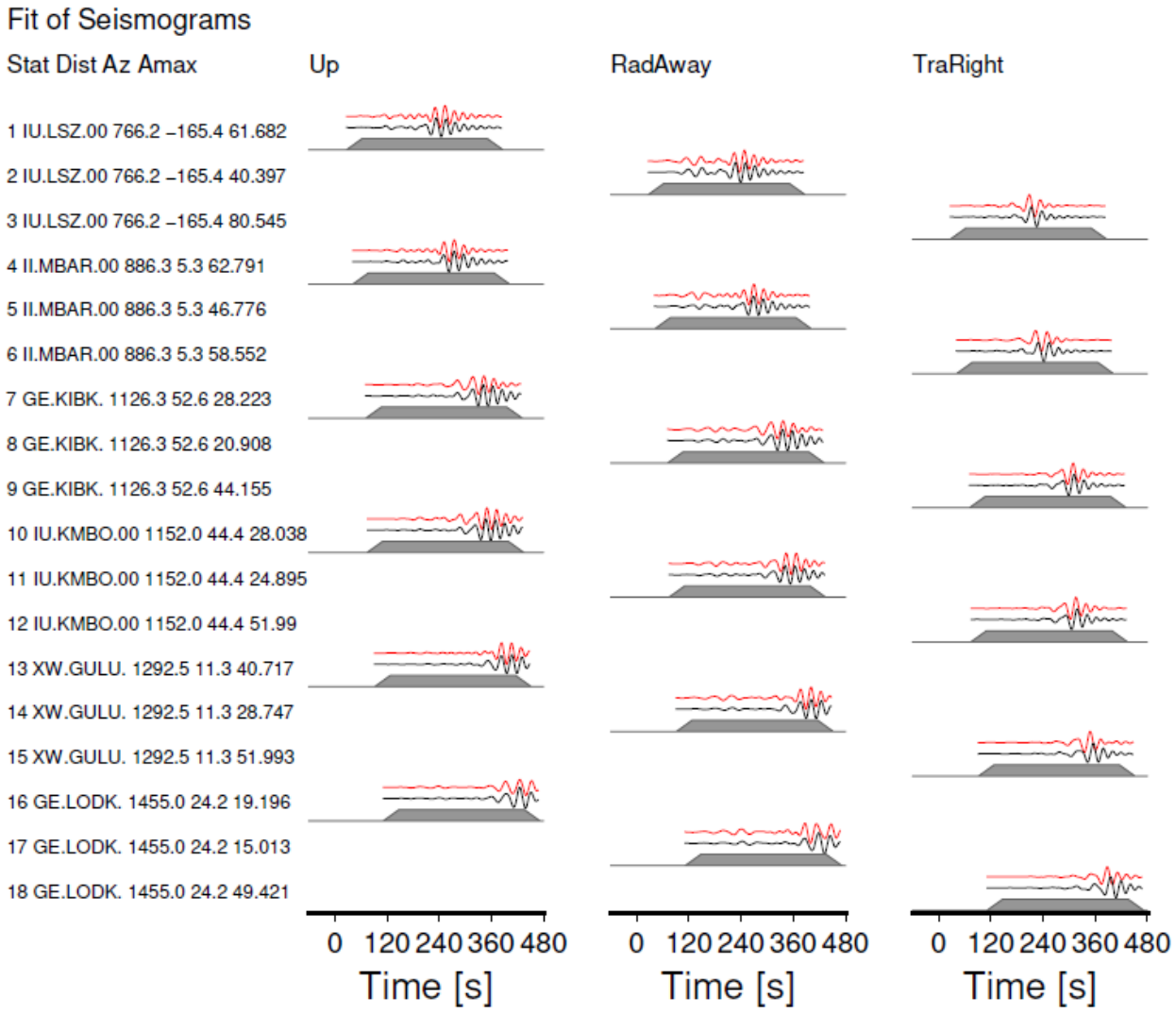


Figure 3.6: An example of generated seismograms of traces from three-component seismic station in time domain for the 2017/02/24 earthquake of Mw 5.9 occurred in Congo. The red color is for data, black is for synthetics.

With G^{-g} is the generalized inverse of G.

The moment-time functions $M_{nk}(\omega)$ can be obtained using equations (3.6.12) and (3.6.13). It can be transformed into time domain using the inverse Fourier transform and factorized as follows:

$$M_{nk}(t) = M_{nk}S(t). \tag{3.6.14}$$

Where M_{nk} is the seismic moment tensor, and $S(t)$ is the source-time function.

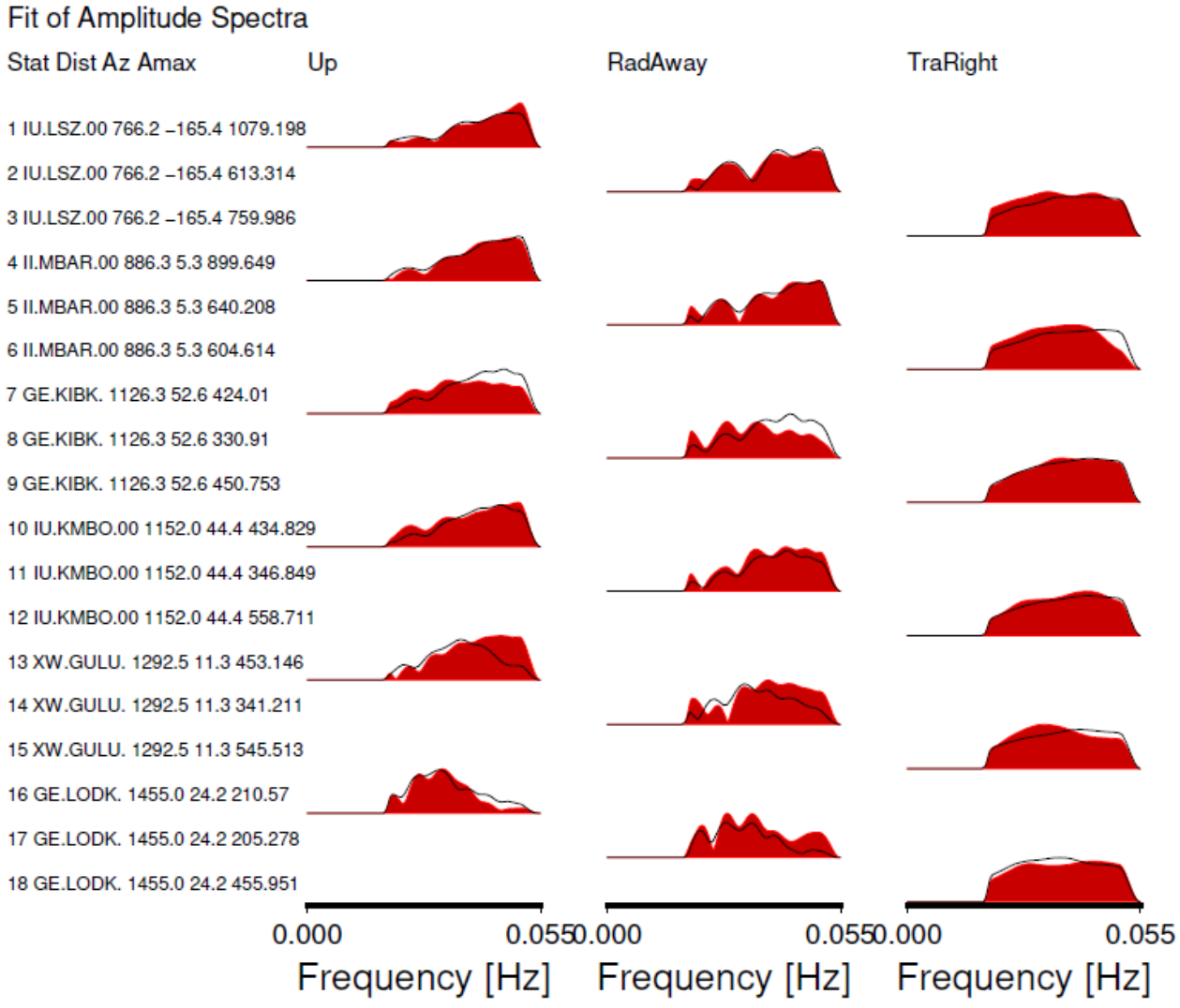


Figure 3.7: An example of generated moment-time functions in frequency domain for the 2017/02/24 event Mw 5.9 occurred in Congo. The red color is for data, black is for synthetics.

In moment tensor inversion, the input Green's functions are taken as known, and the algorithm determines that makes the output agree as possible, in a least squares sense, with the observed

seismograms. Recently an advanced in instrumentation, data management, and computing power have made the routine analysis of moderate to large earthquakes. Automated algorithms of estimating seismic source parameters from body waveform data using the moment tensor source representation have been developed, and are now in use, at both Harvard University and the U.S. Geological Survey (USGS) (Dziewonski et al., 1981; Sipkin, 1982). This method has a potential to substitute other, which is more traditionally used technique to estimates source parameters from P-wave first motion polarities.

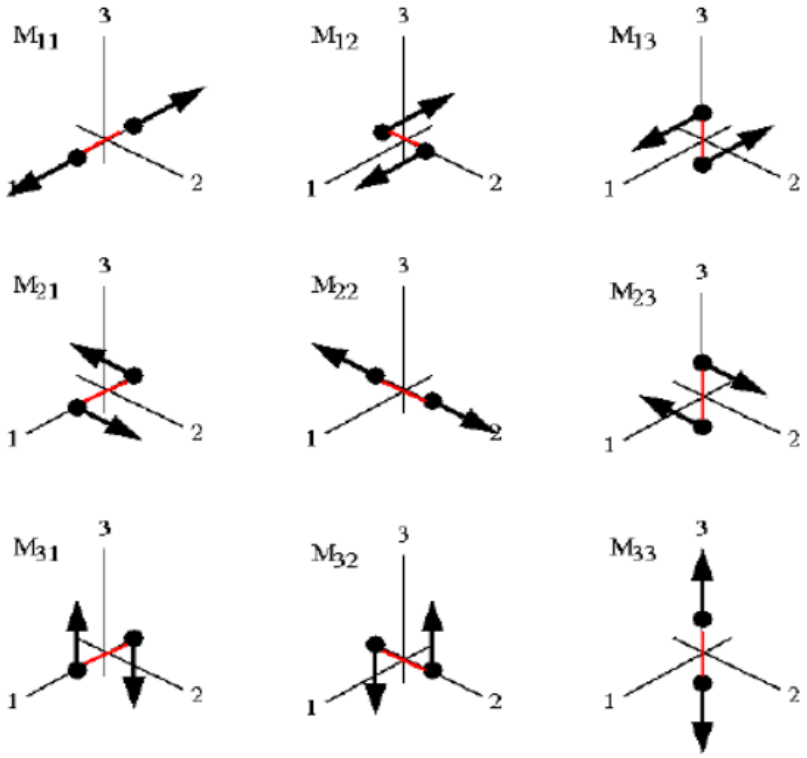


Figure 3.8: Nine couples of equivalent dipole forces forming the moment tensor. The system of force couples representing the components of Cartesian moment tensor.

The techniques can provide a general theoretical framework in describing seismic sources based on generalized force and it is very important tool in seismic source characterization. Moment tensor M is a symmetric tensor describing nine couples of equivalent dipole forces which can act at the earthquake sources. It defines the strength of a seismic source in terms of its seismic

moment, and the radiation pattern of seismic waves. The moment tensor (3×3 matrix) is symmetric and has six independent components. The diagonal elements represent linear vector dipoles and the off diagonal elements represent the force couples with arms as shown in Figure 3.8.

3.6.4 Moment tensor decomposition

For the sake of simplicity, seismic source is physically represented by moment tensor **M**. The moment tensor is usually diagonalized and decomposed into some elementary parts. It can be decomposed into isotropic ISO and deviatoric DEV parts (Vavryuk, 2015):

$$\mathbf{M} = \mathbf{M}_{ISO} + \mathbf{M}_{DEV}, \tag{3.6.15}$$

where,

$$\mathbf{M}_{ISO} = \frac{1}{3}\mathbf{Tr}(M).\mathbf{I}, \tag{3.6.16}$$

and I is identity matrix.

The second term of equation (3.8.1) can be further decomposed into a double couple (DC) and a compensated linear vector dipole (CLVD) components (Knopoff and Randall, 1970), which is further developed by Jost and Herrmann, (1989); Kuge and Lay, (1994), Vavryuk, (2015).

$$\mathbf{M} = M_1\mathbf{e}_1 \otimes \mathbf{e}_1 + M_2\mathbf{e}_2 \otimes \mathbf{e}_2 + M_1\mathbf{e}_3 \otimes \mathbf{e}_3, \tag{3.6.17}$$

where $M_1 \geq M_2 \geq M_3$ and vectors e_1, e_2 and e_3 define the T (tension), N (intermediate or neutral), and P (pressure) axes, respectively. The symbol $\otimes$ is the dyadic product of two vectors. The three terms of equation (3.8.3) can be written (Knoff and Randall, 1970; Jost ad Hermann, 1989) as follow:

$$\mathbf{M}=\mathbf{M}_{ISO} + \mathbf{M}_{DC} + \mathbf{M}_{CLVD},$$

$$\mathbf{M} = M_{ISO}\mathbf{E}_{ISO} + M_{DC}\mathbf{E}_{DC} + M_{CLVD}\mathbf{E}_{CLVD} \tag{3.6.18}$$

where $\mathbf{E}_{ISO}, \mathbf{E}_{DC}$ and $\mathbf{E}_{CLVD}$ are the ISO, DC and $CLVD$ base tensors and M_{ISO}, M_{DC} and M_{CLVD} are the ISO, DC and $CLVD$ moments. The base tensors read,

$$\mathbf{E}_{ISO} = \begin{bmatrix} 1 & 0 & 0 \\ 0 & 1 & 0 \\ 0 & 0 & 1 \end{bmatrix},$$

$$\mathbf{E}_{CD} = \begin{bmatrix} 1 & 0 & 0 \\ 0 & 0 & 0 \\ 0 & 0 & 0 \end{bmatrix},$$

$$\mathbf{E}^{-}_{CLVD} = \tfrac{1}{2} \begin{bmatrix} 2 & 0 & 0 \\ 0 & -1 & 0 \\ 0 & 0 & -1 \end{bmatrix},$$

$$\mathbf{E}^{-}_{ISO} = \tfrac{1}{2} \begin{bmatrix} 1 & 0 & 0 \\ 0 & 1 & 0 \\ 0 & 0 & -2 \end{bmatrix} \quad (3.6.19)$$

Equations (3.8.4 and 3.8.5) uniquely define values as follows:

$$\mathbf{M}_{ISO} = \frac{1}{3}(\mathbf{M}_1 + \mathbf{M}_2 + \mathbf{M}_3), \quad (3.6.20)$$

$$\mathbf{M}_{CLVD} = \frac{2}{3}(\mathbf{M}_1 + \mathbf{M}_3 - 2\mathbf{M}_2), \quad (3.6.21)$$

$$\mathbf{M}_{DC} = \frac{1}{2}(\mathbf{M}_1 - \mathbf{M}_3 - \mid \mathbf{M}_1 + \mathbf{M}_3 - 2\mathbf{M}_2 \mid), \quad (3.6.22)$$

where $\mathbf{M}_{CLVD}$ includes the sign of the elementary CLVD tensor. If CLVD tensor $\mathbf{E}_{CLVD}$ is considered with its sign as in equation (3.8.4), then CLVD can be calculated as the absolute value of equation (3.8.7).

The values of $\mathbf{M}_{ISO}, \mathbf{M}_{DC}$ and $\mathbf{M}_{CLVD}$ can be further normalized and expressed using scalar seismic moment M and relative scale factors C_{ISO}, C_{DC} , and C_{CLVD}:

$$\begin{bmatrix} \mathbf{C}_{ISO} \\ \mathbf{C}_{CLVD} \\ \mathbf{C}_{DC} \end{bmatrix} = \frac{1}{M} \begin{bmatrix} \mathbf{M}_{ISO} \\ \mathbf{M}_{CLVD} \\ \mathbf{M}_{DC} \end{bmatrix}, \quad (3.6.23)$$

where M reads;

$$M = \mid M_{ISO} \mid + \mid M_{CLVD} \mid + M_{DC}. \tag{3.6.24}$$

Equivalently (Bowers and Hudson, 1999):

$$M = \parallel \mathbf{M}_{ISO} \parallel + \parallel \mathbf{M}_{DEV} \parallel, \tag{3.6.25}$$

where $\parallel \mathbf{M}_{ISO} \parallel$ and $\parallel \mathbf{M}_{DEV} \parallel$. Scale factors C_{ISO}, C_{DC} and C_{CLVD} satisfy the following equation:

$$\mid C_{ISO} \mid + \mid C_{CLVD} \mid + C_{DC} = 1. \tag{3.6.26}$$

From equations 3.8.6 to 3.8.10, C_{DC} is always positive and in the range from 0 to 1; C_{CLVD} and C_{ISO} are in the range from -1 to 1. Consequently, the decomposition can be expressed as:

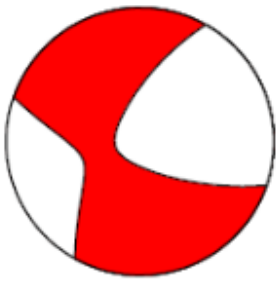
$$\mathbf{M} = M(C_{ISO}\mathbf{E}_{ISO} + C_{DC}\mathbf{E}_{DC} + \mid C_{CLVD} \mid \mathbf{E}_{CLVD}) \tag{3.6.27}$$

where M is the norm of $\mathbf{M}$. The absolute value of the $CLVD$ term in equation 3.8.13 is used because the sign of $CLVD$ is included in the elementary tensor $\mathbf{E}_{CLVD}$.

The decomposed values of $DC, CLVD$ and ISO components have their own physical meaning. Accordingly, the high value of double couple (DC) at the earthquake source indicates a source with shear faulting in isotropic media. A non-double-couple (non-DC) component often displays more general moment tensor (Julian et al., 1998) that can be used investigate a type of faulting (Vavrycuk et al., 2008; Vavrycuk, 2011c) and physical properties of material in the source area (Vavrycuk, 2004). A high percentage of ISO components indicate explosive or implosive source. An example of full moment tensor inversion with moment tensor components is shown in Figure 3.9.

Full MT =

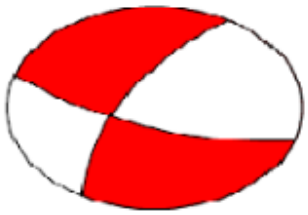
1.150304	−0.543176	−0.222206
−0.543176	−0.077697	−0.457997
−0.222206	−0.457997	0.105199



Decomposition:

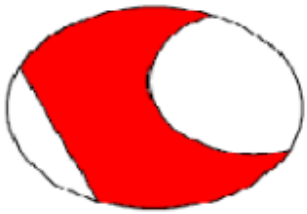
DC =

0.714558	−0.501507	−0.191353
−0.501507	−0.425020	−0.380274
−0.191353	−0.380274	−0.289538



CLVD =

0.043144	−0.041668	−0.030854
−0.041668	−0.045279	−0.077722
−0.030854	−0.077722	0.002135



ISO =

0.392602	0.000000	0.000000
0.000000	0.392602	0.000000
0.000000	0.000000	0.392602

Figure 3.9: Sample results obtained using full moment tensor inversion for 2016/09/10 earthquake around Lake Victoria of Mw 5.7. The moment tensor decomposition values for three components are (DC, CLVD and ISO) are also obtained.

3.7 Seismic phase picking

In this thesis, raw waveform data were collected from different sources with different formats. All waveform data are converted into similar and appropriate format (miniseed) that used for plotting using SEISAN (Earthquake Analysis Software) (Havskov and Ottemöller, 2015). Accordingly, the waveform were plotted and P and S- first arrival times were picked from vertical and horizontal components, respectively as shown in Figure 3.10. Various filtering frequency ranges were used during phase picking.

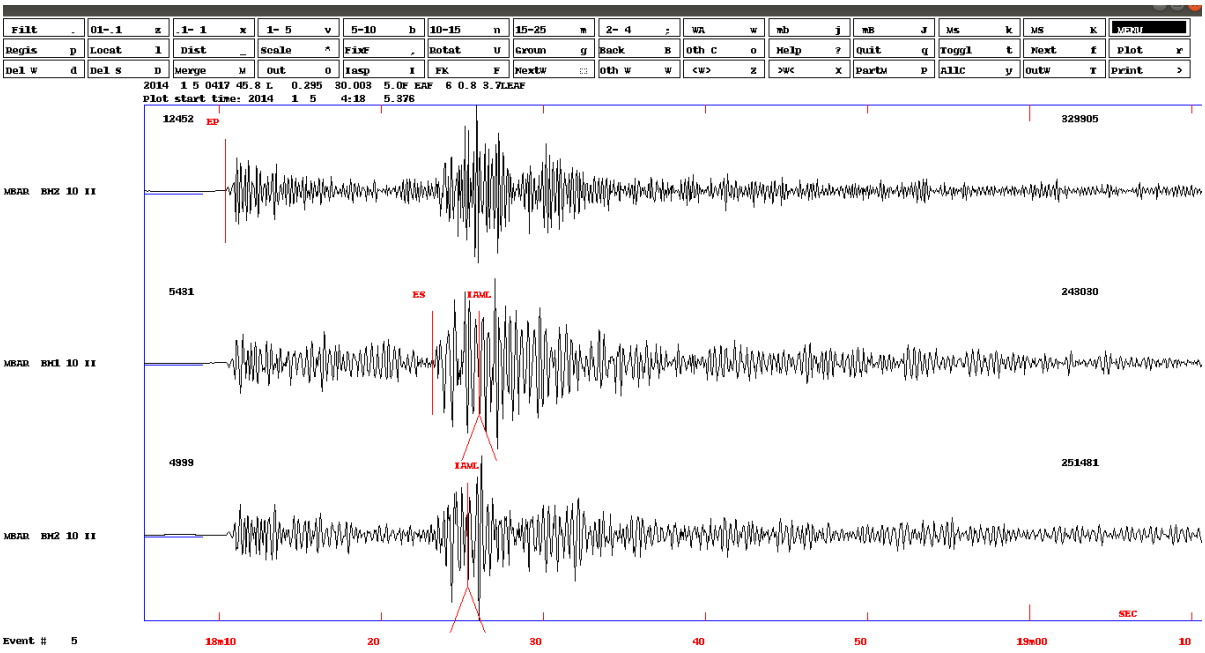


Figure 3.10: A sample of miniseed data recorded at MBAR seismic station. P- and S-phases picks are also shown on the plot. Plot is for earthquake of local magnitude 3.7 recorded on January 5, 2014 at 0.295°N and 30.003°E.

3.8 Earthquakes location technique: Geiger Method

An earthquake location specifies a spatial position and occurrence time of an earthquake. The location may refer to the point within the earth (the hypocenter) or the point on the surface of the Earth immediately above the hypocenter (epicenter) and corresponding origin time. At the beginning earthquake location was performed based up on examining surface faulting, damage, or felt reports. However, at present day earthquakes locations are performed using inverse

problem of various programs using waveform. In inverse problems one can estimate unknown parameters and their uncertainties computed from a combination of the available information on the model parameters and waveform data.

For the purpose of an earthquake location, measuring the arrival times of body waves are very useful. The arrival time of P-wave is better observed on vertical component of the seismogram while arrival time of S-wave is clearly observed on the either of the horizontal components of the seismograms. Earthquake epicenter location is a basic parameter in seismic research, seismic hazards, and in the earthquake engineering.

The Geiger′s method (Geiger, 1912) is one of the known earthquake location which is an iterative approach in solving origin times and earthquake hypocenters. This method initially estimates the event time and the three dimensionalposition coordinates and then updated iteratively based on the arrival time residuals. Geiger′s method starts with a guessed origin time t_0 and hypocentral value.

$$F(t_0, x_0, y_0, z_0) = \sum r_i^2. \tag{3.8.1}$$

If the arrival time measured at receivers is t_i, an estimate of the event hypocenter (x, y, z) and the earthquake time is made, the residual at the i^{th} is calculated based on the observed time at the station t_i, and the estimated event time t_0, and the theoretical travel time from the hypocenter to the receiver coordinates $T(x_0, y_0, z_0)$ is based on the velocity model.

$$r_i = t_i - t_0 - T_0(x_0, y_0, z_0). \tag{3.8.2}$$

t_0 is the event time, t_i is the observed time and T_0 is the calculated travel time.

Alternatively, we can express in terms of model and data vectors,

$$F(m) = d, \tag{3.8.3}$$

where F is an operator on the model vector, is to produce the data vector d. The arrival time can be considered as an element of the data vector while x, y, z and t which are the hypocentral location and origin time, represent the model vector. Thus, equation 3.10.3 can be expressed by

a nonlinear equation given as;

$$F(x, y, z) = d. \tag{3.8.4}$$

The Geiger method aims to minimize the sum of the squared time residuals by adjusting the trial location and timing. In order to solve this equation, first linearize and one can guesses a solution of m^0 with predicted values d^0 and investigates the behavior of d^0 in the neighborhood of m^0. A Taylor series approximation of changes in m^0 is given as;

$$m^1 j = m^0 j + \delta m^0 j. \tag{3.8.5}$$

Where $m^0 j$ is an adjustment of the j^{th} model parameter which improves the fit of the model to the data. After a Taylor series expansion, we can obtain the corresponding change in the predicted data as;

$$F_i^0(x_0, y_0, z_0, t_0) + (\frac{\partial F}{\partial x_0})\delta x_0 + (\frac{\partial F}{\partial y_0})\delta y_0 + (\frac{\partial F}{\partial z_0})\delta z_0 + (\frac{\partial F}{\partial t_0})\delta t_0 = d_i. \tag{3.8.6}$$

Equation (3.8.6) can be written as;

$$(\frac{\partial F}{\partial x_0})\delta x_0 + (\frac{\partial F}{\partial y_0})\delta y_0 + (\frac{\partial F}{\partial z_0})\delta z_0 + (\frac{\partial F}{\partial t_0})\delta t_0 = d_i - F_i^0(x_0, y_0, z_0, t_0). \tag{3.8.7}$$

Which is a system of equations with unknowns and coefficients given by $(\frac{\partial F_i}{\partial m_j})$, evaluated at m^0, which are constants. Equation (3.10.4) can be written as;

$$\delta d_i = \frac{\partial d_i}{\partial m_j}\delta m_j, \tag{3.8.8}$$

where $\frac{\partial d_i}{\partial m_j}$ can be defined as a partial derivative matrix.

This leads to an equation of the form;

$$\triangle d = G \triangle m. \tag{3.8.9}$$

Where changes in model parameters are mapped for improvement in data fit. To linearize the problem, assume that the source coordinates are perturbed by a small value $x_0+\delta x_0, y_0+\delta y_0, z_0+$

δz_0, and a first order Taylor expansion is applied to the travel times T giving an equation for the arrival time to the i^{th} receiver:

$$t_i = t_0 + \delta t_0 + +T(x_0, y_0, z_0) + (\frac{\partial T}{\partial x_0})\delta x_0 + (\frac{\partial T}{\partial y_0})\delta y_0 + (\frac{\partial T}{\partial z_0})\delta z_0. \tag{3.8.10}$$

The residual is determined by the change in event position and time by combining equations 3.10.2 and 3.10.10 we obtain:

$$r_i = \delta t_0 + (\frac{\partial T}{\partial x_0})\delta x_0 + (\frac{\partial T}{\partial y_0})\delta y_0 + (\frac{\partial T}{\partial z_0})\delta z_0. \tag{3.8.11}$$

A set of linear equations is made for all the receivers in the array. The solutions to the set of linear equations in event position and time give:

$$x_1 = x_0 + \delta x_0, y_1 = y_0 + \delta y_0, z_1 = z_0 + \delta z_0, T_1 = T_0 + \delta T_0. \tag{3.8.12}$$

The iteration process is repeated until a set of convergence criterion is met. A non-zero time residual will remain after successive iterations and the method assumes the estimated location close to the true location for the travel-time residuals as a linear function of the event location (Havskov, 2002). Consequently, the final location depends on the initially estimated location. Earthquake location may dependent on a velocity model of a particular region. In this study, the hypocentral locations of earthquakes were determined from phase reading of waveform data using 1-D velocity model of Keranen et al., (2004) which was developed for the part of the East African Rift System. For hypocenter location we applied general program that is based on HYPOCENTER (Lienert et al., 1986; Lienert and Havskov, 1995) using SEISAN earthquake analysis software (Ottemöller et al., 2015). The hypocentral parameters have been estimated from the least-squares solutions and we have searched for the smallest RMS. We have tried to estimate earthquake depth manually by locating a single event starting with a range of different depths, and then we have fixed the one with the lowest RMS. This may significantly improve the reliability of earthquakes depths estimation for the region.

3.9 Magnitude determination: Local and moment magnitude

An earthquake magnitude determination is a basic and essential task in seismology. Earthquake magnitude may use for estimation of energy release. There are several different magnitude scales in use.

The first magnitude scale was defined by Richter, (1935). All other magnitude scales are related to this scale. Local magnitude is an important parameter in earthquake hazard assessments in terms of quantifying the rate and amount of seismicity. The local magnitude estimation is given as:

$$M_L = log(A) - log(A_0) + C, \tag{3.9.1}$$

where A is zero-to-peak amplitude measured on a standard Wood-Anderson seismogram, $log(A_0)$ is a distance correction term and C is the correction term for individual station. Maximum absolute values of zero-to-peak amplitudes are measured from northsouth and eastwest horizontal components of the seismograms.

For the purpose of this study the local magnitude scale determined by Keir et al., (2006b) for the Main Ethiopian rift is used in this study which is given below:

$$log(A_0) = -1.196997 * log(\frac{r}{17}) - 0.001066 * (r - 17) - 2, \tag{3.9.2}$$

where r is the hypocentral distance in kilometers.

On the other hand, the moment magnitude is derived from seismic moment which is defined in terms of rigidity of fracturing material, area of the fractured segment and amount of slip. The seismic moment is defined as:

$$M_0 = \mu AD, \tag{3.9.3}$$

where μ is the modulus of rigidity of the faulted rock, A is the area of the rupture and D is the amount of slip on the rupture.

Seismic moment is related to the moment magnitude, Mw, Kanamori, (1977) and Hanks and Kanamori, (1979) by:

$$M_w = \frac{2}{3}(log_{10}M_0 - 9.1), \tag{3.9.4}$$

where M_0 is the moment measured in Nm. The moment magnitude scale is related to a physical property of the source and it has the advantage of not saturating and convenient for estimating the size of large earthquakes. It is unswerving measure of energy of an earthquake which should be able to be measured from seismographs.

M_0 can be estimated from seismograms using recordings in the time domain or frequency domain.

$$M_0 = \frac{4\pi\rho v^3 r\Omega_0}{R}, \tag{3.9.5}$$

where Ω_0 is the low frequency level of the amplitude spectrum and is equal to the area under the displacement pulse, ρ is the rock density, R is the P- or S- wave radiation pattern correction terms v is the P- or S-wave velocity and r is the source receiver distance. This can be measured directly from the amplitude spectra assuming low frequencies are correctly recorded

CHAPTER 4

Seismicity of the East African Rift System for the period 2013 to 2016

4.1 Introduction

The East African Rift System (EARS) is one of the most active and largest continental rift structures in the world (Ebinger, 1989; Chorowicz, 2005). The activity is demonstrated in terms of faulting and volcanism where significant and damaging earthquakes have been recorded and reported from time to time (Ayele et al., 2007; Yang and Chen, 2010; Craig et al., 2011; Lindenfeld et al., 2012; Ayele et al., 2015; Weinstein et al., 2017; Wilks et al., 2017; Greenfield et al., 2019). Previous studies showed that the EARS exhibits significantly high seismic activity (Kebede and Kulhánek, 1991) and suggested the correlation of earthquakes occurrence with the geologic features (ages) (e.g., Sykes and Landisman, 1964; Maasha, 1975; Fairhead and Stuart, 1982). The whole length of the EARS is composed of several active rift zones and segments initiated at different times during the Cenozoic which exhibit varying intensity of magmatism (George et al., 1998) and seismic activity (Yang and Chen, 2010; Craig et al., 2011) that provide unique opportunities to investigate how continental rifts deform at different length and time scales. Processes of continental rifting are also relevant to current debates regarding the exhumation of sub-continental lithospheric mantle along magma−poor margins, ultraslow spreading ridges, and rheology of the continental lithosphere in general (e.g., Chen and Yang, 2004; Dick et al., 2003).

The EARS comprises several rift segments, some are at advanced developmental stage whereas the Afar Depression demonstrates a prototype oceanic rift setting. Southwards of the MER,

the EARS splits into the western and eastern branches (Fig. 4.1). The western branch is seismically very active and the active faults are providing good spatial coverage for the study of active tectonics (e.g., Foster and Jackson, 1998; Nyblade and Langston, 1995; Shudofsky, 1985). The eastern branch is magmatically active along its length (Albaric et al., 2010). The EARS has a complex structural pattern consisting of several rift segments with time-space tectonic evolutions that are apparently different from each other. The structural connection of the Main Ethiopian Rift (MER) to either of the two branches of the EARS and southwards of the complex tectonic region of the Northern Tanzania Divergence Zone (NTDZ), the direction of propagation of the eastern branch are the most outstanding science questions in the area/region. For example, some studies proposed the linkage of the MER with the western branch of the EARS based on the seismicity distribution (Fairhead and Stuart, 1982; Kebede and Kulhánek, 1991). On the other hand, earthquakes distribution near Lake Turkana (Ayele and Kulhánek, 1997), characteristic of volcanoes and rift formation (Maasha and Molnar, 1972) and deformational age within this region (Ghebreab, 1998; Bellahsen et al., 2003; Bonini et al., 2005) suggested the link of the MER with eastern branch of EARS. Furthermore, southwards of the NTDZ, several suggestions have been given on the direction of the eastern branch using multi study techniques. Based on surface tomography (O′Donnell et al., 2013) and earthquakes distribution (Mulibo and Nyblade, (2016) suggested that the eastern branch propagates southeasterly along the northern boundary of the Ruvuma microplate towards the coast. In contrast Le Gall et al., (2004) proposed the linkage of eastern branch with western branch at the end of Lake Nyasa rift basin using morphostructural interpretation. However, the seismicity data suffers from short observation of instrumental catalogue and sparse station distribution. International agencies like ISC (International Seismological Centre) and NEIC (National Earthquake Information Centre) catalogues are mainly dominated by teleseismic and regional distance earthquakes which made the claimed rift connection poorly known and as a result farther evidence and investigation is required.

Poor distribution of seismic stations along the EARS hinders the detection of intermediate and

small magnitude earthquakes that occur in the region. Moreover, malfunctioning of the already few stations in most countries in the region is quite common and maintenance is difficult for various reasons. In this study, detailed seismicity investigation is made for the 2013 to 2016 period using quality data acquired from permanent and temporary seismic networks.

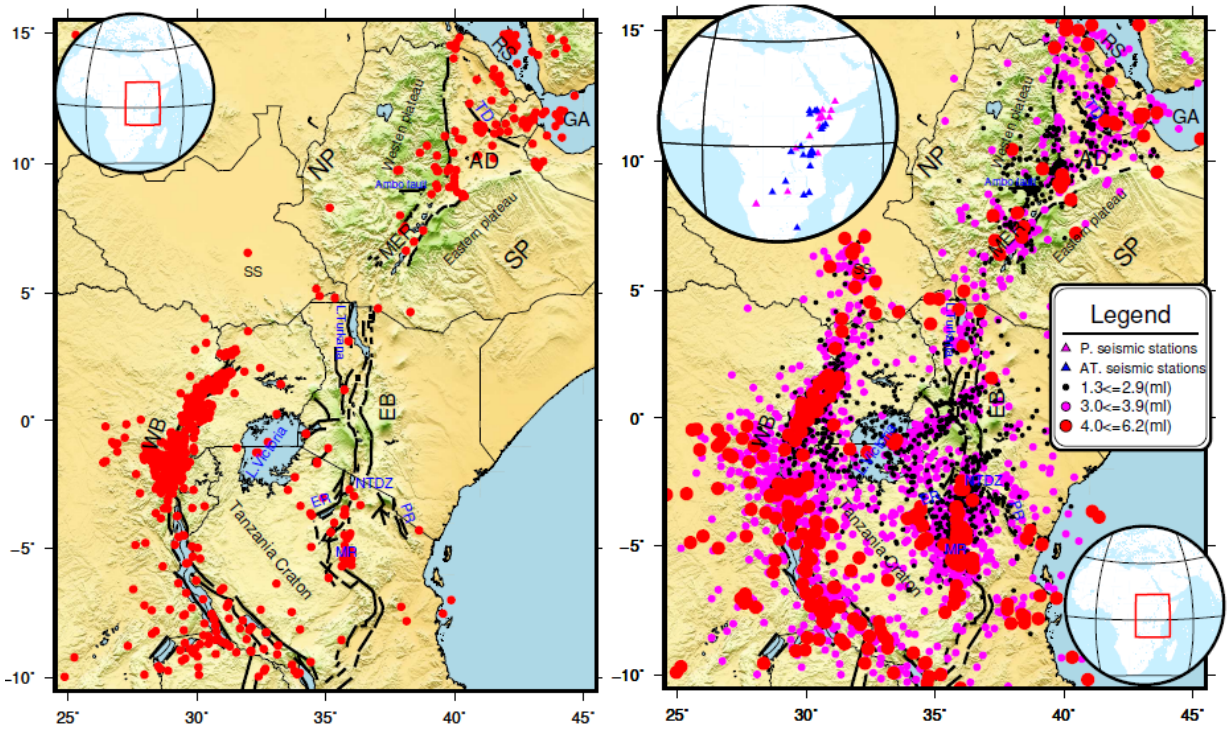


Figure 4.1: Seismicity of the EARS for the period 2013 to 2016: (a) The spatial distribution of earthquakes compiled from the International Seismological Center (ISC) catalog with magnitudes in the range of 0.5 to 6.5, with red circles earthquake epicenters: (b) The spatial distribution of earthquakes in this study with magnitudes in the range of 1.3 to 6.2. Triangles on the inset map are seismic stations used (P. seismic stations, Permanent seismic stations and AT. seismic stations, AfricaArray and Temporary seismic stations). The current study has revealed significant difference as compared to earthquakes captured in International catalog. NP Nubain Plate, SP Somalian Plate, AD Afar Depression, RS Red Sea, GA Gulf of Aden, MER main Ethiopian rift, TD Tendaho Discontinuity, SS Southern Sudan, WB western branch, NTDZ Northern Tanzania Divergence Zone, EY Eyasi rift, MR Manyara rift and PR Pangani rift.

4.2 Data and Methods

4.2.1 Data

In this study, we acquired waveform and phase data for the 2013-2016 time period from various permanent and temporary networks namely: Ethiopian Seismic Station Networks (ESSN), Eastern and Southern Africa Regional seismological working Group (ESARSWG) database, IRIS-PASSCAL broadband three-component temporary seismic stations deployed during the period 2014 to 2016 in the western and eastern Ethiopian plateau and AfricaArray (AF) seismic stations. In addition to this list, we have used data recorded by stations included in the Global Digital Seismograph Network (GDSN) operating in Africa and all of them are displayed in Figure 4.1.

4.2.2 Methods

The data processing was performed using the SEISAN software package (Havskov and Ottemöller, 2015) including an implementation of HYPOCENTER location algorithm by Lienert and Havskov, (1995). We used 1-D velocity model of Keranen et al., (2004) for earthquake location. During event location, the data were filtered using Butterworth band pass filter to enhance the clarity of arrivals. P-wave onsets are initially identified on the vertical components of the seismograms, with all three components subsequently used to refine the picks and S-wave arrival times were picked from horizontal components. All earthquakes were located from arrival times that were manually picked from a minimum of three seismic stations. Local magnitude was estimated using the formula developed by Keir et al., (2006), $M_L = log(A_{WA}) + 1.96997log(\frac{r}{17}) + 0.001066(r - 17) + 2$, where A_{WA} is a maximum horizontal ground amplitudes zero to peak and r is the hypocentral distance. The instrument responses from the horizontal components of seismograms are removed and convolved to that of a Wood-Anderson instrument. The local magnitudes were calculated from the maximum horizontal trace amplitudes from north-south and east-west.

b-value

The historical earthquake records can be analyzed using different statistical methods. The most common one is the frequency-magnitude distribution (FMD) well expressed by the Gutenberg-Richter relation (Gutenberg and Richter, 1954) written as:

$$logN = a - bm. \tag{4.2.1}$$

Where N is the cumulative number of earthquakes with a magnitude greater than or equal to M and a and b are constants; a indicates the activity level of seismicity and exhibits significant variations from region to region. The b-value relates to tectonic stress (Mogi, 1967; Scholz, 1968) and describes the relative abundance of large to small magnitude events. High b-value indicates a larger proportion of small events, and vice versa or a low b-value is considered to be an indicator of a high stress level in a seismogenic zone of interest.

There are different ways to estimate b-value. The first one is the estimation of the b-value by a least squares method which is believed to be statistically unjustified or biased (Weichert, 1980; Bender, 1983; Sandri and Marzocchi, 2007). A b-value calculated from a linear least squares regression has the major drawback of being strongly influenced by the distribution of a few large earthquakes in the FMD. The second method used to estimate b-value is the maximum likelihood method. This method is the most commonly used in b-value estimation with Bootstrapping which has shown to be a robust and unbiased estimation in most of the cases (Wiemer and Wyss, 1997). Thus, we estimated the b-value using a maximum-likelihood method of Aki, (1965) given in equation (4.2.2). The b-value is calculated through the formula:

$$b = \frac{log_{10}(e)}{m' - (m_c - \frac{m_{bin}}{2})} \tag{4.2.2}$$

where, $log_{10}(e) = 0.434$, $m^{'}$ is the mean magnitude of all events. The magnitude of completeness (m_c), which is defined as the minimum earthquake magnitude at which the earthquake catalog is assumed to contain all events and m_{bin} represents the magnitude interval. A value of $m_{bin} = 0.1$ is used in this study. To address the uncertainty of the calculated b-value Shi and Bolt, (1982)

suggested the standard error formula for the magnitude-frequency of b-value as in equation 4.2.3.

$$\sigma(b) = 2.3b^2\sqrt{\frac{\sum_i (m_i - m^{'})^2}{n(n-1)}} \tag{4.2.3}$$

Where "n" is the sample size. We have also calculated the second parameter $'a-value'$ through; $a = log_{10}(n) + b * m_c$ relation.

Seismic energy mapping

Earthquakes result from a sudden release of stored energy mostly in the Earth's crust that creates seismic waves. The amount of seismic energy released by an earthquake is one measure of the potential damage for seismically active areas. A good means of gaining some insight into the change of seismicity in space is energy mapping of an area which may be calculated from earthquakes magnitude (Gutenberg and Richter, 1942; Bath, 1966; Mayeda and Walter, 1996). In this study, we used a generalized formula derived by Ayele and Kulhánek, (1997) for the Horn of Africa that shows a linear relationship of body magnitude with seismic energy (Equation 4.2.4).

$$logE = 4.92 + 1.55m_b, \tag{4.2.4}$$

where seismic energy is measured in joules.

The equation (4.2.4) has been deduced by a formal approach on the basis of all known dependences between earthquake body magnitude and local magnitude relationship used in Bath, (1979). The total energy released within a $1^\circ \times 1^\circ$ window is mapped at the center of block for the time period 2013 to 2016 by using the moving-block method of Bath, (1982), where the block is shifted by 0.5° either in latitude or in longitude at a time.

4.3 Results and Discussion

4.3.1 Spatial and temporal distributions of earthquakes

We located as many earthquakes as we could in the EARS in the time window from 2013 to 2016. The events analyzed in this study are shown in Figures 4.1b and 4.2 whereas the earthquakes compiled from ISC for the same period in the EARS are shown in Figure 4.1a. Only

earthquakes recorded by at least three seismic stations with magnitudes in the range of 1.3 to 6.2 were analysed. The spatial distribution of four years record (Figure 4.1b) shows a typical seismicity pattern of the EARS with some pronounced activity in some places which demonstrates that EARS is seismically active. The spatial pattern is mostly confined to the rift zones which is in agreement with previous studies (Shudofsky, 1985; Iranga, 1992; Nyblade and Langston, 1995). A relatively better detail of seismic activity is captured in this study as compared with the one recorded by ISC due to improved station distribution in the region.

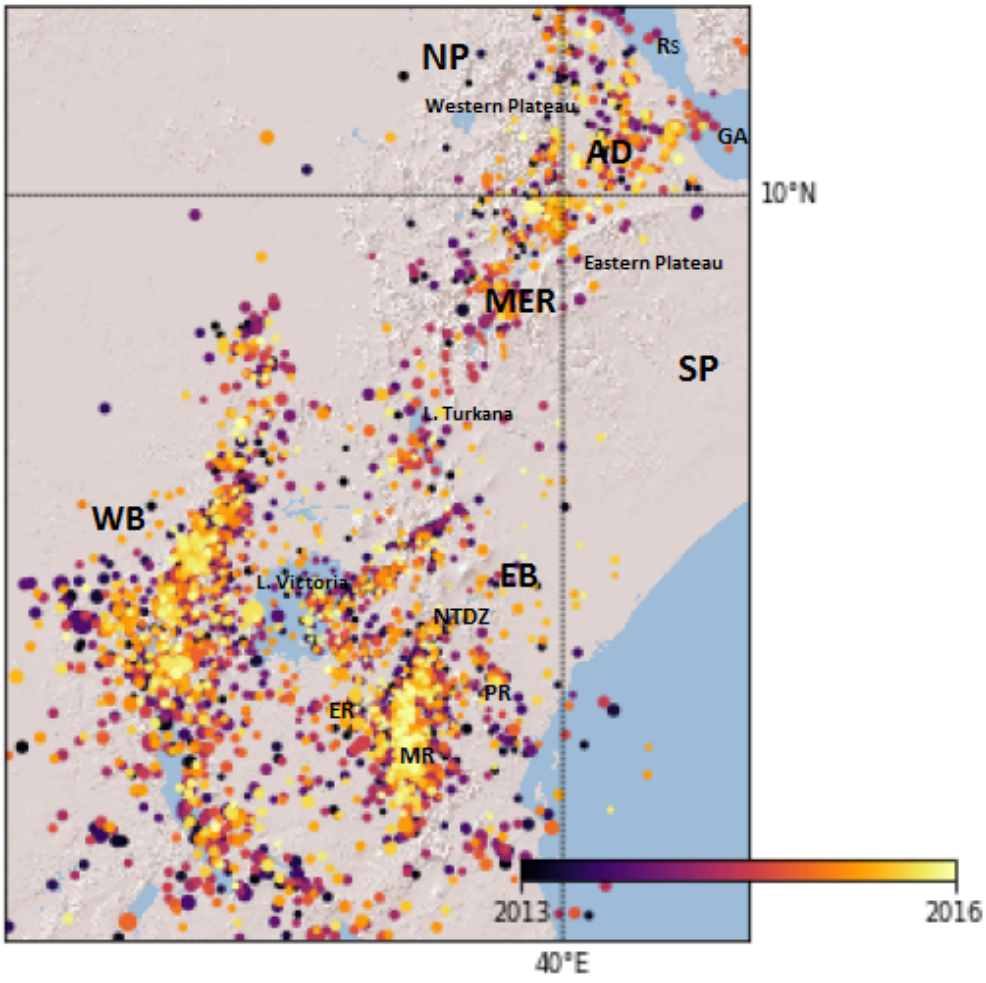


Figure 4.2: Spatio-temporal distribution of earthquakes recorded in the EARS for the period 2013 to 2016. Only events recorded by at least three seismic stations have been considered. The circles with color show the distribution of earthquakes (temporal/year) in the region as shown on legend. NP Nubian Plate, SP Somalian Plate, AD Afar Depression, SS Southern Sudan, WB western branch and EW eastern branch of the East African Rift System.

Afar depression and MER

From the seismicity map shown in Figure 4.1b, it is evident that the rift axis, margins and the western plateau are more seismically active than the eastern plateau which is in agreement with previous studies (Kebede and Kulhánek, 1991; Kebede and Kulhánek, 1994; Ayele and Kulhánek, 1997; Keir et al., 2006; Ayele et al., 2007; Keir et al., 2009). We believe that the transition zone between the attenuated crust of the Ethiopian western rift margin, Afar depression and the thick crust of the Ethiopian plateau region (Makris and Ginzburg, 1987; Beyth, 1991; Makris et al., 1991; Tiberi et al., 2005) and strong density contrast at the rift margin (Tesfaye et al., 2003; Wolfenden et al., 2005; Buck, 2017) might be responsible for the cause of seismic activity mostly at rift margins. The absence of many seismic stations around the region has so far hindered the adequate record of the seismic activity in the main Ethiopian rift. However, analysis of earthquakes from a number of installed permanent seismic stations by IGSSA of Addis Ababa University (Ethiopia) and temporary stations used in this study revealed that the region is relatively seismically active than the previous studies. The continuity of earthquakes distribution in the southwards of the MER to the Lake Turkana clearly showed the structural connection between the main Ethiopian rift and eastern branch the EARS which is in agreement with surface morphology but the extension of the MER towards the western branch is not clearly observed.

Eastern and western branches

From the seismicity map shown in Figure 4.1b, it is evident that the whole length of the rift axis, the eastern and western margins of the rift zones of the western branch of the East African Rift System are seismically very active as compared to the other rift segments of the EARS which is in agreement with previous studies (Nyblade and Langston, 1995; Foster and Jackson, 1998; Albaric et al., 2009). The space-time distribution of seismicity patterns revealed the structural connection between the southern-Sudan and western branch of the EARS.

From the tectonic point of view the eastern branch of the EARS divided into different tectonic settings such as the northern (Kenya rift) and southern parts (Fairhead and Stuart, 1982). The

northern part of the eastern rift shows the absence of earthquakes (e.g., Kebede and Kulhánek, 1991) or the presences of few earthquakes (Ayele and Kulhánek, 1997). As a result, it was believed that the rift is classified as aseismic region (e.g. Bath, 975; Shah, 1986). However, the seismicity maps shown in Figures 4.1b and 4.2 revealed that the northern part of the eastern branch is relatively seismically active.

In the central parts of the eastern branch near 3°S, earthquakes distributions spread over the different rift segments of the Northern Tanzania Divergence Zone which are seismically very active. In this region, earthquakes are concentrated into the well-known three rift segments namely Eyasi rift, Manyara rift and Pangani rift segments. From the observation the Eyasi and Manyara rift segments are more active as compared to the Pangani rift. The seismicity distributions in the Manyara rift follow the N-S trend whereas the seismicity patterns in the Eyasi rift show the ENE-WSW trends which are consistent with the structural trends within the region. It has been also observed that the NW-SE trend of the Pangani rift segment and margins of the Tanzania craton and the craton by itself are relatively seismically active.

From the seismicity patterns we suggest that the eastern branch of the EARS is probably connected to the Davies Ridge offshore along the northern boundary of the Ruvuma microplate. Alternatively, significant amounts of seismicity distribution along Pangani rift segment may suggest the possibility of a zone of extension is developing in northeast Tanzania along Pangani for the eastern branch propagation which is in agreement with the conclusion made by Mougenot et al., (1986). However, the possibility of a structural connection between western and eastern branch towards Malawi proposed by Le Gall et al., (2004) cannot be ruled out, as some earthquake distributions have been observed along transverse fault zone along the margin of the Tanzania Craton.

Generally, the seismicity distributions within the different rift segments of the EARS agree well with distribution of the major tectonic features of the region and the western and eastern branches of the EARS are seismically very active than the other rift segments of the Afar depression and MER.

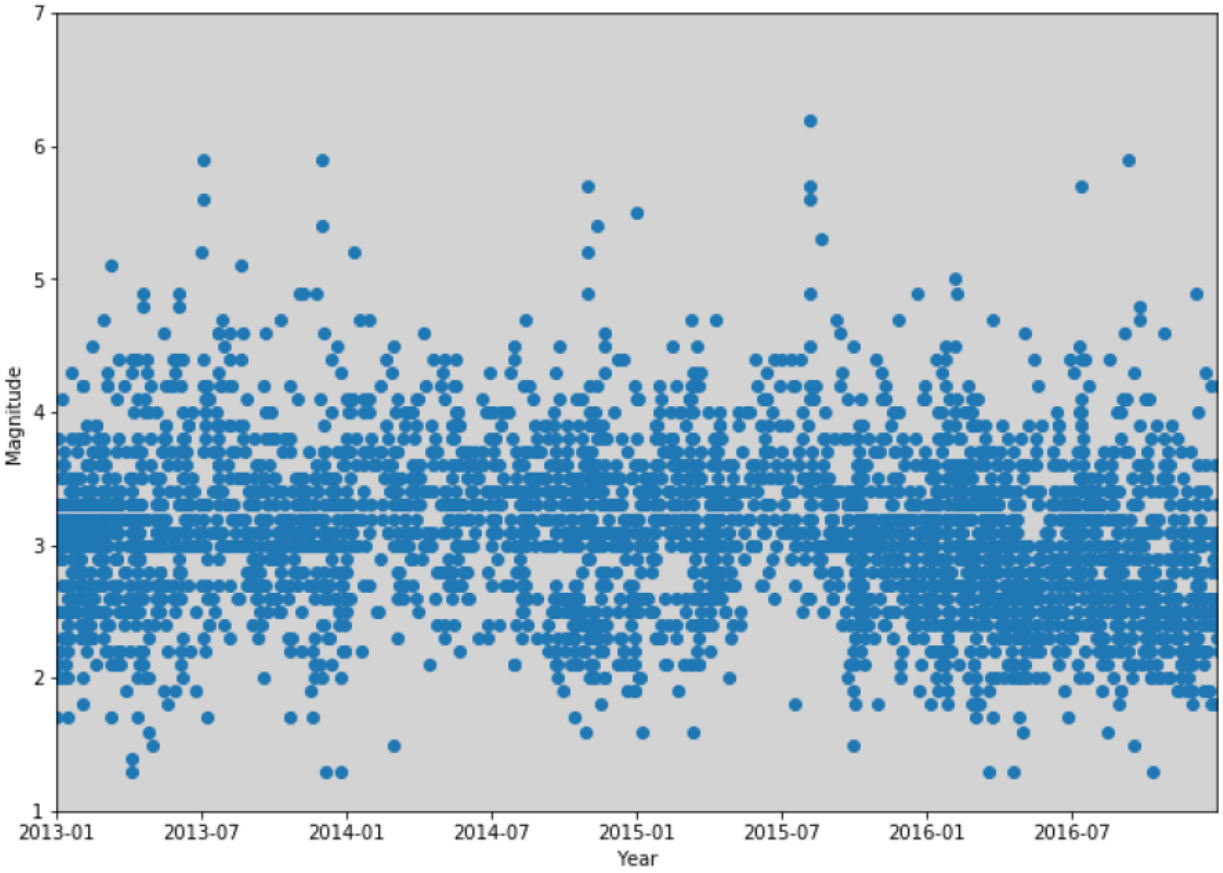


Figure 4.3: Distribution of earthquakes magnitude as a function of time (2013 to 2016) for the entire catalog for earthquakes distribution is shown in Figs. 4.1b and 4.2. The minimum earthquake local magnitude 1.3 and maximum earthquake local magnitude 6.2 have been observed.

4.3.2 Magnitude distributions

During the observation period a number of earthquakes are not uniformly distributed as demonstrated in Fig. 4.6. The number of reported earthquakes is slightly decreasing from year 2013 to 2014 but visibly increasing afterwards. During the study period, the region is highly characterized with earthquakes magnitude less than Ml 4.0 and moderately dominated with magnitudes in between Ml 4.0 to 5.0, while earthquakes with larger magnitude greater than Ml 5.0 are rarely observed (Fig. 4.3). Results of earthquakes magnitudes distribution that make up of the whole database for the period 2013 to 2016 are plotted within the range of local magnitude 1.3 to 6.2 (Fig. 4.3). The distributions of the intermediate magnitudes earthquakes for the whole

years seem similar but variable for earthquakes with smaller magnitudes. Low magnitude events Ml<3.0 are vastly reported in 2016, 2013 and 2015 but with few occurrences in 2014.

4.3.3 Hypocentral depths distribution

Majority of the hypocentral depths of the earthquakes within the EARS are found from the upper crust (0-20 km) (e.g., Figs. 4.4 and 4.5) well in agreement with earlier observations (e.g. Nyblade and Langston, 1995; Camelbeek and Iranga, 1996; Foster and Jackson, 1998; Brazier et al., 2005; Albaric et al., 2009). On the other hand, hypocentral depths of earthquakes within the lower crust (20-30 km) have been observed that is consistent with the results evidenced in the previous studies (e. g., Foster and Jackson, 1998; Brazier et al., 2005; Mulibo and Nyblade, 2016; Asefa and Ayele, 2020) within the East African Rift System. However, relatively a few earthquakes are found down to 35-45 km within the western and eastern branches of the EARS. From Figures 4.4 and 4.5, it is evident that the hypocentral depths of the earthquakes considered in the study time period vary from region to region in the East African Rift System which is increasing from north to south. Earthquakes with shallow depths are observed in the Afar and the main Ethiopian rift. Relatively deeper earthquakes observed in the western and eastern branches of the EARS may reflect relatively larger effective elastic thickness in the southern region of the EARS as compared to the northern part of the East African Rift System in the Afar region and main Ethiopian rift. Some earthquakes which have relatively deep focal depths were also observed by Lapins et al., (2020) in the central MER.

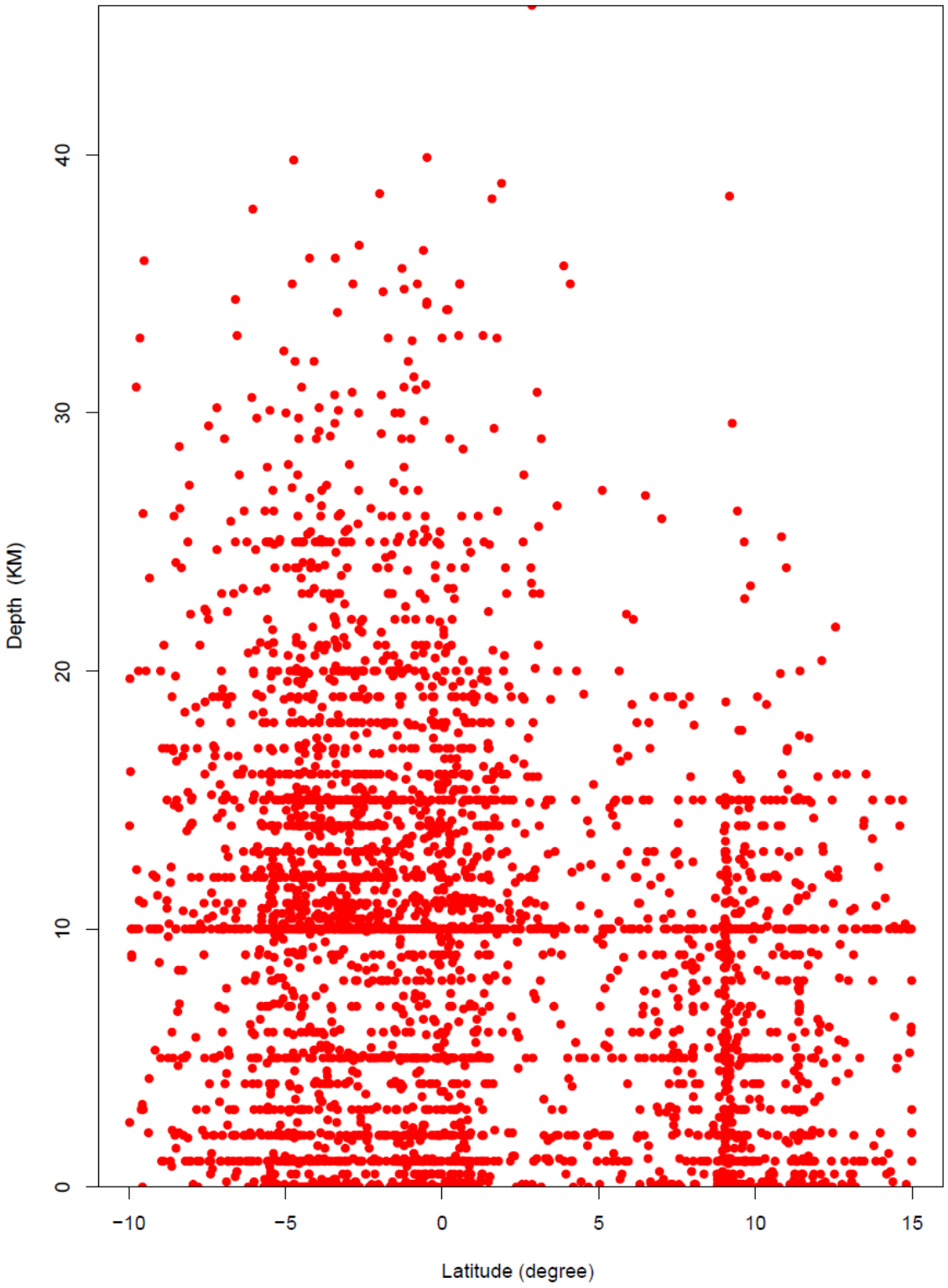


Figure 4.4: Hypocentral depth versus Latitude of earthquakes for the time period 2013 to 2016.

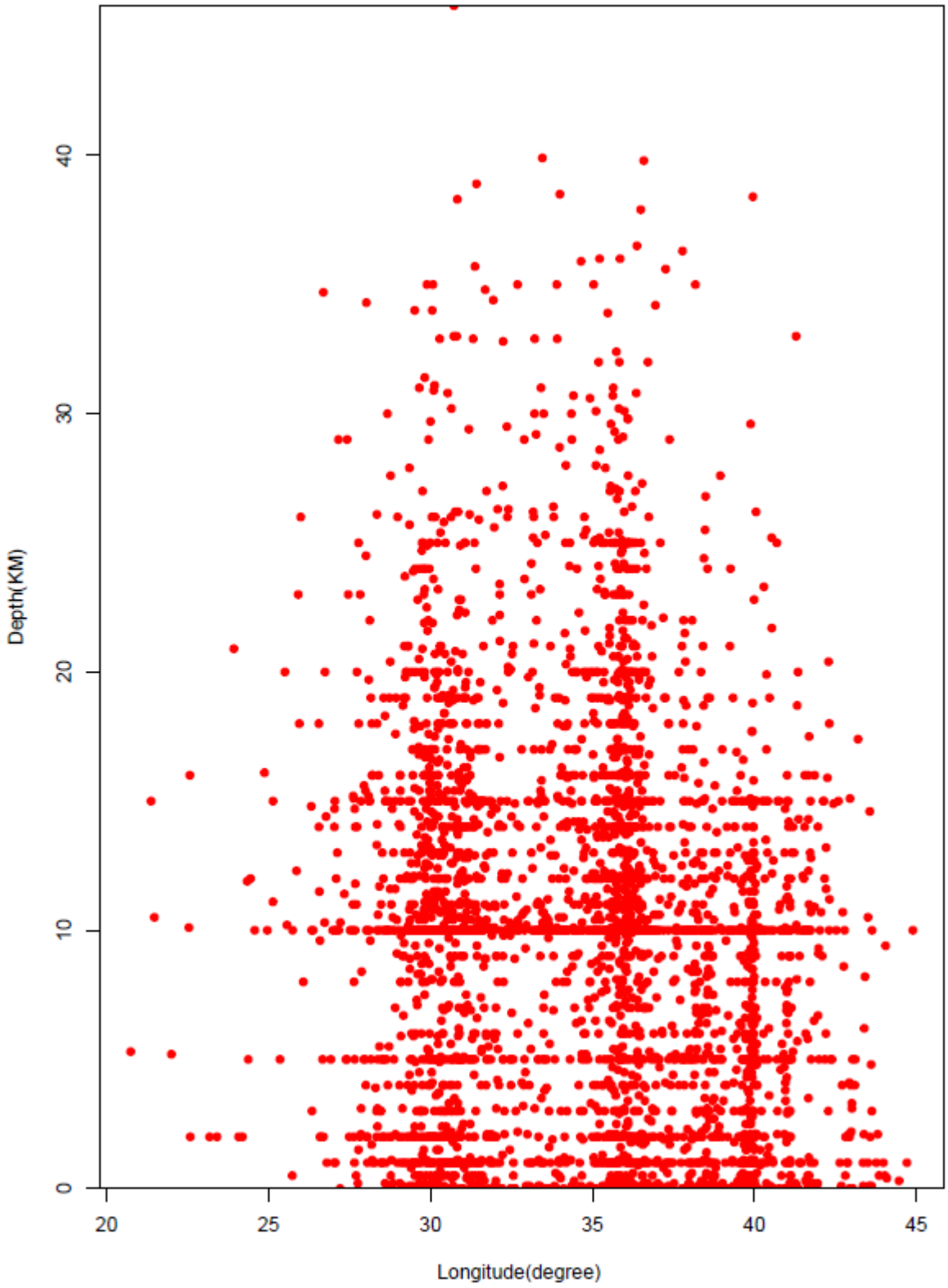


Figure 4.5: Hypocentral depth versus Longitude of earthquakes for the time period 2013 to 2016.

4.3.4 Frequency magnitude distribution

The magnitude of completeness is the magnitude increment at which the lower end of the FMD departs from the linear trend in the log-lin plot (Fig. 4.7). The b-value is estimated using the maximum likelihood method (Aki, 1965) from earthquakes catalog and a threshold magnitude of Mc 3.0 is estimated in this study. An average b-value of ∼1.01 and a-value of ∼6.5 are estimated for the whole region in this study (Fig. 4.7) with standard error of ±0.16. The b-value can be considered as an indicator of the stress condition (Scholz, 1968; Gibowicz, 1974; Henderson and Main, 1992). In regions of relatively high b-values, stress is mostly released by numerous small earthquakes.

For example relatively large b-values (1.0 to 2.5) are usually observed in regions with active

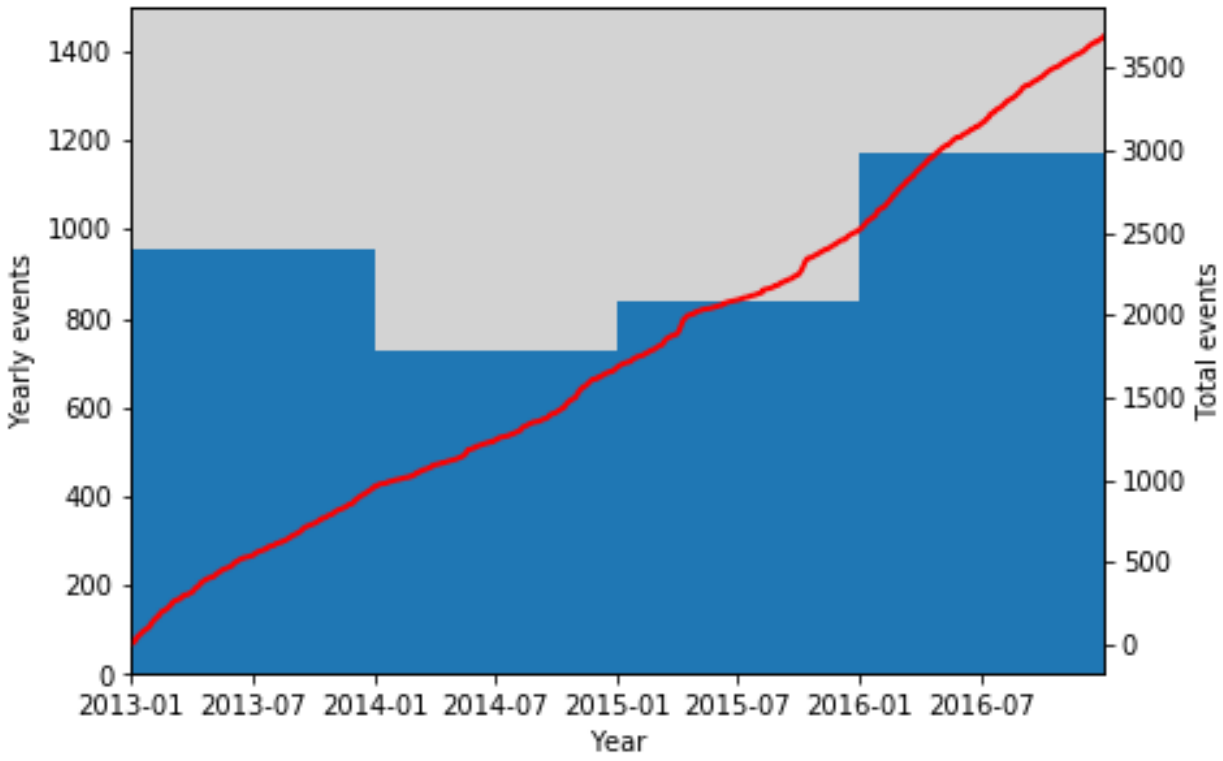


Figure 4.6: Plot of the yearly and total number of earthquakes as a function of time. The left vertical axis is the number of events per year. The right vertical axis is the total of events. The result shows that the number of earthquakes decreases in 2014 but increase again in between 2015 to 2016.

volcanism where seismicity is associated with eruptions and magma movements (e.g., Karpin

and Thurber, 1987). Alternatively, according to Mogi (1967), lower b-values between 0.5 and 1.0 are indicative of tectonic processes in non-volcanic areas. Therefore the obtained b-value of ∼1.01 (Fig. 4.7) is not significantly larger than the one set for tectonic earthquakes which implies that high level of stress is dominating in the East African Rift System mostly released by numerous small to intermediate tectonics earthquakes.

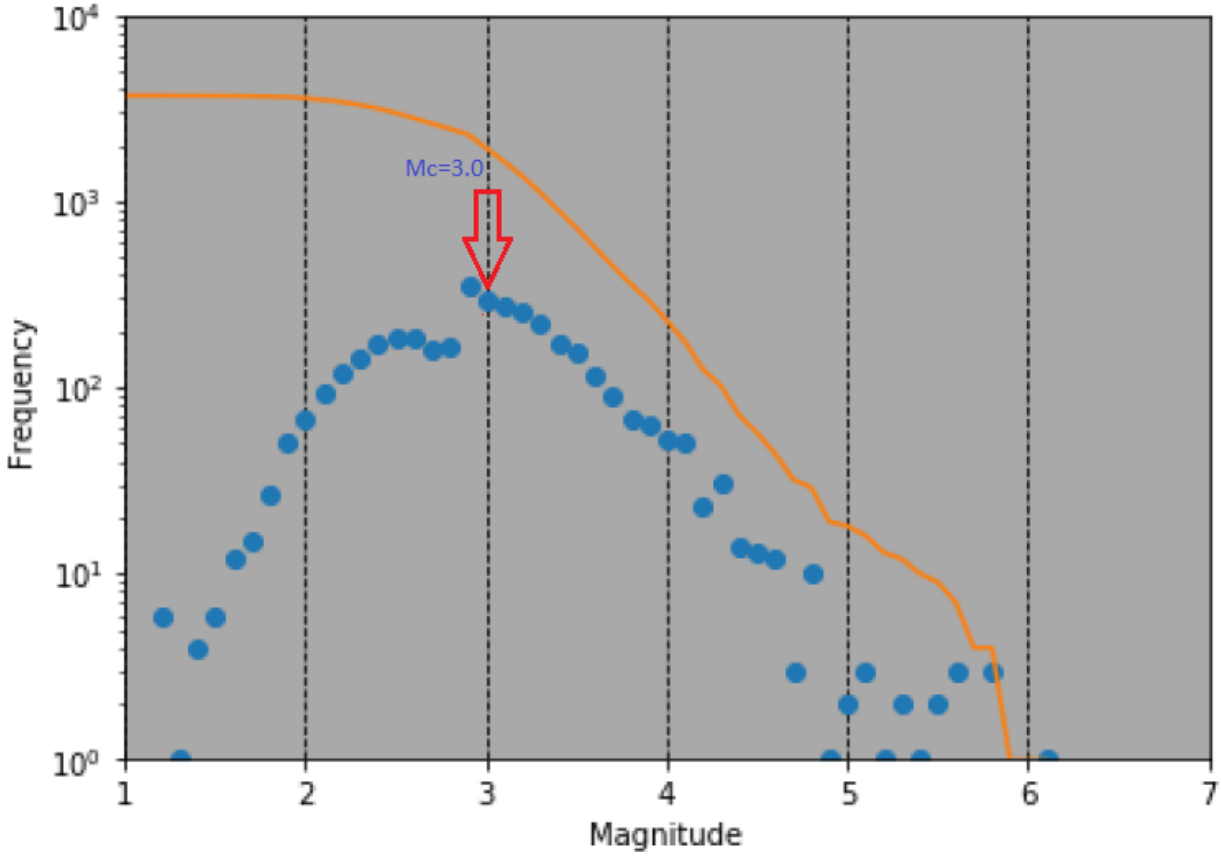


Figure 4.7: Magnitude-frequency distribution of earthquakes in the study area for the catalog. The b-value estimate for the whole region is 1.01 ± 0.16 and a-value with ∼6.5. Magnitude of completeness (Mc) is the magnitude increment at which the lower end of the FMD departs from the linear trend in the log-lin plot. In this study, a visual evaluation can lead to a correct estimate of the completeness magnitude (Mc ∼3.0). Circles represent the discrete (non-cumulative) and the orange line the cumulative distributions of events.

4.3.5 Seismic energy map

The variation of seismic energy released in the region has been calculated using earthquake magnitude for the time window of 2013 to 2016. Dominant energy-release peaks are observed at Afar region, eastern and western branches of the EARS (Fig. 4.8) which could have resulted from either a few larger earthquakes or repeated earthquake sequences of intermediate shocks in the areas than the others. The spatial seismic energy release during the time window considered has revealed that the MER is connected to the eastern branch of the EARS that supports the earthquakes distribution in the region.

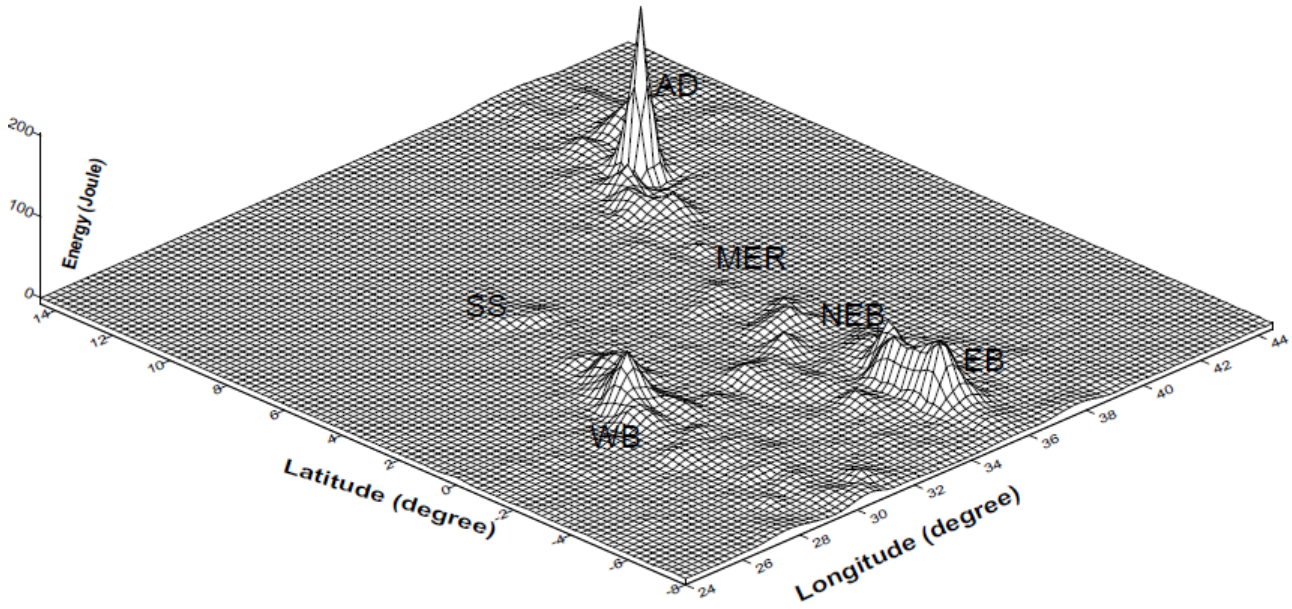


Figure 4.8: Variation of seismic energy released for the period 2013 to 2016 in the EARS. Dominant energy peaks are observed in the Afar depression (AD), main Ethiopian rift (MER), Southern-Sudan (SS), Northern eastern branch (NEB), eastern branch (EB) and western branch (WB).

CHAPTER 5

Complex Tectonic Deformation in Circum-Tanzania Craton: East African Rift System

5.1 Introduction

The Tanzania Craton, embedded in the Victoria microplate, is sandwiched between the eastern and western branches of the East African Rift System (EARS) (Fig. 5.1; Calais et al., 2006b). The eastern branch propagates southward through Kenya and into northern Tanzania, where the rift zone splits into three segments, the Eyasi segment to the west, the Manyara segment in the middle, and the Pangani segment to the east (e.g., Fig. 5.1; Ebinger, 1997; Foster et al., 1997). The circum-Tanzania Craton has experienced enormous seismic activity (Iranga, 1992; Zhao et al., 1997; Foster and Jackson, 1998; Langston et al., 2002; Weeraratne et al., 2003; Kim et al., 2009; Yang and Chen, 2010; Albaric et al., 2010, 2014; Isola et al., 2014). The area is marked by frequent occurrence of small to moderate magnitude earthquakes with rare occurrence of strong events. In 2014 and 2016, the region was shaken by a series of earthquakes that occurred near the margin of the Tanzania Craton. Several earthquakes were felt in 2014 in Manyara rift segment of Maminzi transverse fault zone including the main shock of Mw 5.2 followed by several aftershocks in the magnitude range of Ml 3.0 to 3.7. The magnitude Mw 5.2 event occurred in the northern Dodoma region on October 31^{st}, 2014 which was widely felt in several places, though damage was minimal.

Large and moderate magnitude earthquakes in the East African Rift System are mainly confined to the rift zones (Shudofsky, 1985; Iranga, 1992; Nyblade and Langston, 1995; Nyblade et al., 1996). However, there were rare instrumentally recorded earthquakes known to occur in the

Kagera region of the circum-Tanzania Craton which can be possibly due to longer return period of large magnitude earthquakes and lack of station coverage for small magnitude earthquakes. On September 10, 2016, an earthquake of magnitude Mw 5.7 rocked the western shore of Lake Victoria, in Kagera region. This event was felt a few kms away from the western branch of the East African Rift System and the tremors rippled as far as western Kenya, parts of Uganda, and Rwanda. According to the assessment report prepared by a joint team composed of representatives of the Tanzanian government, UN agencies, UNDAC (United Nations Disaster Assessment and Coordination) team and members of the local and international organizations, 17 people died and 440 people were injured. Furthermore, due to poor building construction practices and low quality construction materials, the region suffered the most serious damage observed in recent times. More than 2,500 houses were completely destroyed and more than 14,500 houses were partially destroyed leaving people with no shelter while, more than 9,000 houses developed minor cracks. According to the report, the earthquake had no major impact on the communication infrastructure including phone networks, roads and bridges.

Even though numerous studies have been conducted to analyze seismic activity and interpret the associated tectonic deformation in the region (Foster and Jackson, 1998; Langston et al., 2002; Mulibo and Nyblade, 2016; Weinstein et al., 2017), details of geodynamic working model in the circum-Tanzania Craton remains poorly understood. Most of the previous works also assessed focal mechanisms of earthquakes using P-wave first motion technique (Mulibo and Nyblade, 2016) which is often highly non-unique (Zahradnk et al., 2015) and has limitation due to data paucity while others applied waveform inversion method from teleseismic data (Shudofsky, 1985; Foster and Jackson, 1998; Brazier et al., 2005). Over the past two decades several studies used a moment tensor inversion method that retrieves reliable and detailed source parameters of earthquakes (Delouis and Legrand, 1999; Kim et al., 2000) even using a three component waveform data from a single station. Therefore, in this study, we apply moment tensor inversion technique using regional waveform data to retrieve detailed source properties of selected events of the 2014 and 2016 earthquake sequences that occurred in the circum-Tanzania Craton

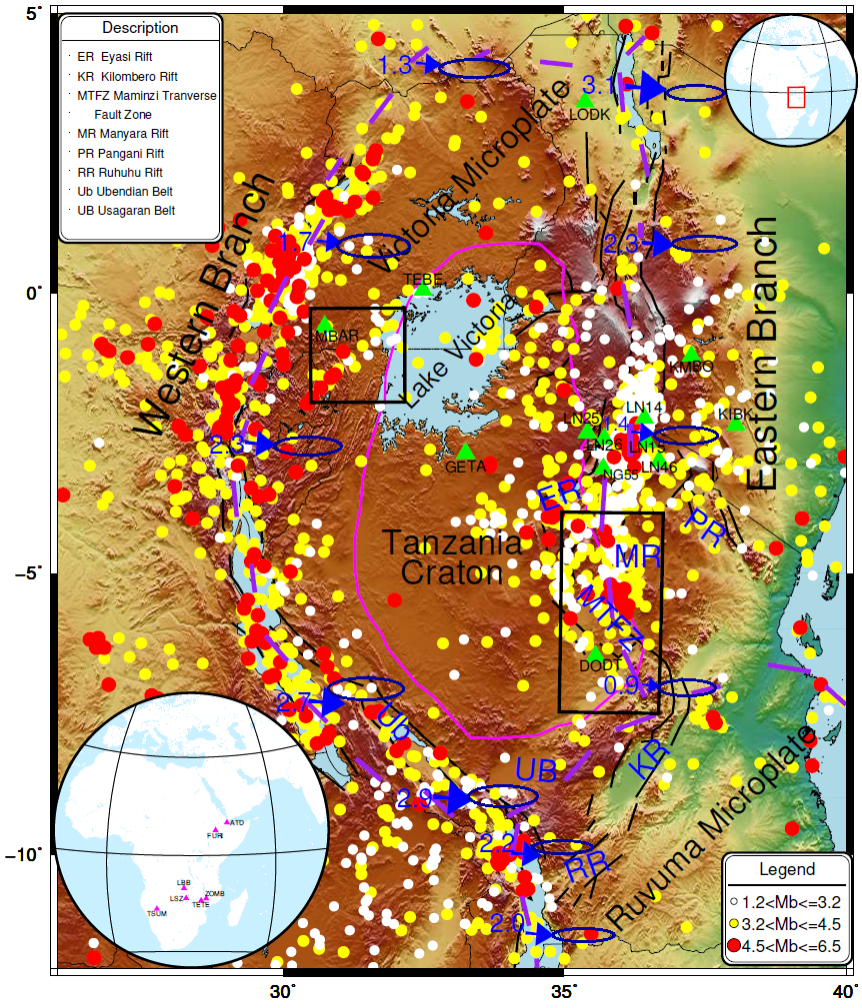


Figure 5.1: Regional tectonic map of the western and eastern branches of the East African Rift System. The magenta loop shows outline of the Tanzania Craton. The Northern Tanzania Divergence Zone (NTDZ) rift segments (Eyasi, Manyara and Pangani), and the mobile belts surrounding the Tanzania Craton. The two black boxes show the study areas and green triangles on the map are local and regional seismic stations while magenta triangles on the inset map show the distant seismic stations used in this study. Solid black lines show major faults and geological features. Major faults are from Le Gall et al., 2004. The purple dashed lines indicate the boundaries of the Victoria and Ruvuma microplates (Stamps et al., 2008). Kinematics symbols are from Saria at el., 2014; the blue arrows show predicted relative motions between plates; numbers are velocities in mm/yr. Seismicity of the western and eastern branches of EARS with body wave magnitudes in the range of Mb 1.2 to Mb 6.5 homogenized using regression analysis for the time period of 1995 to 2013 compiled from the International Seismological Center (ISC) catalogue. Different color circles (white, yellow and red) show the epicenters of earthquakes where circle size is proportional to earthquake magnitude as shown in the legend.

in order to shed light on the dynamics of the Victoria microplate.

5.2 Tectonic setting

For many years the East African Rift System (EARS) is considered as an incipient extensional boundary between the Nubian and Somalia plates (Stamps et al., 2008, 2018) in which rifting is resulted in splitting the African continent into the Nubian and Somalia plates. However, most recently it was discovered that rifting in the EARS has created three recognized microplates: Victoria, Ruvuma and Lwandle (Saria et al., 2014), which are separated by well-defined divergent boundaries of the western and eastern branches of the EARS (Calais et al., 2006a; Stamps et al., 2008; Saria et al., 2013).

The recent plate kinematic studies (Calais et al., 2006b; Stamps et al., 2008; Saria et al., 2013) divided the regions between the Nubian and Somalia plates into the Victoria and Ruvuma microplates (Saria et al., 2014) but Lwandle microplate has only been detected through space geodesy. The Victoria plate is located in the western side of the eastern branch of EARS while the Ruvuma microplate is located in southeastern Tanzania Craton and northern Mozambique. Geodetic evidence (Fernandes et al., 2004; Calais et al., 2006b) indicates that the Victoria and Ruvuma microplates are rotating in a counterclockwise and clockwise with respect to the Nubian plate, respectively. Extension and magmatism are localizing in distinct of western and eastern branches marking the edges of Victoria and Ruvuma microplates extension in East African Rift System. The borders of the Victoria and Ruvuma microplates with the Nubian plate to the west and Somalia plate to the east now represent the most seismically active zones. Thus, the kinematics rotation of these two plates may control the tectonic deformation of the region. The Victoria plate is surrounded by active rift structures with known seismic signatures. Its geodynamic behavior in Cenozoic times is the result of continental rifting on an uplifted East Africa plateau that encompasses relatively undisturbed Archean to early Palaeoproterozoic terranes (Fernandes et al., 2013). Some of the earthquake focal mechanisms observed in this study are generally consistent with the proposed counterclockwise rotation of the Victoria plate.

The circum-Tanzania Craton of this study covers the major complex tectonic provinces of the Victoria microplate and the portion of eastern branch of the EARS which is south of NTDZ. The eastern branch has developed within the Mozambique Belt and partly along the eastern side of the Tanzania Craton which is colder and stronger than surrounding Orogenic Belts (Ebinger, 1997; Delvaux, 2001; Weeraratne et al., 2003). The Tanzania Craton which is found within the Victoria plate is underlain by a 170-250 km thick lithospheric keel (Weeraratne et al., 2003). Rifting in a cratonic lithosphere is strongly controlled by several interacting processes such as crust/mantle rheology, magmatism and stress regime (Plasman et al., 2017).

The eastern branch has N−S trend in northern Tanzania that forms NTDZ with several rift segments propagating southwards (Le Gall et al., 2004; Macheyeki et al., 2008). Some of the rift segments intersect the Tanzania Craton while others pass adjacent to the margin of the Craton. The Eyasi and Manyara rifts intercept the Tanzania Craton (Fig. 5.1) where they are actively opening and propagating through the development of a series of disconnected rift segments (Le Gall et al., 2004; Macheyeki et al., 2008). The eastern branch provides impressive examples of continental breakup with different direction of propagation southwards of the NTDZ within the circum-Tanzania Craton. For example Mougenot et al., (1986) proposed the direction of propagation along the Pangani rift across northeastern Tanzania, while others proposed the direction of propagation through northern edge of Ruvuma plate then connected with Davies Ridge offshore (O′Donnell et al., 2013; Mulibo and Nyblade, 2016). However, Le Gall et al., (2004) suggested the southern link between the western and eastern branches along the margin of the Tanzania Craton. The circum-Tanzania Craton is arguably one of the tectonically complex regions due to its location in seismically active region and due its location at the boundary of several major tectonic plates. In the region, some of structural features are associated with faults and topographic lineaments trending in sub N−S, NNE−SSW and NE−SW to NW−SE directions (Le Gall et al., 2004).

Historically, seismic activity of the East African Rift System is mainly concentrated along the western and eastern branches, and at the edges of the Victoria and Ruvuma microplates. The

eastern branch of the EARS is characterized by earthquakes with shallower focal depths and relatively active magmatism (Albaric et al., 2010) as compared to the western branch where seismicity is featured by higher magnitude and deeper earthquakes (Yang and Chen, 2010; Lindenfeld and R*ü*mpker, 2011).

The particular tectonic provinces of the study areas are including the Kagera region located in the northwestern corner of Tanzania Craton on the Victoria microplate. The September 2016 earthquake of magnitude Mw 5.7 has been rocked in this region. The region is a few kms away from the western branch of the East African Rift System in eastern direction which is towards the Lake Victoria (Fig. 5.1). The second part of the study area is the southeast margin of the Tanzania Craton which is located within the nascent plate boundary between the Victoria and Somalia plates. This region covers some portion of the Manyara-Dodoma rift segment established in Macheyeki et al., (2008). Under this region we have considered two zones: the first one is the northern Kodoa region, towards southern direction of the Lake Manyara region in the eastern branch in which major faults and magmatism developed after $\sim$7 Ma (Mana et al., 2012; Mana et al., 2015). The second zone is the northern Dodoma, which is part of the Manyara-Dodoma rift segment established in (Macheyeki et al., 2008) towards the northern Dodoma town. Currently, this zone is seismically active as indicated by the November Mb 5.5 mainshock (Yang and Chen, 2010), presence of numerous neotectonic features such as active faults (Macheyeki et al., 2008) as well as active deformation as shown by GPS observations (Saria et al., 2014). The seismic activity considered in this region is associated with the active NW$-$SE trending Maminzi transverse fault zone.

5.3 Data and Methods

5.3.1 Data

A dense seismic station network is very important to determine earthquake locations and to detect earthquake down to lower magnitude scales in the region where earthquake occurrence and volcanic manifestation are common phenomena. A few numbers of permanent seismic stations

are available in the circum-Tanzania Craton to capture regional earthquakes. However, a number of existing permanent seismic stations are not sufficient to study the detail seismic activity of the region. Therefore, this study uses broadband seismic data from different sources. Thus, the source properties of earthquakes in the region are investigated. Three-component waveform data recorded on local, regional and distant seismic stations were combined from temporary and permanent seismic stations in and around the study area (Fig. 5.1). Accordingly, earthquake location and moment tensor inversion were performed using waveform data from various sources. The first data source was from seismic stations installed between 12 January 2013 and 6 December 2014 in Tanzania. The network comprised STS-2, Gur-alp 3T and 40T, Trillium 120 sensors with Reftek data loggers from IRIS-PASSCAL instrument pool. We used three-component seismic data of these temporary seismic stations. The second data source was the permanent AfricaArray networks. In this part we have used three-component seismic data from five seismic stations. Along with the temporary and permanent AfricaArray seismic stations, three-component seismic data have been used from eight permanent broadband seismic stations namely ATD, FURI, LSZ, KMBO, MBAR, TSUM, LODK and KIBK.

5.3.2 Methods

5.3.3 Earthquake location

In this study, we located 10 earthquakes from P- and S-waves arrival times picked from waveform data while the location of one event is adopted from the National Earthquake Information Center (NEIC). From the total events, five earthquakes are considered in moment tensor inversion but six events are aftershocks which are not considered in moment tensor inversion due to small magnitudes which may difficult to compute inversion.

Four of 10 earthquakes have been reported by different agencies based on global velocity model, however determination of earthquake parameters such as location and focal mechanism are highly dependent on velocity model of the study area. Therefore, we relocated four events using waveform data from local, regional and teleseismic broadband seismic stations using the local

velocity model. The six aftershocks are located using waveform data from local and regional broadband seismic stations.

During event location, P-wave onsets were initially identified on the vertical components of the seismograms and S-wave arrivals were picked from horizontal components of the seismograms. Event locations were determined using HYPOCENTER (Lienert and Havskov, 1995) program that is incorporated in the SEISAN software (Ottemöller et al., 2015). We used 1-D velocity model of Langston et al., 2002 for earthquake location using a minimum of waveform data from six seismic stations. Events location was analyzed with errors of about 4.3 km and 5.8 km on average in latitude and longitude respectively. For September 10, 2016 Kagera earthquake, the NEIC location is adopted and used in the moment tensor inversion.

5.3.4 Local magnitude estimation

Waveform data obtained from seismic stations were used to measure the size of earthquakes. The local magnitude earthquake was calculated by using empirical relation given below by Richter, 1935: Local magnitude was estimated using the formula developed by Keir et al., (2006),

$$M_L = log(A_{WA}) + 1.96997log(\frac{r}{17}) + 0.001066(r - 17) + 2, \tag{5.3.1}$$

where A_{WA} is a maximum horizontal ground amplitudes zero to peak and r is the hypocentral distance. The instrument responses are removed and convolved with Wood-Anderson instrument response. We measured a maximum absolute value of the zero-to-peak amplitude from north-south and east-west horizontal components of seismograms. An average of earthquake magnitude estimation was carried out from the horizontal components of the seismograms. The results of the estimated magnitudes for all earthquakes are listed on Table 5.1.

5.3.5 Moment tensor inversion

In seismology, characterizing seismic source process especially determining fault plane solutions is one of the major research areas of interest. There are several techniques that can be used

to retrieve fault mechanisms of local and regional earthquakes. Among the techniques, the P-wave first-motion (polarities) reading is one of the most common and well established techniques used to compute focal mechanism of earthquake in different studies (Snoke et al., 1984; Snoke, 2003). However, in this study we applied moment tensor inversion that efficiently reduces non-uniqueness of the polarities solutions, as the source parameters including depth which better characterizes the earthquake source and uses less number of stations (Delouis and Legrand, 1999; Kim et al., 2000).

We applied Ichinose et al., (2014) code which is written based on Gilbert, (1971) approach used to calculate the excitation of the normal modes of the earth due to particular earthquake source. We used deviatoric moment tensor inversion (5 degrees of freedom) and we assumed that there is no volume change (no isotropic component). We generated synthetic seismograms and compared with observed waveform data where interactive inversion is conducted until a reasonable match is found. In this method, a grid search is conducted until a reasonable waveform fit is achieved between observed and synthetic seismograms. Due to small errors from origin time and location of event, the generated synthetic seismograms are shifted relative to the observed for a few seconds after or before the origin time. Long-period seismic waves were used because long-period seismic waves are relatively not sensitive to the effects of lateral velocity and density heterogeneities (Ritsema and Lay, 1995; Larson and Ekstrm, 2006) and stable source parameters can be obtained.

Moment tensor inversion is computed using 1-D velocity model Langston et al., (2002) with band-pass filtering in the range of 0.014-0.05 Hz. The solutions scheme for moment tensor inversion is constrained to allow double couple and compensated linear vector dipoles (CLVD) components. The solutions for the inversion were computed at 2 km depth increments. We calculated the percentage of variance reduction, double couple, source mechanism and source depth versus origin time. We selected our results that have the highest percentage of double couple and variance reduction, and choose the depth at the best fit between observed and synthetic seismograms. In some cases, when a good signal-to noise ratio waveform data are

available only on a few seismic stations, a smaller number of seismic stations is required to get a reasonable source parameter. In fact moment tensor inversion method could retrieve a reliable source parameters even using a three component waveform of a single station (Delouis and Legrand, 1999; Kim et al., 2000).

In the second part of moment tensor inversion, we applied Cesca et al., (2010) code for the September 10, 2016 Kagera earthquake of magnitude Mw 5.7 to estimate source parameter of the event. We used a mixed approach inversion both in time and frequency domains. Time traces and spectra amplitude are fitted at the same time at regional distances. A set of information are used for a better constraint of the source parameters, including the fit of amplitude spectra and displacement phases. We generated synthetic seismograms both in time and frequency domain and fitted synthetic seismograms with the observed seismograms using bandpass filtering of 0.015- 0.04 Hz in both cases. Generally, in the first and second moment tensor inversion methods applied in this study, our solutions quality were determined by the goodness of the fit of synthetic to the observed data. The reported Global Centroid Moment Tensor (GCMT) solution for focal mechanism is used as a priori knowledge to validate our technique. Generally, as we applied the moment tensor inversion, the value of variance reduction that determines the quality of our result is higher for larger magnitude earthquake than for the lower magnitude earthquake might be influenced by signal-to-noise ratio.

5.4 Results and Discussion

In this work, a total of 11 earthquakes (Table 5.1) that occurred in the circum-Tanzania Craton were analyzed. Four of the 11 earthquakes felt in 2014 (Mw 4.1 to 5.2) that were reported in the International Agencies are relocated by integrating phase readings from local, regional and distant waveform data with good signal-to-noise ratios to reduce uncertainties. Of the 11 events, six are aftershocks of the 31^{st} October 2014 main shock of magnitude Mw 5.2. The magnitudes of aftershocks are too small to be reported by neither the NEIC nor the ISC. These aftershocks are used for interpretation by incorporating with the trend of focal mechanism of the

Table 5.1: Source parameters for selected five earthquakes felt in 2014 and 2016 which are considered for the moment tensor inversion and associated aftershocks that occurred in the circum-Tanzania Craton. The symbol $*$ indicates aftershocks that are obtained in this study.

Date	*Lat.*(∘)	*Long.*(∘)	*Strike*(∘)	*Dip*(∘)	*Rake*(∘)	*Depth*(*km*)	*Magn.*
28-01-2014	-4.531	35.726	125,357	23,75	-140,-72	16.0	Mw4.1
21-11-2014	-4.50	36.039	158,355	32,59	-104,-81	12.0	Mw4.2
31-10-2014	-5.464	36.207	145,52	73,78	-167,-18	16.0	Mw4.8
31-10-2014	-5.402	35.914	154,153	69,64	-157,-24	14.0	Mw5.2
31-10-2014$*$	-5.695	36.565	–	–	–	6.6	Ml3.2
31-10-2014$*$	-5.636	36.439	–	–	–	12.0	Ml3.7
31-10-2014$*$	-5.379	35.811	–	–	–	8.0	Ml3.6
31-10-2014$*$	-5.575	35.845	–	–	–	12.0	Ml3.0
31-10-2014$*$	-6.033	36.544	–	–	–	6.4	Ml3.4
31-10-2014$*$	-5.442	35.837	–	–	–	5.6	Ml3.0
10-09-2016	-1.23	31.37	32,287	61,66	-152,-32	20.9	Mw5.7

main shock. One of the 11 events is the 2016 Kagera earthquake of magnitude Mw 5.7 that was strongly felt around the western shore region of Lake Victoria. There seems to be no aftershocks with significant magnitude associated with the Kagera earthquake that could be recorded at regional distances. In this study, except for the aftershocks the source parameters of each event is computed from the moment tensor inversion. Accordingly, the moment tensor inversion has revealed reliable source parameters as analyzed from the seismological data.

Ten of the 11 events are located within seismically active border of Tanzania Craton which is near boundary between Victoria and Somalia plates, and within the eastern branch that associated to the portion that extends southwards from the North Tanzanian Divergence down to the Dodoma region (the Manyara−Dodoma rift segment) (Macheyeki et al., 2008). Two of the events of magnitude Mw 4.1 and 4.2 in the 2014 earthquake sequence considered in this study occurred in northern Kondoa region in the highly segmented Manyara fault associated with mainly N−S trending direction. The events of magnitude Mw 4.8 and Mw 5.2 are felt in the northern Dodoma region with aftershocks distributed around the Maminzi transverse fault zone that are aligned roughly along NW−SE direction.

The compiled epicenters of earthquakes from International Seismological Center database (Fig.

5.1) show that the highest seismicity in the western and eastern branches of the East African Rift System is confined in the rift axis and at rift margins (Nyblade and Langston, 1995; Albaric et al., 2010; Lindenfeld and Rümpker, 2011). The results show a comprehensive small to large magnitudes earthquakes. As we compare the two branches of the East African Rift System, the western branch is featured by higher magnitude earthquakes (Fig. 5.1; Yang and Chen, 2010) than the eastern branch. Majority of earthquakes in the eastern branch are distributed in the NTDZ (Nyblade et al., 1996; Foster and Jackson, 1998; Albaric et al., 2010), encompassing the Eyasi and Manyara rift segments with no much distribution of events in Pangani rift segment. The portion of Manyara−Dodoma rift segment (Macheyeki et al., 2008) is seismically very active. The region has relatively higher magnitudes as compared to northern Tanzania which has high level of microseismicity. Majority of the earthquakes are distributed along a broad N−S trend, mainly between 35° and 36°. The compiled earthquakes show also the alignment in NNE-trending at the northern Tanzania and the N−S trending in the Kondoa fault system. Earthquakes distribution is also observed within the Tanzania Craton and near Lake Victoria. All events analyzed in this study have focal depths varying from 5.6 to 26 km (Table 5.1). We obtained the maximum depth of 26 km, while a maximum focal depth of 21.4 km was reported by Mulibo and Nyblade, (2016) for 25/03/2011 event of magnitude Ml 4.6 in which the focal mechanism of the event has been computed using polarity reading in surrounding area.

The resulted focal depths distributions in this study are in agreement with previous studies in the circum-Tanzania Craton (Nyblade and Langston, 1995; Nyblade et al., 1996; Zhao et al., 1997; Langston et al., 2002; Brazier et al., 2005; Yang and Chen, 2010; Albaric et al., 2010, 2014; Mulibo and Nyblade, 2016). Several interpretation have been given for the presence of deep crustal earthquakes depths that reported in East African Rift System (Keir et al., 2009; Lindenfeld et al., 2012; Albaric et al., 2009, 2014; Weinstein et al., 2017). The presence of relatively deep crustal earthquakes in the circum-Tanzania Craton of this study is interpreted to be due the presence of relatively stronger and thicker lithosphere of the Tanzanian surrounding orogenic belts (Weeraratne et al., 2003; Craig et al., 2011) as compared to other areas in the

East African Rift System. The earthquakes are even generally deeper in the circum-Tanzania Craton due to the presence of thicker and stronger lithosphere (Albaric et al., 2009; Albaric et al., 2010) under the Tanzania Craton than in the northern part of the East African Rift System in the Main Ethiopian rift and Afar region.

The well constrained moment tensor inversion we calculated in this study provided reliable focal depths and mechanisms for earthquakes considered. Our focal mechanism is very similar to the Global Centroid Moment Tensor (GCMT) solution but our focal depths obtained from moment tensor inversion for 4 earthquakes from 12 to 26 km for the magnitudes Mw 4.1−5.2 is deeper than the ones estimated by the GCMT solutions and ISC catalogue while the depth estimate of Kagera earthquake in our study is 20.9 km which is shallower than the one obtained by GCMT. Our results characterize the seismogenic deformation of the area in detail. Moment tensor inversions have been done for five events using long-period seismic waves which provide reliable estimates compared to P-wave first motion techniques. Reasonable good waveform fits are obtained for the observed and synthetic seismograms and a sample of waveform fit between generated synthetic and observed seismograms from the conducted inversion and the source parameters results for all events are summarized in Table 5.1. The inversion results are obtained at maximum percentage of double couple and variance reduction, thus, the source parameters like focal depth, seismic moment, moment magnitude, and strike, dip and rake angles are extracted (Figs. 5.2; 5.3; 5.4; 5.5; 5.6; 5.7).

Our results indicate that the upper and deep crustal seismicity in the circum-Tanzania Craton containing normal faulting oriented N−S and normal faulting with significant strike-slip oriented NW−SE within cratonic margin and at the plate boundary. The focal mechanisms of earthquakes obtained in this study are interpreted in light of the regional tectonics (Fig. 5.1). For ease of discussion, the studied events are grouped into three: (1) the northern Kondoa region, which is south of Lake Manyara (Manyara rift segment); (2) the northern Dodoma region, a part of the Maminzi transverse fault zone. The two regions are associated with the N−S trending rift portion that extends southwards from the Northern Tanzania Divergence Zone down to the

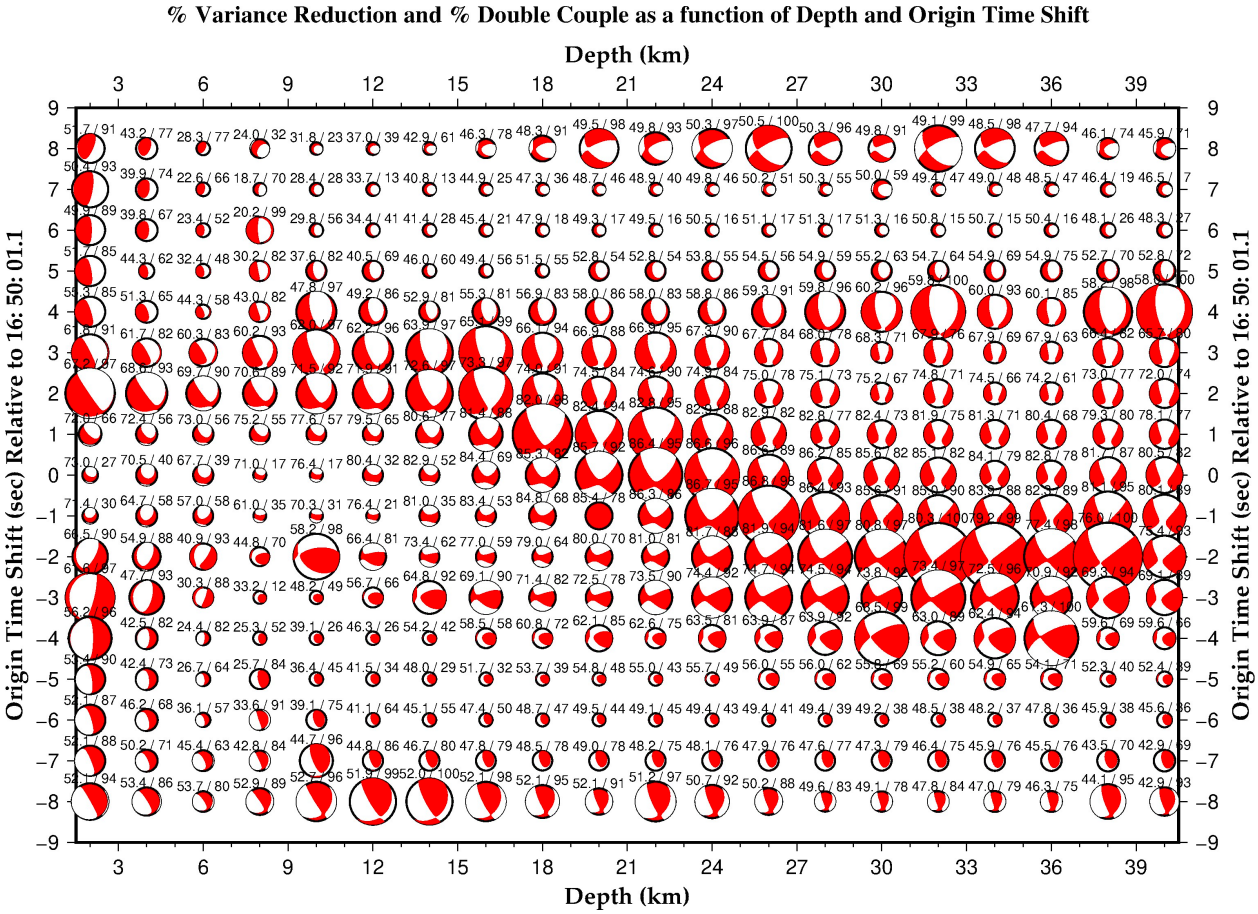


Figure 5.2: Percentage of variance reduction, double couple and source mechanism for 2014/10/31 earthquake with origin time 16:50:01.1 as a function of focal depth variations from 2 to 40 km. The optimal origin time shift is -1 s and preferred focal depth is 26 km. The size of beach ball is proportional with the value of variance reduction (VR) and percentage of double couple (DC) solution.

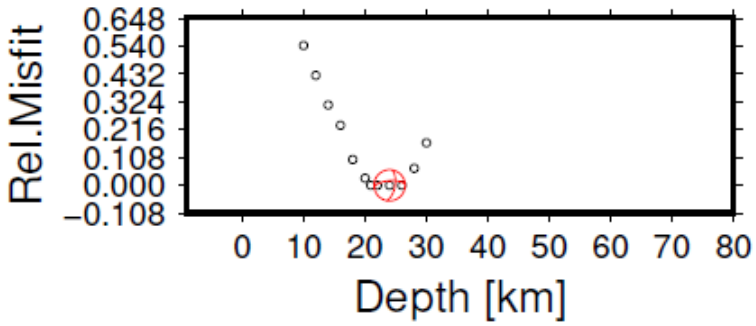


Figure 5.3: Relative misfit versus focal depths of September 10, 2016 Kagera earthquake of magnitude Mw 5.7 computed from moment tensor inversion. The best solution for focal depth of the event has been chosen at the smallest misfit.

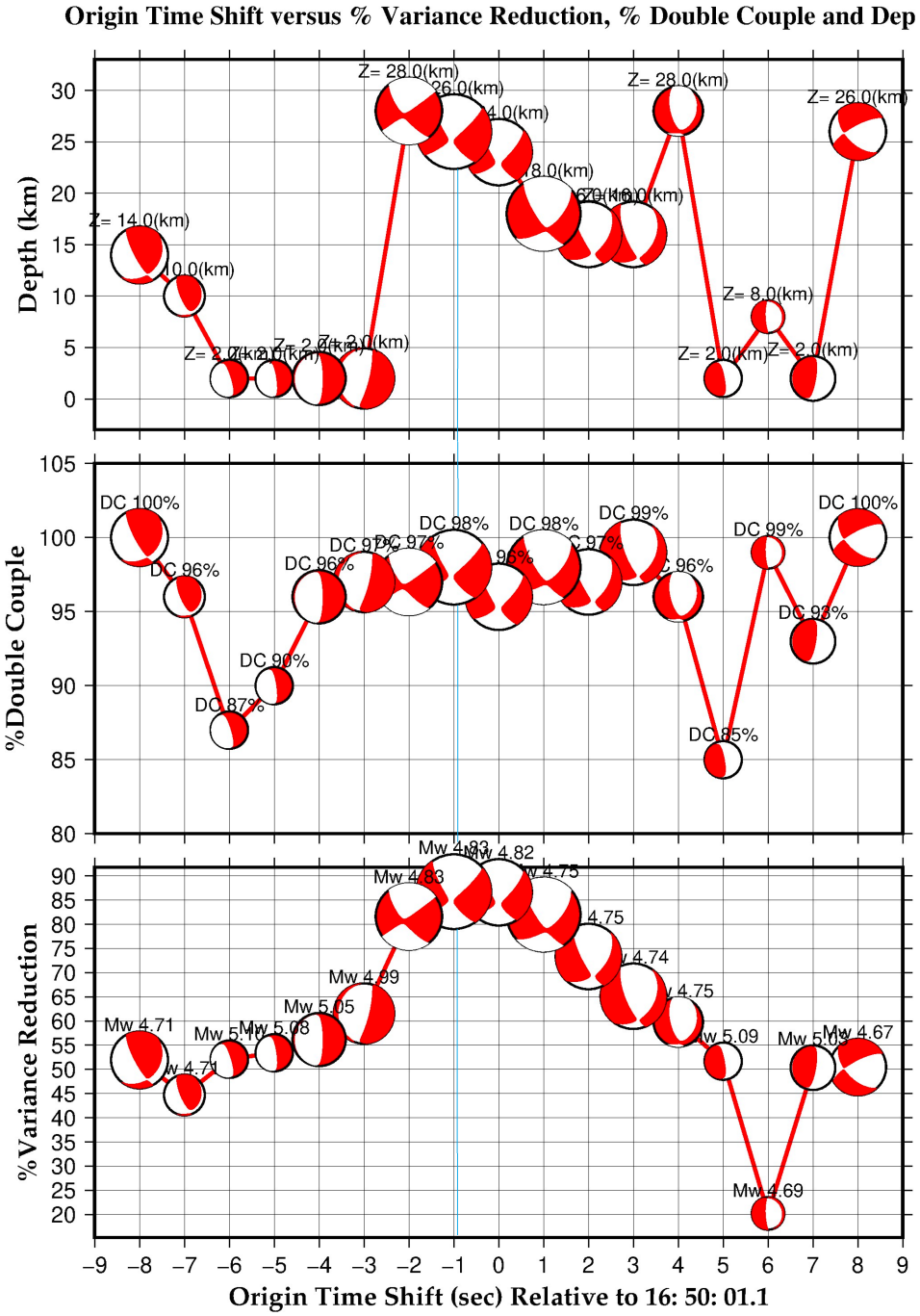


Figure 5.4: These plots show values of variance reduction, double couple and depth versus origin time shift of -1 s relative to origin time for lower, middle and upper panels, respectively. The blue line shows the value of results adopted in this study (depth 26 km, Mw 4.8 and focal mechanism).

Dodoma region (the Manyara-Dodoma rift segment) as described in Macheyeki et al., (2008). (3) the Kagera region, a part of the western shore of Lake Victoria. The regions are explained earlier under the tectonic setting part.

5.4.1 The Northern Kondoa region

There are two moderate size earthquakes of magnitudes Mw 4.1 and 4.2 which were felt in northern Kondoa in 2014 and considered for the moment tensor inversion in this group. The two events of the northern Kondoa region are interpreted to rupture along the N−S trending fault system in the Manyara rift segment (Fig. 5.1). For earthquakes in this group, waveform data are used from five and three broadband (three-component) seismic stations to compute moment tensor inversion for Mw 4.1 and 4.2 earthquakes, respectively. The inversion result of an earthquake of magnitude Mw 4.1 is obtained with the highest values of variance reduction and percentage of double couple results (VR 73.6% and DC 98%), respectively. The respective values of seismic moment and moment magnitude are 1.56E+22 (dyne*cm) and Mw 4.1. On the other hand, the inversion result of the event with magnitude Mw 4.2 is obtained with the highest values of variance reduction and percentage of double couple (VR 83.7% and DC 98.4%), respectively. The values of seismic moment and moment magnitude are 2.72E+22 (dyne*cm) and Mw 4.2. Good waveform fits are obtained between observed and synthetic seismograms at focal depths of 16 and 12 km for earthquakes with magnitudes Mw 4.1 and 4.2, respectively, as all are shown in Table 5.1.

The focal mechanisms of the two events of magnitude Mw 4.1 and 4.2 show normal faulting related to the complex tectonic setting of the Northern Tanzania Divergence Zone (NDTZ) consistent the south of Manyara rift segment. The focal mechanism of the Mw 4.1 earthquake is possibly consistent with NNW−SSE trending to sub E-W extension of the eastern branch of the East African Rift System and the focal mechanism of Mw 4.2 earthquake shows normal faulting slightly with N−S trending under E−W eastern branch of the East African Rift System opening (Fig. 5.8). The two focal mechanisms which have NNW−SSE and slightly N−S trending are

consistent to the Kondoa faults at the north of Kondoa town which are assigned in the southern part of the Lake Manyara in Macheyeki et al., (2008). The focal mechanisms result is in good agreement with the previous results of Brazier et al., (2005); Macheyeki et al., (2008) in the eastern branch of the East African rift system. However, focal mechanisms of earthquakes which have trends in NNE−SSW and NE−SW trends which are consistent with some of the main faults in the region have been reported (Albaric et al., 2014) but quite far from the current study which is towards north direction of Kondoa region.

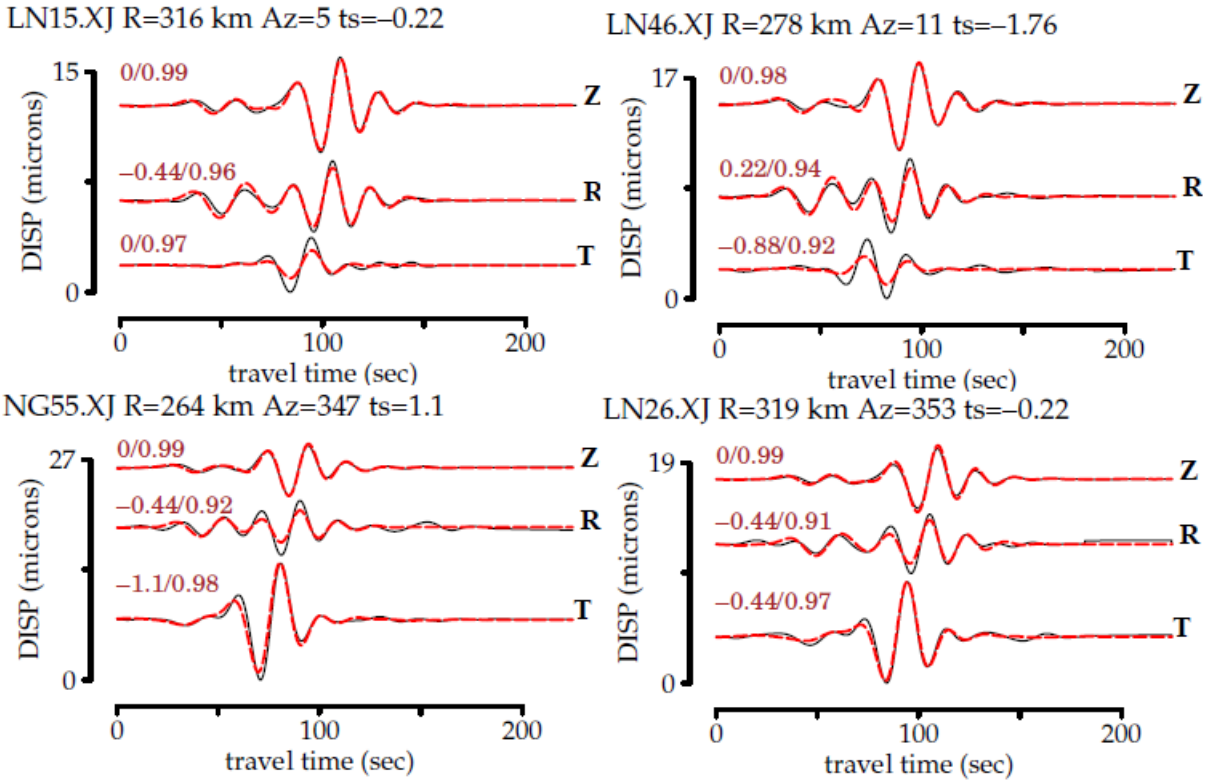


Figure 5.5: Moment tensor inversion result for waveform fits of the observed (red lines) and synthetic seismograms (black lines) displacement waveforms for the preferred focal mechanism deduced at 26 km source depth. The epicentral distance (km) and azimuth (degree) of each station is written above their trace. Z, R, T indicate vertical, radial and transverse components, respectively.

5.4.2 Northern Dodoma region

Here we consider two earthquakes with magnitudes Mw 4.8 and 5.2 that were felt in 2014 for moment tensor inversion. Aftershock distributions are also incorporated for interpretation. Four

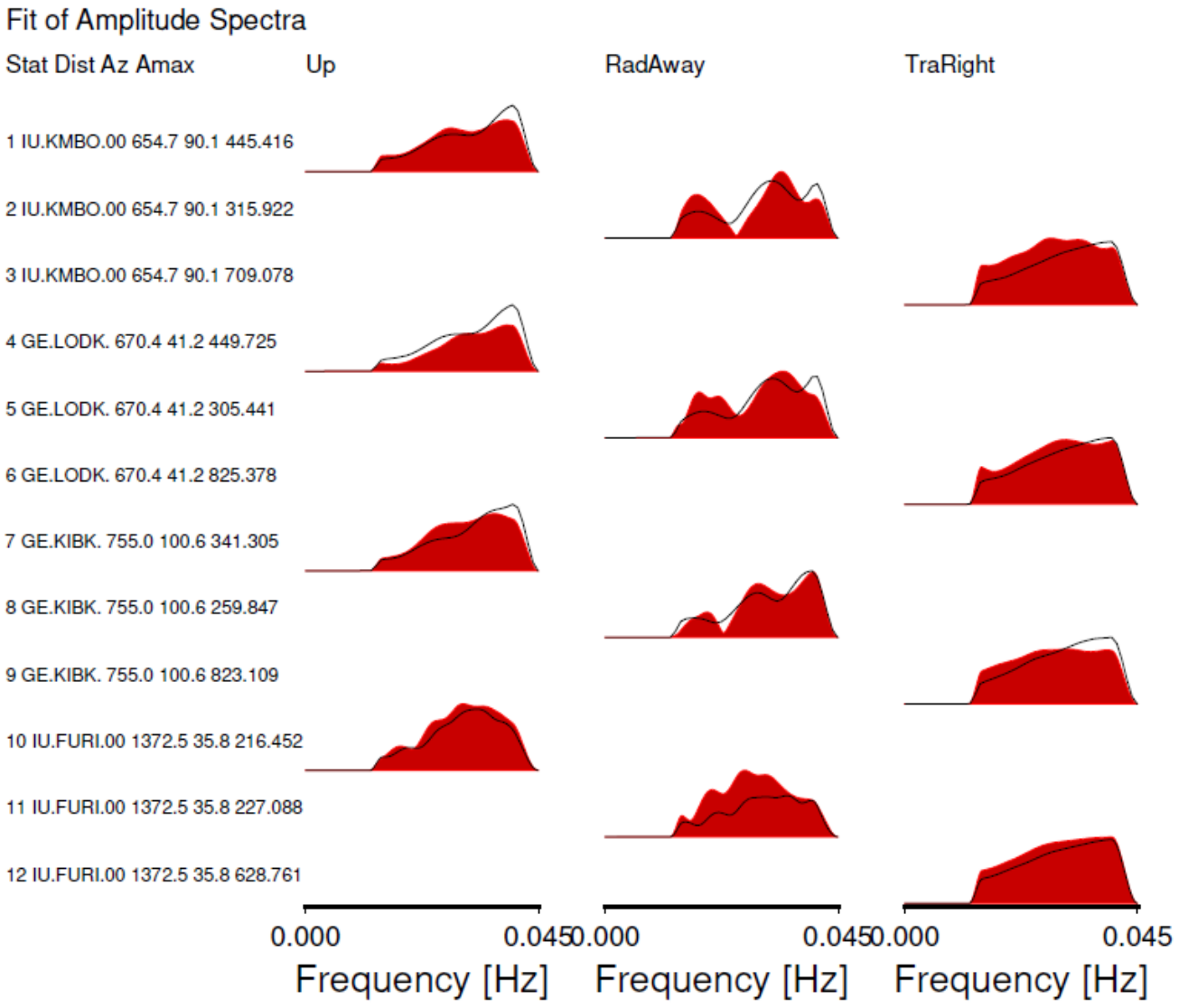


Figure 5.6: Moment tensor inversion in frequency domain for the 2016 Kagera earthquake with magnitude Mw 5.7 for spectra amplitude fit. The panel is dedicated to spectra comparison (red color is used for data, black for synthetics). Stations are sorted on the base of epicentral distances, with station name, distance, azimuth and maximal amplitudes provided on the left side. Up, RadAway, TraRight of each station is written above the fits of data and synthetics.

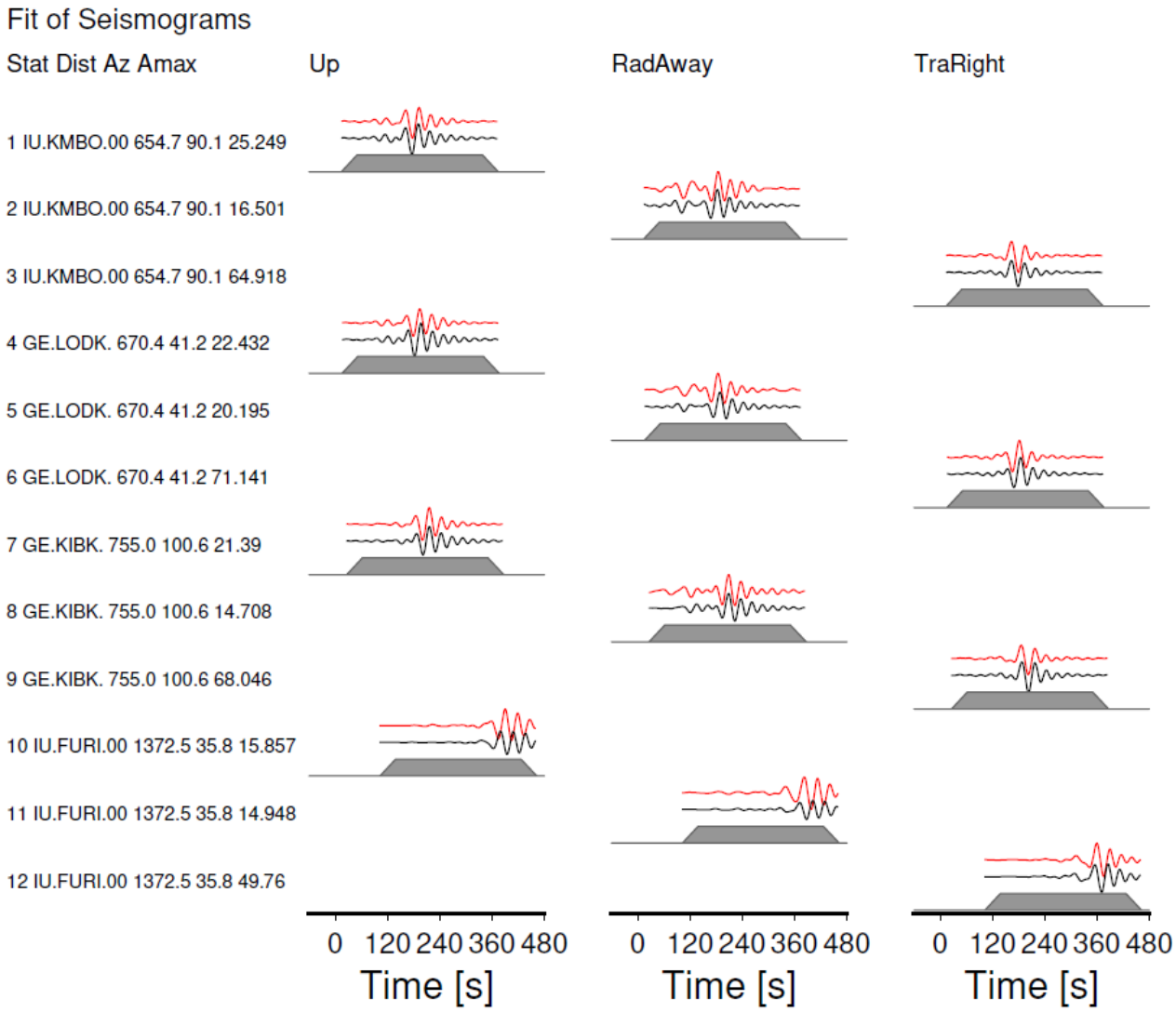


Figure 5.7: Moment tensor inversion in time domain of 2016 Kagera earthquake with magnitude Mw 5.7 for amplitude and phase fits. The panel is dedicated to waveform comparison (red color is used for data, black for synthetics). Stations are sorted on the base of epicentral distances, with station name, distance, azimuth and maximal amplitudes provided on the left side. Up, RadAway, TraRight of each station is written above the fits of data and synthetics.

broadband (three-component) seismic stations are used in inversion for each earthquake. The inversion results for earthquake with magnitude Mw 4.8 are shown as example on Figs. 5.2, 5.4 and 5.5. The reliable source parameters are obtained by plotting the origin time of the event versus depth, for depths range from 2 to 40 km (Figs. 5.2 and 5.4). The inversion revealed reliable source parameters at focal depth of 26 km with -1 s time shift. Our results obtained at the maximum values of variance reduction and percentage of double couple (VR 86.8% and DC 98%) respectively. The seismic moment and moment magnitude obtained are 2.19 E+23 dyne∗cm and Mw 4.8. Similarly, inversion was performed for earthquake with magnitude Mw 5.2. The reliable source parameters of the event are obtained in the maximum values of variance reduction and percentage of double couple (VR 87.2% and DC 98.5%) respectively. The seismic moment value 7.0 E+23 dyne∗cm and Mw 5.2 are obtained. A good waveform fit is obtained between observed and synthetic seismograms at depths of 26 and 14 km for earthquakes with magnitude Mw 4.8 and 5.2 respectively, as results are shown in (Table 5.1).

We interpreted focal mechanisms of the two earthquakes in the region by considering the tectonic setting of the region associated with the distribution of aftershocks of the 2002 Mb 5.5 and the 2014 Mw 5.2 sequences felt in the northern Dodoma region (Fig. 5.8). The region is currently tectonically active as indicated by November 2002 Mb 5.5 earthquake (Yang and Chen, 2010) and the presence of numerous neotectonic features such as the presence of open fractures (Macheyeki et al., 2008). Current kinematics analysis of GPS observations (Saria et al., 2014) also show that the region is active. In the region several moderate magnitude earthquakes have been reported. For example the November 4, 2002, an earthquake of Mb 5.5 struck the northern Dodoma area (Macheyeki et al., 2008). On the other hand, in 2014 earthquakes of Mw 4.8 and Mw 5.2 followed by several aftershocks of this study were felt in the region. An earthquake of magnitude Mw 5.2 event struck the Dodoma region on October 31^{st}, 2014 which was widely felt in several places, though damage was minimal. Therefore, this area is located in seismically very active region but the region has not attracted much attention to seismologists (Macheyeki et al., 2008), hence the estimation of reliable source parameters and the details interpretation of earthquakes in the

region are very crucial. The two Mw 4.8 and 5.2 earthquakes are initiated nearly in the same area with the 2002 Mb 5.5 mainshock (Macheyeki et al., 2008; Yang and Chen, 2010). The main shocks distribution of this study, in the northern Dodoma region are along a broad alignment along the NW−SE similar trend with the aftershocks of the November 4, 2002 Mb 5.5 and the October 31, 2014 Mw 5.2 sequences (Fig. 5.8). The spatial distribution of the aftershocks of Mb 5.5 and Mw 5.2 have similar alignment along NW−SE.

The fault plane solutions of the 2014 earthquakes with magnitude Mw 4.8 and 5.2 computed from moment tensor inversion of this study show normal faulting with significant strike-slip or oblique slip components. The slip directions are oriented in NW−SE and NE−SW depending on which nodal planes chosen as a fault plane. The NE−SW nodal plane is chosen as auxiliary plane that has no structural significance on the area, whereas the nodal plane along NW−SE trend is chosen as fault plane which pursuit with the distribution pattern of aftershocks of the 2002 Mb 5.5 and 2014 Mw 5.2 sequences. The mechanisms interpretation of these two events emphasis that the study area is dominated by N-S oriented normal faults and NW−SE oriented strike-slip which is in agreement of the counterclockwise rotation of Victoria microplate relative to Somalia plate (Calais et al., 2006b; Déprez et al., 2013; Saria et al., 2013, 2014; Stamps et al., 2008, 2018). Therefore, the mechanisms of these events indicate a complicated stress pattern with possible sense of dextral strike-slip motion. From the aftershocks distribution and source mechanisms, we confirm and illustrate that rift faulting and active deformation ongoing in the northern Dodoma region, probably resulted from the counterclockwise rotation of Victoria microplate within the circum-Tanzania Craton.

5.4.3 Kagera region

There is only one earthquake considered for the moment tensor inversion in this group. For this particular event of magnitude Mw 5.7, we used waveform data from four broadband (three-component) seismic stations for inversion both in time and frequency domains. Reliable source parameters have been obtained for the 2016 Kagera earthquake of magnitude Mw 5.7 that felt

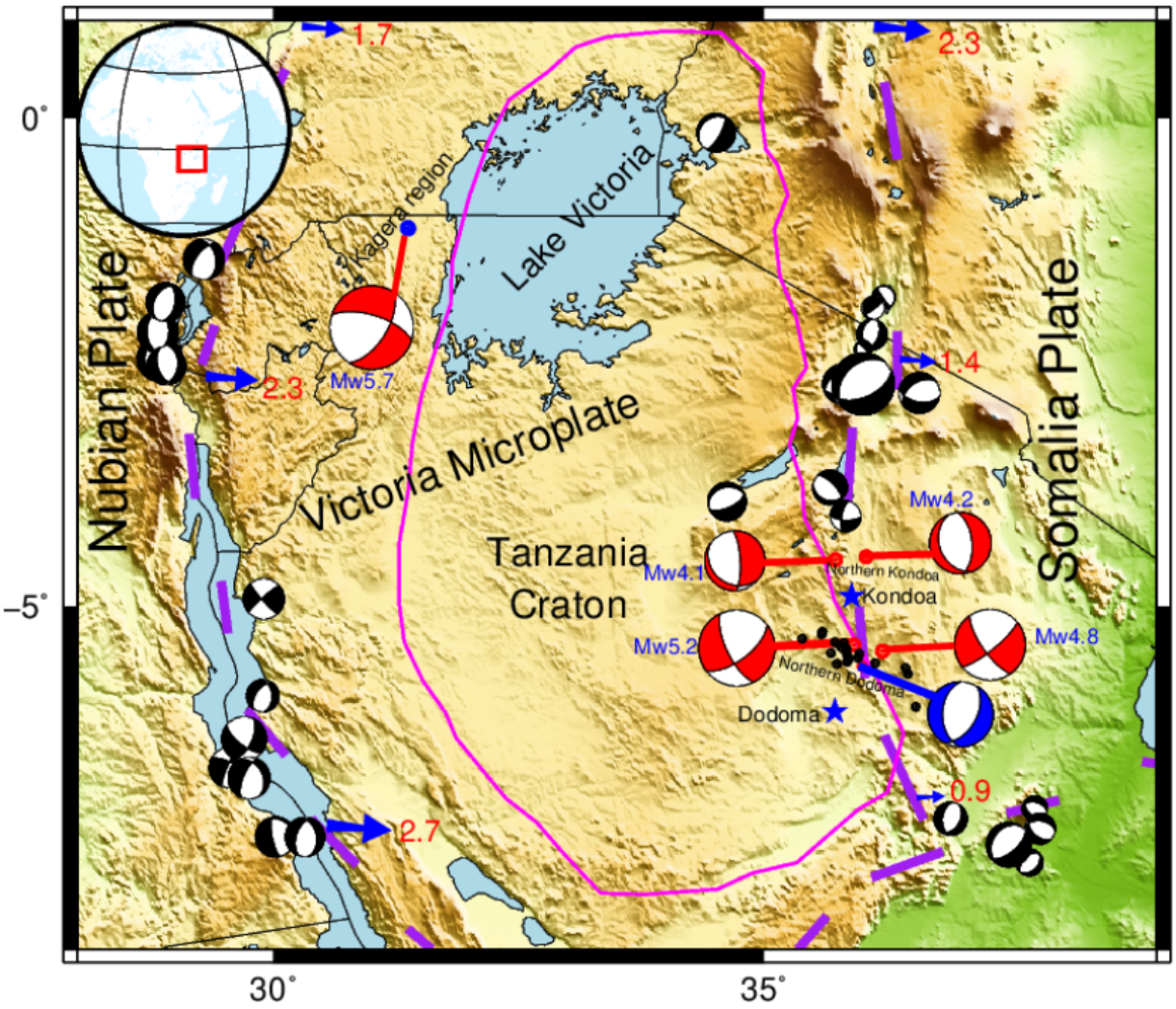


Figure 5.8: Plots of five earthquakes fault plane solutions determined in this study and previous studies. The red and white beach balls are mechanisms of earthquakes from moment tensor inversion of this study, black and white beach balls are mechanisms from Brazier et al., (2005); Mulibo and Nyblade, (2016); Weinstein et al., (2017) and GCMT solutions, while the blue and white is mechanism of the 2002 Mb 5.5 main shock (Yang and Chen, 2010). The size of beach ball is proportional to the magnitude of earthquake. Color coded circles show the epicenters of the four earthquakes that felt in 2014 (red), the 2016 Kagera earthquake (blue) and aftershocks of Mw 5.2 and Mb 5.5 (black) sequences. The purple dashed lines indicate the boundaries of the Victoria microplate (Stamps et al., 2008). The blue vectors represent surface motion velocities in mm/yr (Saria at el., 2014). Blue stars: the two major towns of Tanzania.

in Kagera region at good spectra amplitude fit between observed and synthetic seismograms. We obtained good amplitude and phase fits (Figs. 5.6 and 5.7) between observed and synthetic seismograms. Seismic moment (M0 4.91E+20 dyne*cm), moment magnitude (Mw 5.7) and focal depth (20.9 km) have been obtained (Table 5.1). The well-constrained focal source depth of this event shows a shallow oblique faulting within the thick lithosphere in the eastern branch (Nyblade and Langston, 1995; Mulibo and Nyblade, 2009; Yang and Chen, 2010). There were few instrumentally recorded earthquakes occur in the Kagera region of the circum-Tanzania Craton which can be possibly due to longer return period of large magnitude earthquakes and lack of station coverage to capture small magnitude earthquakes. Thus, earthquakes focal depths in the region have been not well-studied and the detail source parameters reported from the previous studies not available. Even different focal depths have been reported by several agencies for this earthquake of magnitude Mw 5.7. Therefore, the reliable source depth result of this study might be improving various confusing results reported by several agencies and might be used as an input for future study.

In the surrounding of circum-Tanzania Craton a combination of normal and strike-slip faulting with sinistral motion have been observed along the boundary between the Victoria and Ruvuma microplates (Mulibo and Nyblade, 2016) which are resulted from the clockwise rotation of the Ruvuma microplate (Calais et al., 2006a, 2008; Stamps et al., 2008; Saria et al., 2013, 2014). On the other hand, focal mechanisms of earthquakes with left and right-lateral strike-slip were observed from stress inversions (Delvaux and Barth, 2010) in the western branch of East African Rift System. Therefore, the 2016 earthquake in Kagera region with magnitude Mw 5.7 of this study likely resulted from the counterclockwise rotation of the Victoria microplate relative to Nubian plate with dominantly normal faulting with strike- slip component (Fig. 5.8). The focal mechanism result indicates a complicated stress pattern with the two nodal planes oriented NNE−SSW and WNW−ESE. The nodal plane oriented along NNE−SSW possibly chosen as auxiliary plane, whereas striking along WNW−ESE direction with possible dextral sense of motion is chosen as fault plane which might be consistent to counterclockwise rotation

of the Victoria microplate (Saria et al., 2013, 2014) and regional tectonic setting of the area. Thus, focal mechanism of this earthquake shows dominantly normal faulting with strike-slip component in WNW−ESE trending with the dextral sense of motion. The interpreted fault orientation for the Kagera earthquake seems to agree with macroseismic information and aftershock distribution which were recorded by seismic stations deployed immediately after the main shock (Mulibo, 2019) where macroseismic orientation might be influenced by site effects while the aftershock distribution is too far to claim association.

Most of the previous studies about the present-day tectonic stress in the Northern Tanzania Divergence Zone to Dodoma have been studied by using earthquakes focal mechanisms that are available from different sources (e.g., Harvard Centroid Moment Tensor catalogue; Brazier et al., 2005). However, the available focal mechanisms of earthquakes in the region are might be not sufficient to study the details of the tectonic stress of the region. Therefore, the well estimated results of focal mechanisms of this study might be used as an input for further study. Furthermore, from the seismicity distribution and moment tensor inversion results, this study confirms that the tectonically deformed of the circum-Tanzania Craton seems to be seismically very active. Even though few earthquakes are analyzed, the focal mechanisms and the trend of aftershocks distribution may indicate the propagation direction of the eastern branch is southeasterly along the northern boundary of the Ruvuma microplate towards the coast (O′Donnell et al., 2013; Mulibo and Nyblade, 2016). It′s also possible for the southern link between the eastern and western branches of the EARS to the southeast of the Tanzania Craton along the Maminzi transverse fault zone, Kilombero and Ruhuhu rifts (Le Gall et al., 2004).

CHAPTER 6

Deep Rupture Process of the 3rd of April, 2017 Botswana Earthquake

6.1 Introduction

The African continent is a tectonic plate with diverse geological domains that include seismically active and aseismic regions where the seismic activity is mainly characterized by earthquakes with shallow depths of 0-70 km (Adagunodo et al., 2018). The part of the continent, the East African Rift System (EARS) has been the site of occurrence of small to large magnitude earthquakes for many years (Shudofsky, 1985; Nyblade and Langston, 1995; Nyblade et al., 1996; Foster and Jackson, 1998; Langston et al., 2002; Weeraratne et al., 2003; Kim et al., 2009; Yang and Chen, 2010; Albaric et al., 2010, 2014; Ayele et al., 2007, 2016; Isola et al., 2014). In particular the Botswana region has been the site of several small to moderate earthquakes (Fig. 6.1; Nthaba et al., 2018) with different tectonic settings (Figs. 6.1 and 6.2). The April 3, 2017 Botswana earthquake of magnitude Mw 6.5 has occurred within the Paleoprotozoic Limpopo Orogenic Belt, a tectonic area involves a collisional suture between the Kaapvaal and Zimbabwe Cratons (Khoza et al., 2013), which is a region of geologic province with historically low seismic activity (Stamps et al., 2014).

The April 3, 2017 Botswana earthquake struck central Botswana and the shaking was felt in different neighboring countries with Modified Mercalli intensities of VI (Midzi et al., 2018) was estimated. The event is unique and drew attention as its occurrence is quite far from the frequent locations of earthquakes in the EARS over a period of time. Major historical earthquakes recorded in Botswana are mainly located north of the April 3, 2017 Botswana main shock near

Okavango Delta Region (ODR) where the young arm of the EARS is developing and thought to be an incipient rift (Modisi, 2000). Previously, the region has been rocked by the 11^{th} of September and 11^{th} of October 1952 earthquakes with magnitudes are of 6.1 and 6.7 ML (Nthaba et al., 2018), respectively.

The April 3, 2017 Botswana earthquake has been investigated in many studies using various methods which ended with different interpretations. The geometric and kinematic characteristics of the causative fault were estimated from the modeling of Sentinel-1 InSAR interferograms and the best-fit solution for the main shock was represented by a normal fault located at a depth greater than 20 km and classified the event as a natural intra-plate earthquake (Albano et al., 2017). Gardonio et al., (2018) proposed a reservoir of elastic stress that can be released episodically, as a result of deep fluid migration for the event at the depth of 29 $\pm$ 4 km, likely requires a transient pulse of fluids from a deep source to activate brittle faulting. On the other hand, Moorkamp et al., (2019) suggested the event may be a sign of future activity, controlled by the collocation of a weak upper mantle and a weak crustal structure using a result of an integrated geophysical study. Moreover, Materna et al., (2019) attempted to generate synthetic waveforms in the time domain from teleseismic broadband waveform, and suggested that the event appears to have occurred in an ancient zone of weakness.

Earthquake source characterization is challenging due to poor understood earthquake source investigation in the Botswana region. Studying such a large earthquake of the 3^{th} April, 2017 of Mw 6.5 Botswana earthquake may help to refine estimates of source parameters and expand our understanding of a reliable hypocentral depth of the event in a region where present-day deformation is believed to be negligible, which implies unusually deeper hypocentral depth. The April 3, 2017 Botswana earthquake is relatively deep which has never been observed before in the earthquake history of the region. An accurate hypocentral depth estimation of an earthquake is a critical parameter for understanding the tectonics and evaluating earthquake hazards of a region in the context of the occurrence of great earthquake. However, hypocentral depth estimation of an earthquake is usually the most difficult to nail down with great accuracy. Thus,

techniques used in order to determine earthquakes depths (Maggi et al., 2000) should be improved. Therefore, the main purpose of this effort is to obtain reliable source parameters of the April 3, 2017 Botswana main shock using a mixed approach moment tensor inversion. The result of this study will provide a base for earthquake disaster risk reduction research potential involving assessment for the future damaging earthquake to contribute in the minimization of loss of human life, property damage, and economic disruption attributable to earthquakes in the region.

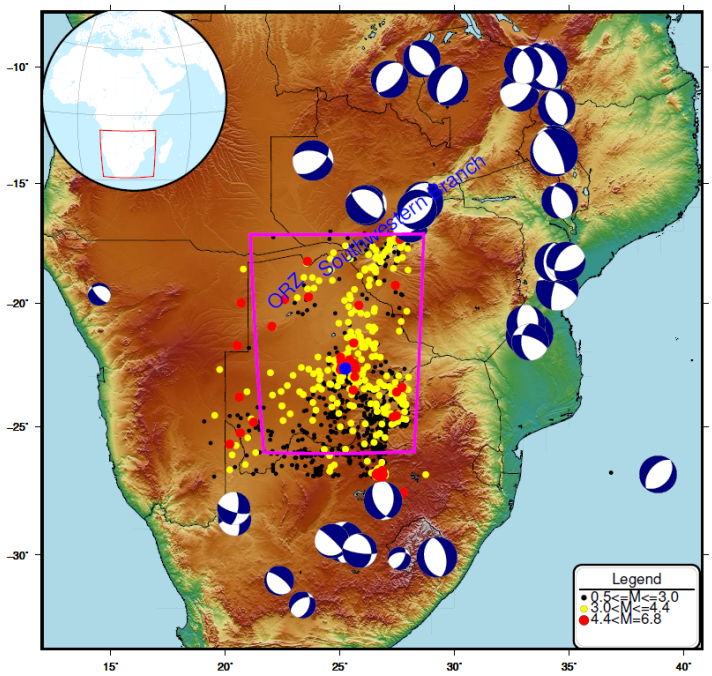


Figure 6.1: Seismicity of the Botswana with (earthquake magnitudes in the range of 0.5 to 6.8) for the time period 2000 to 2017 compiled from the ISC catalog. The region is dominated by lower magnitude earthquakes within the range of 0.5 to 3.0 and the southern part of the study area is seismically active as compared to the other parts of the region. Different color circles (black, yellow and red) show the epicenters of earthquakes where circle size is proportional to earthquake magnitude as shown in the legend. The large blue circle is the location of the April 3, 2017 Botswana main shock. The magenta box on the map shows the study area.

6.2 Geological and tectonic setting

The EARS propagates southward direction through Ethiopia (Beyene and Abdelsalam, 2005) then forms two main rifts; the eastern and western branches. Furthermore, the third branch of the EARS which is called the southwestern branch (e.g., Girdler, 1973; Chapman and Pollack, 1974; Ballard et al., 1987; Modisi, 2000; Scholz and Koczynski, 2007; Mosley et al., 2012) propagates towards southwest direction in Botswana. It's NE−SW trending faults have similar orientation with Lake Kariba (Figs. 6.1) and the localized seismic activity led many authors since the late 1960′s to be considered as the final extension of the EARS. Therefore, the southwestern branch of the EARS is believed to be as an incipient rifting zone (Modisi, 2000; Scholz and Koczynski, 2007; Mosley et al., 2012).

The basement of the Botswana geology is dominated by complex tectonic inheritance of early Archean Cratonic blocks and Belts (Fig. 6.2). The well-known three major Cratons are the Congo, Zimbabwe and the Kaapvaal Cratons. Thus, the diverse tectonic features of the region encompasses the Kaapvaal, Zimbabwe and the Congo Cratons (Fadel et al., 2018) with several mobile belts found in the region; the Limpopo, Magondi, and Damara Belts (Key and Ayres, 2000). The main provinces of the ORZ and the current study area are sandwiched between the Neoproterozoic Congo Craton to the northwest (Yu et al., 2015), the Kaapvaal Craton in the south, and Zimbabwe Craton in the east−southeast (Fig. 6.2.; Kinabo et al., 2008; Begg et al., 2009) respectively. Most of the Botswana region is dominated by the basement rocks of the Kaapvaal and Zimbabwe Cratons that are extending in the east and southeast with metamorphic rocks of Archaean age and Limpopo Belt (McCourt et al., 2004). The collision between the Kaapvaal and Zimbabwe Cratons during late Archean caused dominant planar surface along the Limpopo Belt (Roering et al., 1992). The Limpopo Paleoproterozoic orogenic Belt encloses a lithospheric scale suture zone resulted from the collision of these two Cratons. It′s a Neoarchean orogenic belt which has a width of 250 km and 600 km length that located between, the Zimbabwe Craton to the north and the Kaapvaal Craton to the south (Ranganai

et al. 2002).

The current study also focuses on the April 3, 2017 Botswana earthquake of Mw 6.5 that has occured within the Paleoprozoic Limpopo Orogenic Belt (Fig. 6.2). The Cratonic margins and some intra-cratonic domains boundaries may have a major role in the tectonics of the region. Boundaries may have localized successive cycles of extension, rifting, and the ongoing development of the East African Rift. On the other hand, uplift topographic feature of the region has been affected by African Superswell (Brandt et al., 2012). Thus, the African Superswell is responsible for the cratonic movement resulted in the formation of southern African tectonic region with the major axis in Botswana and Zimbabwe (Begg et al., 2009).

The southwestern branch of the EARS and Botswana region are one of the least studied areas in the African continent as compared to the other parts of regions with diverse tectonic features and several mobile belts which may the cause of earthquakes in the region. Earthquake distributions can be found in several parts of the region mainly in the mobile belt area like ODR. The historical earthquakes of 1952 were occurred within the Okavango Rift Zone at the end of the southwestern branch of the East African Rift System (Modisi, 2000). A relatively high level of seismicity distribution within the Okavango Rift Zone suggests rifting in the Bostawana is due to the extension of the EARS. The initiation and early-stage development of the rift are mostly due to lithospheric stretching resulted from the relative motion between the Archean Congo and Kalahari cratons along preexisting ancient orogenic zones (Yu et al., 2016).

Majority of the largest earthquakes in the African continent are concentrated towards the nearest tectonic plate boundary where the continent is pulling apart due to the EARS. Botswana region does not show any strong earthquakes in instrumented history, the clustering of small magnitude events in the Okavango Delta has led to speculation of an incipient rift in the ORZ (Leseane et al., 2015) which may represent the southwestern continuation of the EARS (Fadel et al., 2018). However, the April 3, 2017 Botswana main shock shows a resulted earthquake from normal fault pulling apart roughly in NE-SW direction which is unique from trends of earthquakes focal mechanims within the East African Rift System.

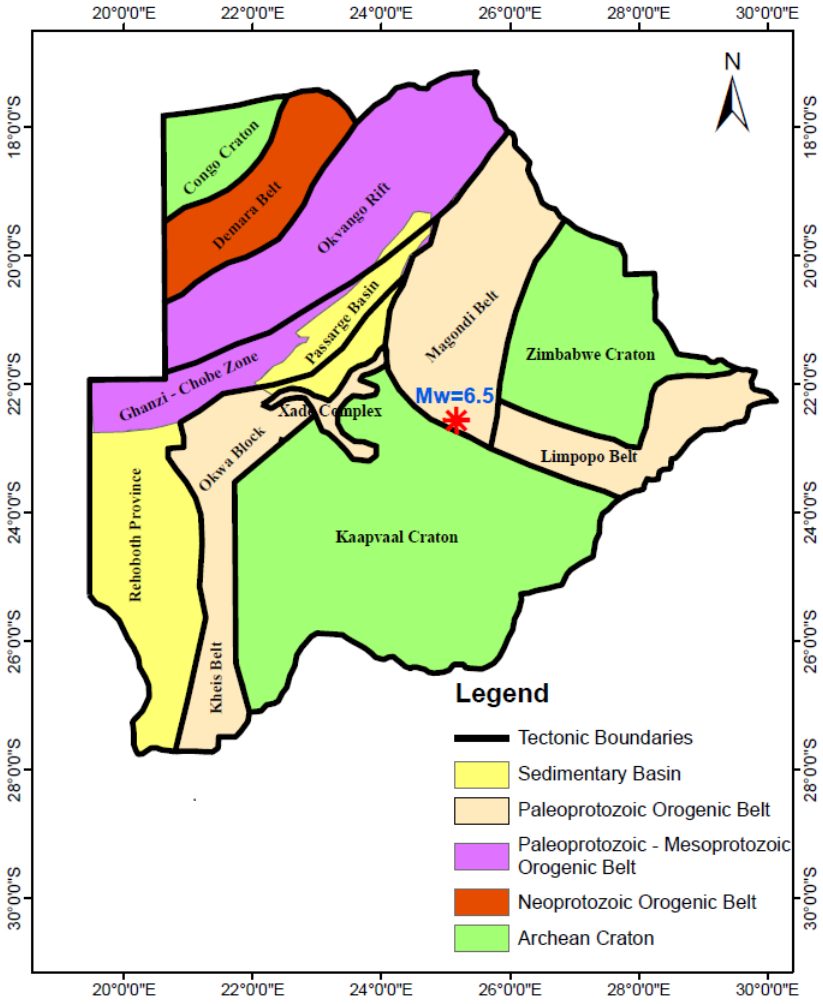


Figure 6.2: An overview of the tectonic and geologic map of Botswana and its surroundings. The epicentral location of the April 3, 2017 Botswana earthquake of Mw 6.5 is shown by red asterisk. Black lines represent the tectonic boundaries from Fadel et al., (2018) modified after Singletary et al. (2003) and McCourt et al., (2013). Geologic map of Archean Cratons and Proterozoic Orogenic Belts in Botswana and surroundings are after Leseane et al., (2015).

6.3 Data and Method

In this study three-component broadband waveform data and instrument response information were obtained from the Data Management Center of the Incorporated Research Institutions for Seismology (IRIS DMC) for all of the stations at regional distances which successfully recorded the April 3, 2017 Botswana earthquake. We selected six broadband seismic stations with high

quality waveform data (e.g., Fig. 6.3) located at various azimuths and distances from the source. We applied the approach developed by Cesca et al., (2010) to estimate source parameters of the April 3, 2017 Botswana earthquake of magnitude Mw 6.5. We used moment tensor inversion in both frequency and time domains. To illustrate the approach, we used a combined fit of amplitude spectra and phases at regional distances. We generated synthetic seismograms in both time and frequency domain and compared to the observed seismograms. The reliable source parameters of the event were extracted at the best fits between synthetic and waveform data using the bandpass filtering range from 0.02 to 0.05 Hz. We calculated our uncertainty with an error misfit of L2 norm which is equal to $sqrt((d-s)**2)$, where d are data and s are synthetics. For amplitude spectra inversion, we used regional waveforms and applied bandpass filtering to waveform data to fit amplitude spectra, instead of the classical one in the time domain. An amplitude spectra inversion has advantages than in the time domain inversion (Dahm et al., 1999; Cesca et al., 2006). This technique is less sensitive to a precise trace alignment and phase shifting owing to mismodeling of the crustal structure (Cesca et al., 2010) and it is very helpful to serach more precise source depth estimation because in the inversion procedure the fitted result is only amplitude spectra. In the time domain inversion, we used the same bandpass filtering range as for the amplitude spectra inversion. Both the amplitude and phase fits of the seismograms have been considered in this inversion technique. After the inversions, the values of strike, dip, rake, and hypocentral depth are estimated. Two indicators were identified and considered in an evaluation of the quality of solutions. The first indicator was the misfit value that reflects the quality of the solutions. The best solution of the inversion assumed to be the lowest misfit. The second indicator was relative misfit curves for strike, dip and rake perturbations. This stability indicator prefers solutions, for which a common perturbation of strike, dip or rake angles will induce a major variation of the misfit values. An example of the three-component waveform data recorded on seismic station SOE that were used in the inversion for the April 3, 2017 Botswana earthquake of magnitude Mw 6.5 is plotted in Figure 6.3.

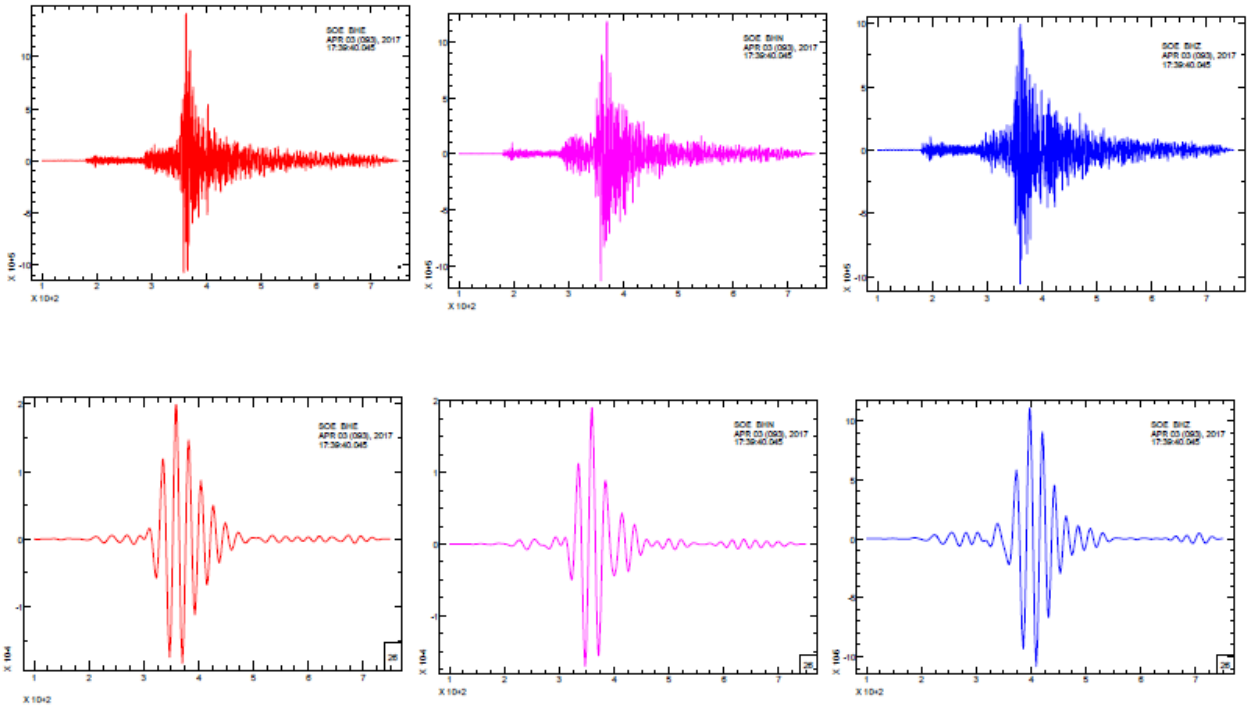


Figure 6.3: Seismograms of the April 3, 2017 Botswana main shock recorded at SOE seismic station. a) The raw data for three-component seismograms. b) The three-component seismograms filtered at bandpass filtering range from 0.02 to 0.05 Hz (after instrument response removed) which are used in inversions. E, N, Z indicate (E-W), (N-S) and vertical components respectively.

6.4 Results

After conducting the moment tensor inversion for the April 3, 2017 Botswana earthquake, the hypocentral depth, which is of 38.4 km, has been estimated with an error misfit of 0.296 (L2 norm misfit sense). The moment magnitude of Mw 6.5 was estimated for the event which is consistent with the magnitude estimated by the Global CMT Mw 6.5 solution. The extensional normal fault plane solution is obtained from the inversion in both frequency and time domains. A good waveform fit is obtained for the observed and synthetic seismograms in both inversion techniques (Figs. 6.4 and 6.5). The extracted source parameters are shown in Figs. 6.6; 6.7.

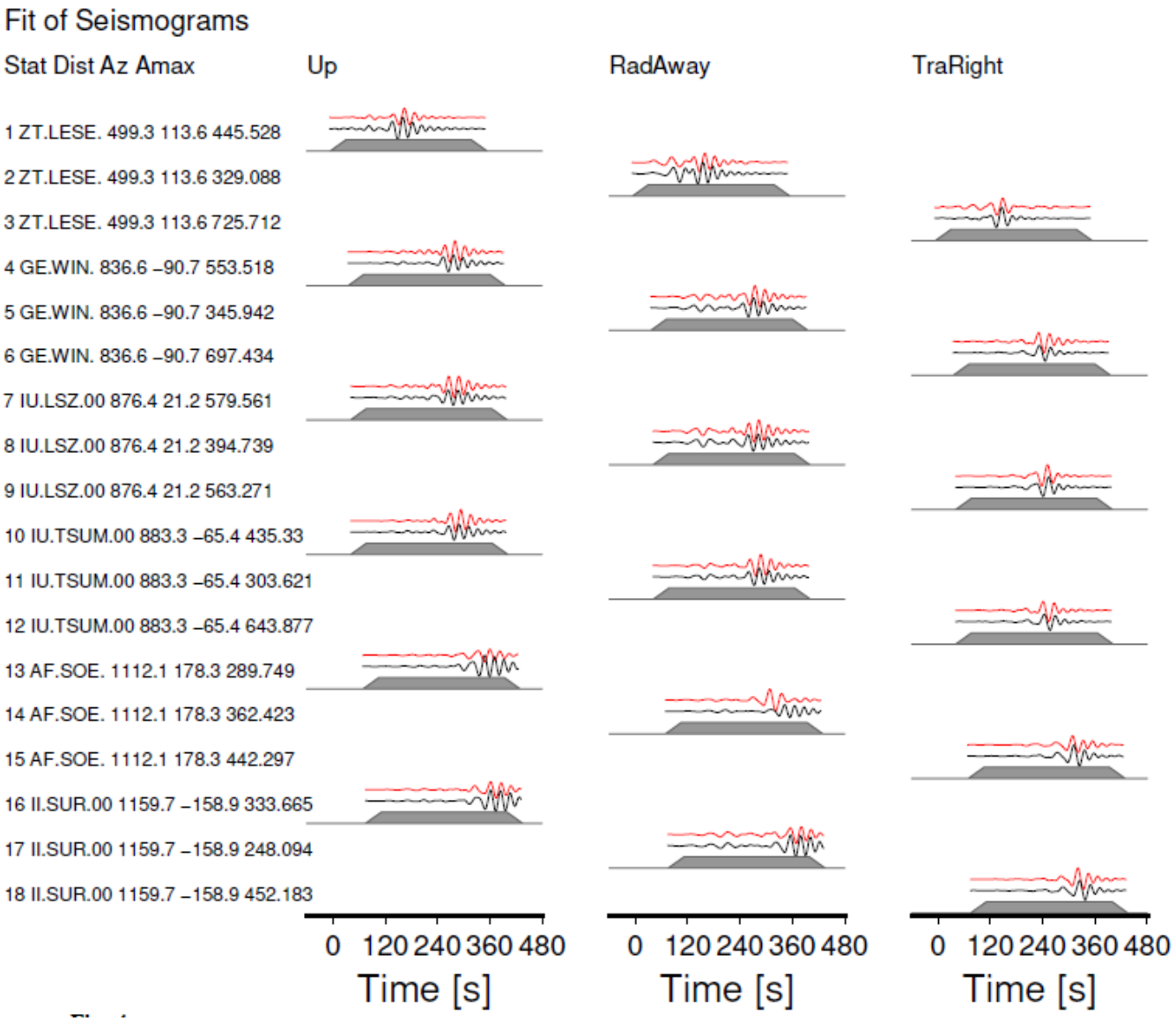


Figure 6.4: Regional waveform fits of the April 3, 2017 Botswana main shock using moment tensor inversion in the time domain. The panel is dedicated to waveform comparison (the red color is for data, black is for synthetics). Stations are sorted according to epicentral distances, with station name, distance, azimuth and maximal amplitudes provided on the left side.

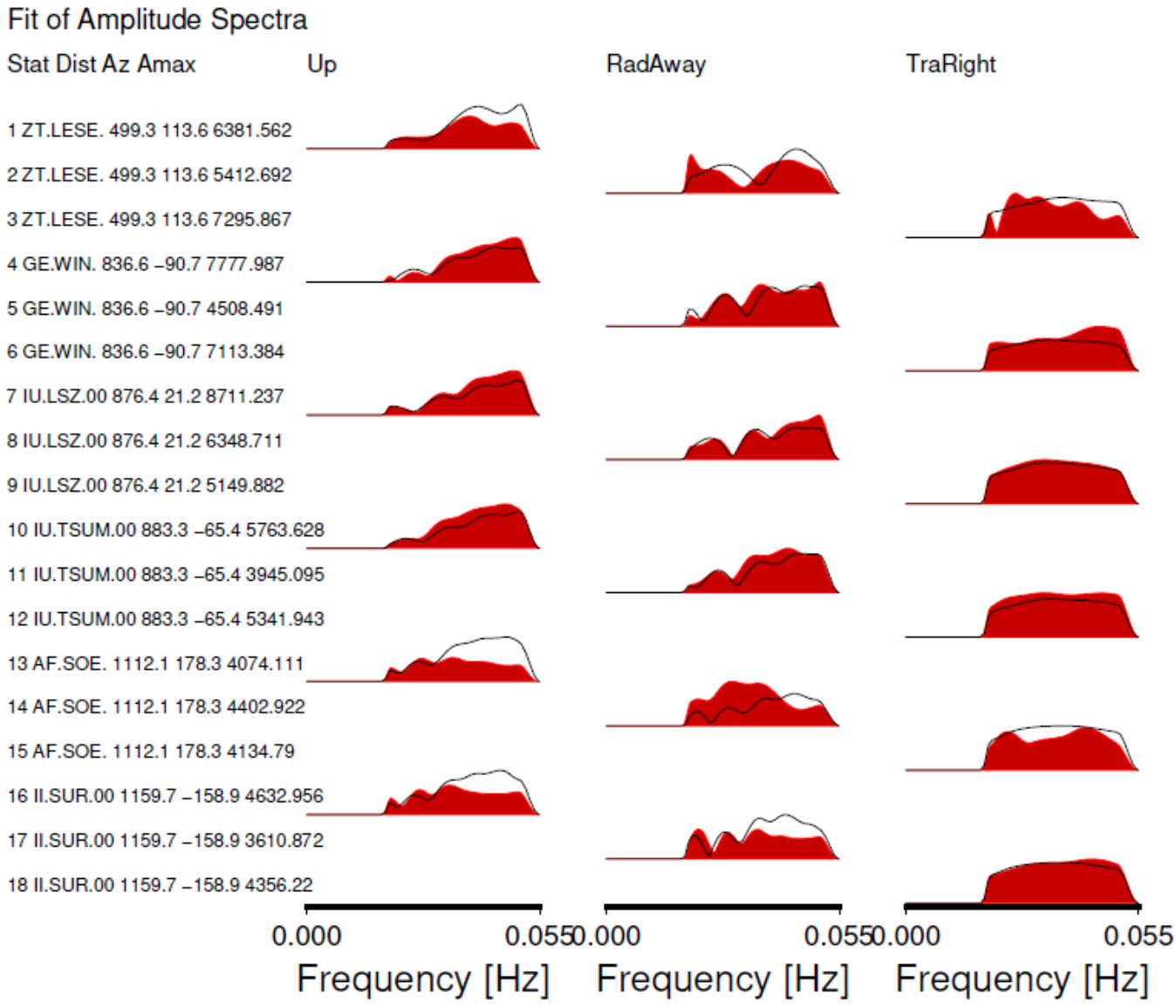


Figure 6.5: Spectra amplitude fits of the April 3, 2017 Botswana main shock using moment tensor inversion in frequency domain. The panel is dedicated to spectra comparison (the red color is for data, black is for synthetics). Stations are sorted based on epicentral distances, with station name, distance, azimuth and maximal amplitudes provided on the left side.

6.5 Discussion

The over all distribution of aftershocks (Fig. 6.8) of the April 3, 2017 Botswana earthquake roughly show NW−SE trending, consistent with the trend of the focal mechanism of the main shock (purely normal faulting) with extension. The southward propagation of the EARS extends to the southwest into Botswana where it forms a southwestern branch (Modisi, 2000) towards the ORZ and weakness zones initiate strain, when coupled with favorable plate kinematics can lead to continental break-up.

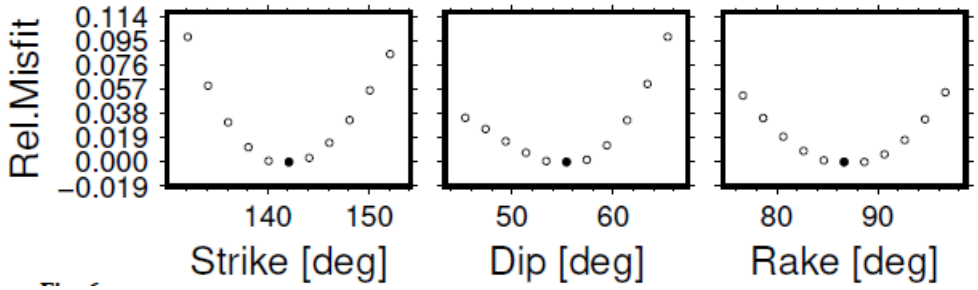


Figure 6.6: The relative misfits (illustrate how our misfit increases when we perturb one single parameter) versus Strike, Dip and Rake angles for the fault plane solution estimated using moment tensor inversion and obtained at a hypocentral depth of 38.4 km. The bold black dots represent the values at which the three angles are selected from the minimum variance.

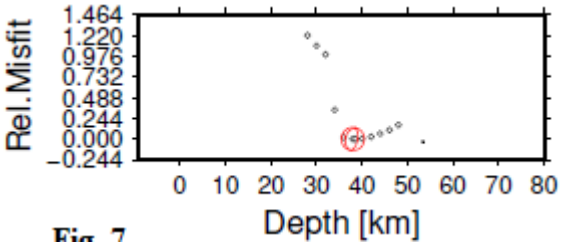


Figure 6.7: Relative misfits versus hypocentral depths of the April 3, 2017 Botswana earthquake of magnitude Mw 6.5 computed from the moment tensor inversions. The best solution has been chosen at smallest misfit for the hypocentral depth (38.4 km).

Thus, the ORZ contains a rift related faults and a zone of extensional faults (Kinabo, 2007) that might be responsible for seismicity of the region. On the other hand, the low velocity anomaly observed at the upper mantle beneath the EARS (Adams et al., 2012) seems to affect the crust through weak low velocity zones at the Okavango Rift Zone and the border of the Kaapvaal

Craton.

Therefore, we believe that the extension of the East African Rift System until the border of the Kaapvaal Craton (Yu et al., 2016) might be the cause for the occurrence of the large April 3, 2017 Botswana earthquake of magnitude 6.5 Mw with its NE−SW extensional focal mechanism. The well-constrained hypocentral depth of the event is estimated to be at 38.4 km, near the lower crust and the upper mantle boundary. The source is reflecting relatively a deep hypocentral depth that is rare in the occurrence of earthquakes in the EARS. In a previous study Moorkamp et al., (2019) suggests the crustal and mantle weak zones control seismicity of the 2017 Botswana earthquake sequence using the result of geophysical evidence. The Okavango Rift Zone is at the developmental stage of continental rifts in which the pre-existing rift structures are strongly controlling the linking rift basins (Ring, 1994). Therefore, a relatively deep hypocentral depth of this study may suggest the reactivation of pre-existing NW−SE trending geological structure or from the early rift faults within the stress region during rift initiation beneath the area.

On the other hand, most of large magnitude earthquakes occur at plate boundaries where a stress and strain concentration is believed to pose a significant threat to human lives and infrastructure. However, quite a low value of maximum intensity values of VI (according to the Modified Mercalli Intensity scale) was estimated, but the epicentral region is expected in a national park which is sparsely populated (Midzi et al., 2018). But here, we present a striking feature of the event is its deep depth that suggests the event may be a sign of future activity. Therefore, we believe that the hypocentaral deep is from a weak upper mantle and weak lower crust that might be a reason for low intensity value. Our suggestion may supports a hypothesis of the fluid leaks from the upper mantle have triggered the event (Gardonio et al., 2018), as the lower crust thickness of the area is around 35 km thick (Tedla et al., 2011; Youssof et al., 2013). The Mw 6.5 Botswana earthquake is one of the largest instrumentally recorded events within the Botswana territory, though the event caused little to no damage, but its effect was felt over a wide area, might be due to the deep hypocentral source of the event.

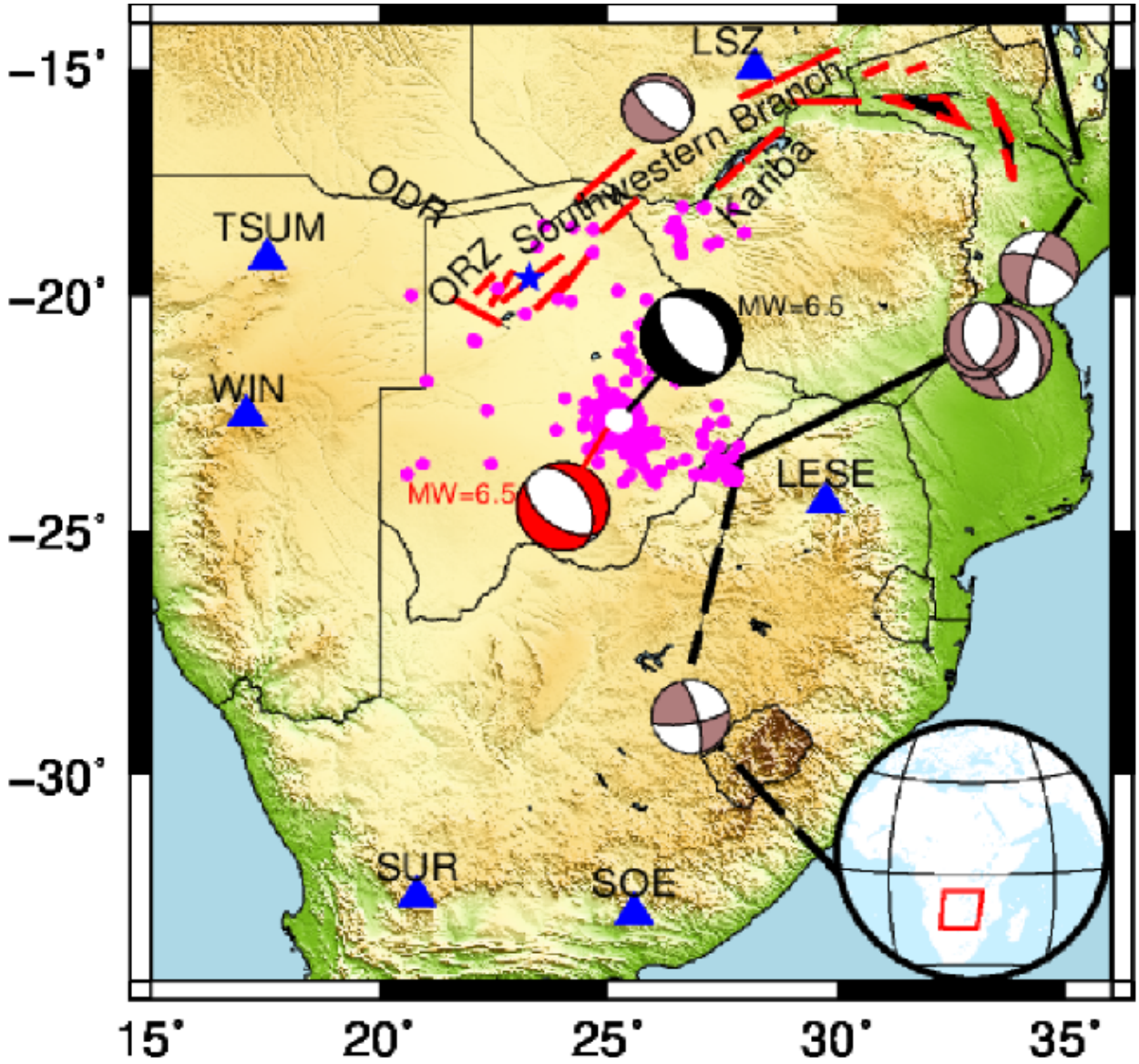


Figure 6.8: Focal mechanism of the April 3, 2017 Botswana main shock (black and white color beach ball) and its aftershocks distribution. The white dot represents the location of main shock and magenta dots represent the epicenter location of aftershocks. The blue triangles represent the seismic stations used and the blue star is the location of historical earthquakes of the 11^{th} of September and 11^{th} of October 1952 earthquakes with magnitudes of 6.1 and 6.7 ML. The red and white beach ball is the focal mechanism for 2017 Botswana main shock from GCMT solution while pink and white are for some earthquakes from GCMT solutions. Broken red lines represent the fault system of the Okavango Rift Zone (ORZ) and Southwestern Branch, ODR represents Okavango Delta Region modified from Kinabo, (2007). Heavy black lines represent plate boundaries modified from Bird, (2003). Inset map shows the study area.

CHAPTER 7

Conclusions and Recommendation

The current study focuses on the recent seismicity for the period 2013 to 2016 and rupture process of some selected earthquakes across the different tectonics regimes of the EARS. The seismically and volcanically active area of the EARS drew an interest on several researchers to conduct research on the current understanding of the seismic activity of the region. Currently, the region is a characterized by earthquake sequences and demonstrated by several seismic crisis from time to time. The region is located in seismically active areas and a site of a few large magnitude earthquakes, the systematic way of detecting the occurrence of earthquakes down to lower magnitude and determination of source parameters of regional earthquakes are generally poorly understand due to sparsely distributed seismic networks and owing to lack of the proper techniques used in the region. In addition, a gap in the International database suggests a need for a further investigation to show a clear seismicity picture of the region.

Therefore, in this dissertation we combined earthquakes waveform data from permanent seismic networks, AfricaArray networks, local permanent seismic networks (Ethiopian Seismic Network) and some temporary seismic networks deployed in the region to improve our current understanding of seismic activity and the source parameters of earthquakes in the region. We analyzed earthquake location from phase picking of P-and S-wave arrival times recorded on three or more seismic stations with a reasonable error. In this investigation different works have been organized in different chapters and concepts, mainly the results of chapter four to chapter six. Chapter four is submitted for publication and under review, chapter five is already published and chapter six is accepted after revision.

In this investigation three different works have been conducted. In the first part of the thesis, we have tried to investigate the recent seismicity of the EARS (Afar, main Ethiopian rift, Southern-Sudan, western and eastern branches) for the period of 2013 to 2016. Spatial and temporal distribution of earthquakes in the EARS has been investigated for the years 2013 to 2016. The part of the EARS which is considered in this study have small to moderate magnitudes earthquakes Ml 1.3 to 6.2. Seismicity of the region is concentrated along active spreading rift segments and active faults. A relatively high level of seismicity has been obtained in this study compared to the International Seismological Centre catalogue database for the same time period which implies the region is seismically more active than we thought. This might be due to the recently expanded network and good monitoring system used in this study. Results of this study could be handy in an attempt to achieve a better picture of seismicity of the EARS and probably has a positive contribution towards hazard mitigation of the region for the future works.

In addition to the rift floor, the rift margins and the surroundings plateaus are found to be seismically active. It has been observed that certain rift segments are characterized with higher seismic activity. For example the western and eastern branches of the East African Rift System are experiencing the most seismic activity of the EARS for the time period considered. The spatial earthquakes distribution in the time window considered has revealed that the main Ethiopian rift is structurally connected to the eastern branch of the East African Rift System but southwards of the Northern Tanzania Divergence Zone, it is difficult to suggest the direction of propagation of the eastern branch. In addition, the spatial earthquakes distribution seems to mark the structural connection of the southern-Sudan with western branch of the EARS.

The local and regional seismic networks used in this study revealed threshold magnitude completeness of Mc 3.0 for the region which is the minimum value that has never been observed previously for such large area. Thus, this value indicates that completeness of the catalog for the time period 2013 to 2016 is more refined than the previous studies for such large area of

the EARS. The frequency-magnitude distribution of earthquakes during this study period provided an average b- and a -values of ∼1.01 and ∼6.5, respectively. The relatively lower b-value obtained during the study period may suggest relatively high stress with tectonic origin of earthquakes occurrence dominating the region.

The seismic energy mapping of the region has provided the peaks seismic energy release at Afar, eastern and western branches of the East African Rift System. In addition, the spatial distribution of energy mapping has revealed that the MER is structurally connected to the eastern branch of the EARS which is consistent to earthquakes distribution within the region. For the time period considered in this study, the hypocentral depth of earthquakes is shallower in the Afar and MER than the eastern and western branches of the EARS. This may due to the presence of the thicker seismological lithosphere at the southern part of the EARS (eastern and western branches) than the northern parts of EARS such as the main Ethiopian rift and the Afar region.

In the second part of this thesis, we have investigated the complex tectonic deformation of the circum-Tanzania Craton by analyzing the earthquakes that occurred within the region. The source parameters for the selected earthquakes have been investigated using moment tensor inversion. The study was mainly focused on ongoing active tectonic deformation in the circum-Tanzania Craton of the EARS namely, northern Kondoa, northern Dodoma and Kagera regions. The regions are demonstrated by the seismic crisis of Mb 5.5 and Mw 5.2 in northern Dodoma in 2002 and in 2014, and the seismic crisis of Mw 5.7 in Kagera region in 2016. The regions are located in seismically very active areas and a site of a few large magnitude earthquakes. The source parameters (depths, focal mechanisms), the current deformation associated to earthquakes and the current deformation in relationship with dynamic change of Victoria plate rotation are generally poorly understood owing to the lack of the proper techniques such as moment tensor inversion. Even the source parameters of earthquakes in the regions were widely obtained from P-wave first motion polarities which are often highly non-unique. Here, we investigated the details of the source parameters of the selected 2014 and 2016 earthquake sequences of the study

region using moment tensor inversion.

The selected fault plane solution has been generally in agreement with the Global Centroid Moment Tensor (GCMT) solution but our depth estimates range from 12 to 26 km for the northern Kondoa and the northern Dodoma regions earthquakes which are deeper and shallower for Kagera earthquake with depth of 20.9 km. The relatively deep focal depth of this study is might be implying relatively larger effective elastic thickness compared to the northern part of the East African Rift System in the Afar region. The relatively deeper earthquakes might be due to the presence of relatively stronger and thicker cratonic lithosphere in the circum-Tanzania Craton. Different focal mechanisms have been obtained in the region: normal faulting and normal faulting with significant strike-slip component. From a summary of fault plane solutions pure normal faulting of earthquakes have been obtained in the northern Kondoa region, whereas normal faulting with significant strike-slip motion have been observed in the northern Dodoma and Kagera regions. The resulted normal focal mechanisms indicate the E-W extension of the eastern branch of the EARS. The presences of normal faulting with significant strike-slip focal mechanisms are performing a complex tectonic interpretation of the region. From the aftershocks distribution and source mechanisms, we confirm and illustrate that active deformation is ongoing in the northern Dodoma region, might be resulted from the counterclockwise rotation of Victoria microplate. The estimated reliable focal depth of earthquake in Kagera region might be improve various confusing results reported by several agencies for this event and it may help as an input for future study. Furthermore, the implication of the inversion results that involve focal mechanisms of normal faults (in northern Kondoa) and normal faults with significant strike-slip components (in northen Dodoma and Kagera region) deformation seems to be influenced by the extensional stress regime of the EARS and the counterclockwise rotation of the Victorian plate respectively. The results of this part may increase the number of the focal mechanisms used to estimate recent stress field (Delvaux and Barth, 2010) and give impending proper interpretation for the complex tectonic deformation in the circum-Tanzania Craton.

Finally, the upper and lower crustal deformation associated to large size earthquakes in the region could cause a serious loss of life and damage on property as urbanization and some projects are growing and high population size is concentrated near by the seismically active areas of Dodoma and Kondoa towns. Therefore, special attention should be given by government of the country to minimize the loss of life and damage of property.

In the last part of the thesis, we have investigated the rupture processes of the April 3, 2017 Botswana main shock. To analyze the earthquake, we applied time and frequency domain moment tensor inversion techniques from regional waveform data to determine reliable source parameters of the April 3, 2017 Mw 6.5 Botswana earthquake. The moment magnitude of Mw 6.5 is estimated using the broad bandpass frequency range of 0.02 to 0.05 Hz in contrast to the GCMT solution a relatively narrow frequency range of 0.02 to 0.025 Hz. Our fault plane solution shows normal faulting on NW−SE trending fault and NE−SW extension direction. Thus, the propagation of the southwestern branch of EARS towards Botswana may be the main cause for the occurrence of this rare event as its mechanism shows extension.

The well-constrained hypocentral depth of this event is estimated to be 38.4 km, which is relatively deeper than the previous results. The relatively deep hypocentral depth, which is close to Moho depth, may suggest the reactivation of a deep weak pre- existing fault or from the early rift faults within the stress region during a rift initiation beneath the area. Accordingly, we suggested that due to a relatively deep hypocentral depth of the event, relatively a low maximum intensity value of VI (according to the Modified Mercalli Intensity scale) is estimated. The result of the inversion for the focal mechanism of the event is in agreement with the GCMT solution with extensional consistent to the majority of the focal mechanism in the East African Rift System.

An examination of the source parameters of the event relies relatively differences between this study and the globally reported one (IPGP and GCMT). For instant, the hypocentral depth of the event leads to approximately 8.4 km difference. The difference of this order can be attributed to a combination of several factors. Therefore, the approaches used to compute the

source parameters, a different velocity model and different frequency bands are the key factors for the differences. However, we are confident that the final source parameters obtained in this study are robustly determined.

As a general recommendation, the structural connection between the main Ethiopian rift and the eastern branch of the EARS has been investigated from this study, however additional investigation is needed by deploying some of broadband seismic stations in northern Kenya for a better understanding of the seismicity distribution around Lake Turkana in future. This may improve a clear structural connection between the main Ethiopian rift either with the eastern branch or with western branch of the EARS. In addition, revisiting the regional database to improve earthquake catalogue in EARS is very important from time to time. Furthermore, to boost current monitoring and archiving capacity of national seismic networks in EARS, attention should be given by governments of the regions.

Adagunodo, T., Lning, S., Adeleke, A., Omidiora, J., Aizebeokhai, A., Oyeyemi, K., and Hammed, O., (2018). Evaluation of $0 \leqslant M \leqslant 8$ Earthquake Data Sets in African−Asian Region during 19662015. Data in Brief 17:588−603. doi: 10.1016/j.dib.2018.01.049.

Adamova, P., Sokos, E., and Zahradnik, J., (2009). Problematic non-double-couple mechanism of the 2002 Amfilochia Mw5 earthquake, Western Greece. J. Seis., 13(1), 1−12. https://doi.org/10.1007/s10950-008-9112−4.

Adams, A., Nyblade, A., and Weeraratne, D., (2012). Plateau : Evidence for a Deep , Plateauwide Low Velocity Anomaly. 123−42.

Aki, K., (1965). Maximum Likelihood Estimate of b in the Formula log N = a -b×M and its confidence Limits. Bull. Earthq. Res. Inst., 43, pp. 237−239.

Aki, K., and Richards, P., (1980). Quantitative Seismology: Theory and Methods. V., I.

Aki, K., and Richards, P., (2002). Quantitative Seismology, 2nd Ed.

Albano, M., Polcari, M., Bignami, Ch., Moro, M., Saroli, M., and Stramondo, S., (2017). Did Anthropogenic Activities Trigger the 3 April 2017 Mw 6.5 Botswana Earthquake? Remote Sensing 9(10):1−12.

Albaric, J., Dverchre, J., Petit, C., Perrot, J., Le Gall, B., (2009). Crustal rheology and depth distribution of earthquakes: Insights from the central and southern East African Rift System. Tect.,, 468(1−4), 28−41. https://doi.org/10.1016/j.tecto.2008.05.021.

Albaric, J., Perrot, J., Dverchre, J., Deschamps, A., Le Gall, B., Ferdinand, R., Songo, M., (2010). Contrasted seismogenic and rheological behaviours from shallow and deep earthquake sequences in the North Tanzanian Divergence, East Africa. J. Afr. E, Sci., 58(5), 799−811. https://doi.org/10.1016/j.jafrearsci.2009.09.005.

Albaric, J., Dverchre, J., Perrot, J., Jakovlev, A., Deschamps, A., (2014). Deep crustal earthquakes in North Tanzania, East Africa: Interplay between tectonic and magmatic processes in an incipient rift. Geoch. Geoph. Geosy., 15(2), 374−394. https://doi.org/10.1002/2013GC005027.

Ambraseys, N., (2007). The Rukwa earthquake of 13 December 1910 in East Africa. Terra Nova 3(2):202 −211 doi: 10.1111/j.1365-3121.1991.tb00873.x.

Asefa, J., and Ayele, A., (2020). Complex tectonic deformation in Circum-Tanzania Craton: E ast African Rift System. J. Afr. Earth Sci., 170. https://doi.org/10.1016/j.jafrearsci.2020.103893",.

Asfaw, L., (1990). Implication of shear deformation and earthquake distribution in the East African Rift between 4°N and 6°N. J. Afr. Earth Sci., 10, 745−751.

Ayele, A., (1995). Earthquake catalogue of the Horn of Africa for the period 1960 − 1993; Seismological Dept., Uppsala Univ., Report, 3−95, 1−9.

Ayele, A., and Kulhánek, O., (1997). Spatial and temporal variations of the seismicityin the Horn of Africa from 1960 to 1993. Geophys. J. Int., 130, 805−810.

Ayele, A., and Arvidsson, R., (1998). Fault mechanisms and tectonic implication of the 1985−1987 earthquake sequence in south-western Ethiopia. J. Seis., 1, 383−394.

Ayele, A., (2000). Normal left-oblique fault mechanisms as an indication of sinistral deformation between Nubia and Somalia plates in the Main Ethiopian Rift. J. Afr. Earth Sci., 31 (2), 359−367.

Ayele, A., and Kulhánek, O., (2000). Reassessment of source parameters for three major earthquakes in the East African rift system from historical seismograms and bulletins. Annali Di Geofisica, 43, 81−94.

Ayele, A, Stuart, G., and Kendall, J., (2004). Insights into rifting from shear wave splitting and receiver functions: an example from Ethiopia. 354−362. https://doi.org/10.1111/j.1365−246X. 2004.02206.x.

Ayele, A., Stuart, G., Bastow, I., and Keir, D., (2007). The August 2002 earthquake sequence in north Afar: Insights into the neotectonics of the Danakil microplate. J. Afr. Earth Sci., 48, 70 − 79.

Ayele, A., Ebinger, C., Alstyne, C., Keir, D., Nixon, C., Belachew, M., and Hammond, J., (2015). Seismicity of the central Afar rift and implications for Tendaho dam hazards. Geological Society, London, Special Publications, 420, 341−354. https://doi.org/10.1144/SP420.9.

Babiker, N., Halim, A., Nadi, H., Mula, A., and Eisawi, A., (2015). Seismicity and Seismotectonics of the Sudan and South Sudan. 2(5), 142−149.

Bagley, B., and Nyblade, A., (2013). Seismic anisotropy in eastern Africa, mantle flow, and the African superplume. Geophy. Res. Letters, 40(8), 1500−1505. https://doi.org/10.1002/grl.50315.

Ballard, S, Pollack, N., and Skinner, N., (1987). Terrestrial Heat Flow in Botswana and Namibia. 92:6291−6300.

Bastow, I., and Keir, D., (2011). The protracted development of the continentocean transition in Afar. Nature Geoscience 4:248−250. doi: 10.1038/ngeo1095.

Bath, M., (1966). Earthquake energy and magnitude, Physics and Chemistry of the Earth, vol 7, L H. Ahrens, F Press, S. K Runcorn, and H C. Urey, Editors, Pergamon Press, New York, 117−165.

Bath, M., (1975). Seismicity of the Tanzania region.Tectonophysics, 27: 353−379.

Bth, M., (1979). Introduction to seismology. Birkhauser, 2ndedition Verlag.

Bath, M., (1982). Seismic energy mapping applied to Turkey. Tect., 82, 69−87.

Begg, C., Griffin, W., Natapov, L., O′Reilly, S., Grand, S., O′Neill, C., Hronsky, J., Djomani, Y., Swain, Y., Deen, T., and Bowden, P., (2009). The Lithospheric Architecture of Africa: Seismic Tomography, Mantle Petrology, and Tectonic Evolution. Geosphere 5(1):23−50.

Bellahsen, N., Faccenna, C., Funiciello, F., Daniel, J., and Jolivet, L., (2003). Why did Arabia separate from Africa? Insights from 3-D laboratory experiments. Earth and Plan. Scie. Letters, 216(3), 365−381. https://doi.org/10.1016/S0012-821X(03)00516−8.

Bender, B., (1983). Maximum likelihood estimation of b values for magnitude-grouped data, Bull. seism. Soc. Am., 73, 831−851.

Bendick, R., McClusky, S., Bilham, R., Asfaw, L., and Klemperer, S., (2006). Distributed Nubia−Somalia relative motion and dike intrusion in the Main Ethiopian Rift. Geoph. J. Inter., 165(1), 303−310. https://doi.org/10.1111/j.1365−246X.2006.02904.x.

Beyene, A., and Abdelsalam, M., (2005). Tectonics of the Afar Depression: A Review and Synthesis. J. Afr. Earth Sci., 41(1−2):41−59.

Beyth, M., (1991). Smooth and rough propagation of spreading Southern Red Sea-Afar depression. J. Afr. Earth Sci. 13 (2), 157−171.

Biggs, J., Bastow, I., Keir, D., and Lewi, E., (2011). Pulses of deformation reveal frequently recurring shallow magmatic activity beneath the Main Ethiopian Rift. Geoch. Geophy. Geosy., 12(9), 1−11. https://doi.org/10.1029/2011GC003662.

Bird, P., (2003). An Updated Digital Model of Plate Boundaries. Geoche. Geoph. Geosy., 4(3).

Bolton, M., Storchak, A., and Harris, J., (2006). Updating default depths in the ISC bulletin. Phys. Earth and Plan. Inter., 158(1), 27−45. https://doi.org/10.1016/j.pepi.2006.03.004.

Bonini, M., Corti, G., Innocenti, F., Manetti, P., Mazzarini, F., Abebe, T., and Pecskay, Z., (2005). Evolution of the Main Ethiopian Rift in the frame of Afar and Kenya rifts propagation. Tect., 24(1), 1−21. https://doi.org/10.1029/2004TC001680.

Bosworth, W., (1985). Geometry of propagating continental rifts. Nature, 316(6029), 625−627. https://doi.org/10.1038/316625a0.

Boyd, O., Smalley, R., and Zeng, Y., (2015). Crustal deformation in the New Madrid seismic zone and the role of postseismic processes, J. Geoph. Res., 120 (8), 5782−5803.

Braile, L., Keller, G., Wendlandt, R., Morgan, P., and Khan, M., (1995). The East African Rift sys-tem, in Continental Rifts: Evolution, Structure, Tectonics,Dev. Geotectonics, vol. 25, edited by K. H.Olsen, pp. 213− 231, Elsevier, New York.

Brandt, M., Grand, S., Npyblade, A., and Dirks, P., (2012). Upper Mantle Seismic Structure beneath Southern Africa: Constraints on the Buoyancy Supporting the African Superswell. Pure

and Appl. Geophy. 169(4):595−614.

Brazier, R., Miao, Q., Nyblade, A., Langston, C., Ayele, A., (2005). Local Magnitude Scale and Seismicity for Ethiopia, East Africa. AGU Fall Meeting Abstracts, 88(3), 712−721. Retrieved from https://pubs.geoscienceworld.org/ssa/bssa/article-abstract/88/3/712/102755.

Brazier, R., Nyblade, A., Florentin, J., (2005). Focal mechanisms and the stress regime in NE and SW Tanzania , East Africa. 32, 24−27.

Buck, W., (1991). Modes of continental lithospheric extension. J. Geoph. Res., 96(B12), 161−178. https://doi.org/10.1029/91jb01485.

Buck, W., (2017). The role of magmatic loads and rift jumps in generating seaward dipping reflectors on volcanic rifted margins. Earth and Plane. Sci. Letters, 466, 62−69.

Bungum, H., and Nnko, A., (1984). Seismicity and tectonics of the Stiegler′s Gorge Area, Tanzania. J. Geoph. Res., 89, B3. https://doi.org/10.1029/JB089iB03p01874.

Camelbeeck, T., and Iranga, M., (1996). Deep crustal earthquakes and active faults along the Rukwa trough, eastern Africa. Geoph. J. Inter., 124(2), 612−630. https://doi.org/10.1111/j.1365-246X.1996.tb07040.x.

Calais, E., Dong, L., Wang, M., Shen, Z., and Vergnolle, M., (2006). Continental deformation in Asia from a combined GPS solution. Geoph. Resea. Letters, 33, L24319. doi:10.1029/2006GL028433.

Calais, E., Camelbeeck, T., Stein, S., Liu, M., and Craig, T., (2016). A New Paradigm for Large Earthquakes in Stable Continental Plate Interiors. Geophys. Res. Letterrs, 43, 10,621−10,637, doi:10.1002/2016GL070815.

Calais, E., Ebinger, C., Hartnady, C., Nocquet, J., (2006a). Kinematics of the East African Rift from GPS and earthquake slip vector data. Geological Society, London, SpecialPublications, 259(1), 9−22. https://doi.org/10.1144/gsl.sp.2006.259.01.03.

Calais, E., Ebinger, C., Hartnady, C., Nocquet, J., (2006b). Kinematics of the East African Rift from GPS and earthquake slip vector data. Geol. Socie. Spec. Publ., 259(June 2014), 9−22. https://doi.org/10.1144/GSL.SP.2006.259.01.03.

Calais, E., D′Oreye, N., Albaric, J., Deschamps, A., Delvaux, D., Dverchre, J., Wauthier, C., (2008). Strain accommodation by slow slip and dyking in a youthful continental rift, East Africa. Nature, 456(7223), 783−788. https://doi.org/10.1038/nature07478.

Casey, M., Ebinger, C., Keir, D., Gloaguen, R., and Mohamed, F., (2006). Strain accommodation in transitional rifts : extension by magma intrusion and faulting in Ethiopian rift magmatic segments. (2003), 143−163.

Cesca, S., Buforn, E., and Dahm, T., (2006). Amplitude spectra moment tensor inversion of shallow earthquakes in Spain. 839−854. https://doi.org/10.1111/j.1365−246X.2006.03073.x.

Cesca, S., and Dahm, T., (2008). A frequency domain inversion code to retrieve time-dependent parameters of very long period volcanic sources. Comp. and Geosc., 34(3), 235− 246. https://doi.org/10.1016/j.cageo.2007.03.018.

Cesca, S., Heimann, S., Stammler, K., Dahm, T., (2010). Automated procedure for point and kinematic source inversion at regional distances. J. Geophy. Res., 115(6), 1−24. https://doi.org/10.1029/2009JB006450.

Chambers, E., Harmon, N., Keir, D., and Rychert, C., (2019). Using Ambient Noise to Image the Northern East African Rift. Geoch. Geoph. Geosy., doi:10.1029/2018gc008129.

Chapman, S., and Pollack, N., (1974). Heat Flow and Heat Production in Zambia: Evidence for Lithospheric Thinning in Central Africa.

Chen, W., P., and Yang, Z., (2004). Earthquakes beneath the Himalayas and Tibet: Evidence for strong lithospheric mantle, Science, 304, 1949−1952, doi:10.1126/science.1097324.

Cornwell, D., Mackenzie, G., England, R., and Maguire, P., (2006). Northern Main Ethiopian Rift crustal structure from new high-precision gravity data. 307−321.

Chorowicz, J., (2005). The East African rift system. J. Afr. Earth Sci., 43(1−3), 379−410. https://doi.org/10.1016/j.jafrearsci.2005.07.019.

Corti, G., van Wijk, J., Cloetingh, S., and Morley, C., (2007). Tectonic inheritance andcontinental rift architecture: Numerical and analogue models of the East African Rift system. Tect., 26(6). https://doi.org/10.1029/2006TC002086.

Corti, G., (2009). Continental rift evolution: From rift initiation to incipient break-up in the Main Ethiopian Rift, East Africa. Earth-Science Reviews, 96(1−2), 1−53. https://doi.org/10.1016/j.earscirev.2009.06.005.

Corti, G., Sani, F., Philippon, M., Sokoutis, D., Willingshofer, E., and Molin, P., (2013). Quaternary volcano-tectonic activity in the Soddo region , western margin of the Southern Main Ethiopian Rift. https://doi.org/10.1002/tect.20052

Craig, T., Jackson, J., Priestley, K., and Mckenzie, D., (2011). Earthquake distribution patterns in Africa: Their relationship to variations in lithospheric and geological structure, and their rheological implications. Geoph. J. Inter., 185(1), 403−434. https://doi.org/10.1111/j.1365-246X.2011.04950.x.

Dahm, T., Manthei, G., and Eisenbltter, J., (1999). Automated Moment Tensor Inversion to Estimate Source Mechanisms of Hydraulically Induced Micro-Seismicity in Salt Rock. Tect., 306(1):1−17.

Davidson, A., and Rex, D., (1980). Age of volcanism and rifting in southwestern Ethiopia. Nature, Vol. 283, pp. 657−658. https://doi.org/10.1038/283657a0.

Dawson, J., (1992). Neogene tectonics and volcanicity in the North Tanzania sector of the Gregory Rift Valley: contrasts with the Kenya sector. Tect., 204(1−2). https://doi.org/10.1016/0040-1951(92)90271-7.

Dick, H., Lin, J., and Schouter, H., (2003). An ultraslowspreading class of ocean ridge. Nature, 426, 405−412, doi:10.1038/nature02128.

Delouis, B., Legrand, D., (1999). Focal mechanism determination and identification of the fault plane of earthquakes using only one or two near-source seismic recordings. Bull. Seism. Soci. Amer., 89(6), 1558−17.

Delvaux, D., (2001). Tectonic and palaeostress evolution of the Tanganyika-Rukwa-Malawi rift segment, East African Rift System. Peri-Tethys Memoir 6: Peri-Tethyan Rift/Wrench Basins and Passive Margins, 545−567.

Delvaux, D., and Barth, A., (2010). African stress pattern from formal inversion of focal mechanism data. Tect., 482(1−4), 105−128. https://doi.org/10.1016/j.tecto.2009.05.009.

Delvaux, D., and Macheyeki, A., (2012). Geodynamic significance of the TRM segment in the East African Rift (W- Tanzania): Active tectonics and paleostress in the Ufipa plateau and Rukwa basin. (April). https://doi.org/10.1016/j.jsg.2012.01.008.

Deprez, A., Doubre, C., Masson, F., Ulrich, P., (2013). Seismic and aseismic deformation along the east african rift system from a reanalysis of the GPS velocity field of africa.

Donatian, M., (1992). Seismicity of Tanzania : distribution in time , space , magnitude , and strain release. 209, 313−320.

Doser, D., and Yarwood, D., (1991). Strike-slip faulting in continental rifts : examples from Sabukia , East Africa (1928), and other regions. 197, 213−224.

Dreger, D., and Woods, B., (2002). Regional distance seismic moment tensors of nuclear explosions. Tect., 356(1−3), 139−156. https://doi.org/10.1016/S0040−1951(02)00381−5.

Dverchre, J., Petit, C., Gileva, N, Radzimiovitch, N, Melnikova, V., and San′kov, V., (2001). Depth distribution of earthquakes in the Baikal rift system and its implications for the rheology of the lithosphere, Geophys. J. Int., 146, 714−730, doi:10.1046/j.0956540x.2001.1484.484.x.

Dziewonski, A., Chou, T., and Woodhouse, J., (1981). Determination of earthquake source parameters from waveform data for studies of global and regional seismicity. J. Geoph. Res., 86(B4), 2825−2852. https://doi.org/10.1029/JB086iB04p02825.

Ebinger, C., Crow, M., Rosendahl, B., Livingstone, D., and Lefournier, J., (1984). S tructural evolution of Lake Malai, Africa. Nature, 308(5960), 627−629. https://doi.org/10.1038/308627a0.

Ebinger, C., and Sleep, N., (1998). Cenozoic magmatism throughout east Africa resulting from impact of a single plume. Nature, 395(6704), 788−791. doi:10.1038/27417 .

Ebinger, C., (1989). Tectonic development of the western branch of the East African rift system. Geol. Soc. Amer. Bull., 101(7), 885−903. https://doi.org/10.1130/0016-7606(1989)101<0885:TDOTWB>2.3.CO;2.

Ebinger, C., Yemane, T., Woldegabriel, G., Aronson, J., and Walter, R., (1993). Late Ecocene-Recent volcanism and faulting in the southern main Ethiopian rift. J. Geol. Soc., 150(1), 99−108. https://doi.org/10.1144/gsjgs.150.1.0099.

Ebinger, C., Djomani, Y., Mbede, E., Foster, A., Dawson, J., (1997). Rifting archaean lithosphere: the eyasi-manyara-natron rifts, East Africa. J. Geol. Soc. 154 (6), 947960. https://doi.org/10.1144/gsjgs.154.6.0947.

Ebinger, C., (1998). Cenozoic magmatism throughout east Africa resulting from impact of a single plume. (October). https://doi.org/10.1038/27417.

Ebinger, C., and Casey, M., (2001). Continental breakup in magmatic provinces: An Ethiopian example. Geology, 29(6), 527−530. https://doi.org/10.1130/0091- 7613(2001)029¡0527:CBIMPA>2.0.CO;2.

Ebinger, C., Yemane, T., Harding, D., Tesfaye, S., Kelley, S., and Rex, D., (2000). Rift deflection, migration, and propagation: Linkage of the Ethiopian and Eastern rifts, Africa. gsa Bull., 112, 163−176.

Ebinger, C., (2005). Continental breakup: The East African perspective. 46, 2, 2.16−2.21. https://doi.org/10.1111/j.1468-4004.2005.46216.x.

Ebinger, C., Keir, D., Bastow, I., Whaler, K., Hammond, J., Ayele, A., Hautot, S., (2017).

Crustal Structure of Active Deformation Zones in Africa: Implications for Global Crustal Processes. Tect., 36(12), 3298−3332. https://doi.org/10.1002/2017TC004526.

Fadel, I., Meijde, M., and Paulssen, H., (2018). Crustal Structure and Dynamics of Botswana. J. Geoph. Res., 123(12):10,659−10,671.

Fairhead, J., and Girdler, R., (1971). The Seismicity of Africa. 271−301.

Fairhead, J., and Girdler, R., (1972). The Seismicity of the East African Rift System. Company, Elsevier Publishing.

Fairhead, J., (1980). The structure of the cross-cutting volcanic chain of Northern Tanzania and its relation to the East African rift system. Tect., 65, 3−4, 193−208. https://doi.org/10.1016/0040-1951(80)90074-8.

Fairhead, J., and Stuart, G., (1982). The seismicity of the East African rift system and comparison with other continental rifts. 41−61. https://doi.org/10.1029/gd008p0041.

Fairhead, J., and Stuart, G., (2011). The seismicity of the East African rift system and comparison with other continental rifts. 8, 41−61. https://doi.org/10.1029/gd008p0041.

Fernandes, R., Ambrosius, B., Noomen, R., Bastos, L., Combrinck, L., Miranda, J., Spakman, W., (2004). Angular velocities of Nubia and Somalia from continuous GPS data: Implications on present-day relative kinematics. Earth and Plan. Sci. Letters, 222(1), 197−208. https://doi.org/10.1016/j.epsl.2004.02.008.

Fernandes, R., Miranda, J., Delvaux, D., Stamps, D., Saria, E., (2013). Re-evaluation of the kinematics of victoria block using continuous GNSS data. Geoph. J. Inter., 193(1), 1−10. https://doi.org/10.1093/gji/ggs071.

Fossen, H., (2010). Structural Geology.Cambridge University Press.

Foster, A., Ebinger, C., Mbede, E., Rex, D., (1997). Tectonic development of the northern Taiizaiiian sector of the East African Rift System. Journal of the Geological Society, 154(4), 689−700. https://doi.org/10.1144/gsjgs.154.4.0689.

Foster, A., Jackson, J., (1998). Source parameters of large African earthquakes: implications for crustal rheology and regional kinematics. Geoph. J. Inter., 134(2), 422−448. https://doi.org/10.1046/j.1365-246X.1998.00568.x.

Furman, T., (2007). Geochemistry of East African Rift basalts : An overview. 48, 147−160. https://doi.org/10.1016/j.jafrearsci.2006.06.009.

Gardonio, B., Jolivet, R., Calais, E., and Leclre, H., (2018). The April 2017 Mw6.5 Botswana Earthquake: An Intraplate Event Triggered by Deep Fluids. Geoph. Res. Letters, 45(17):8886−96.

Gashawbeza, E., Klemperer, S., Nyblade, A., Walker, K., and Keranen, K., (2004). Shear-wave splitting in Ethiopia : Precambrian mantle anisotropy locally modified by Neogene rifting -wave splitting in Ethiopia. https://doi.org/10.1029/2004GL020471.

Gaulon, R., Chorowicz, J., Vidal, G., Romanowicz, B., and Roult, G., (1992). Regional geodynamic implications of the May-July 1990 earthquake sequence in southern Sudan. 87−103.

Geiger, L., (1912). Probability method for the determination of earthquake epicenters from the arrival time only, Bull. St. Louis Univ. 8, 60−71.

Ghebreab, W., (1998). Tectonics of the Red Sea region reassessed. Earth Sci. Reviews, 45(1−2), 1−44. https://doi.org/10.1016/S0012- 8252(98)00036-1.

Gibowicz, S., (1974). Frequencymagnitude, depth, and time relations for earthquakes in Island Arc: North Island, New Zealand, Tect., 23, 283−297.

Gilbert, F., (1971). Excitation of the Normal Modes of the Earth by Earthquake Sources. Geoph. J. Royal Astr. Soc., 22(2), 223−226. https://doi.org/10.1111/j.1365-246X.1971.tb03593.x.

Giordano, F., D′Antonio, M., Civetta, L., Tonarini, S., Orsi, G., Ayalew, D., Isaia, R., (2014). Genesis and evolution of mafic and felsic magmas at Quaternary volcanoes within the Main Ethiopian Rift: Insights from Gedemsa and Fanta Ale complexes. Lithos., 188, 130−144.

Girdler, R., (1973). The Great Negative Bouguer Gravity Anomaly Over Africa. 516−19.

Greenfield, T., Keir, D., Kendall, J., and Ayele, A., (2019). Seismicity of the Bora-Tullu Moye Volcanic Field, 2016−2017. Geoch. Geoph. Geosy., 20(2), 548−570. https://doi.org/10.1029/2018GC007648.

Grimison, N., and Chen, W., (1988a). Earthquakes in the Davie RidgeMadagascar region and the southern Nubian-Somalian Plate boundary. J. Geoph. Res., 93, 10 439−10 450.

Gouin, P., (1979). Earthquake history of Ethiopia and the Horn of Africa. Inter. Dev. Res. Center, Ottawa, Ont., pp. 258.

Gutenberg, B., and Richter, C., (1942). Earthquake magnitude, intensity, energy, and acceleration. Bull. Seism. Soc. Amer., 32 (3). pp. 163−191. ISSN 0037−1106.

Gutenberg, B., and Richter, C., (1954). Seismicity of the Earth and associated Phenomena, 2nd edn, Princeton University Press, Princeton.

Gutenberg, B., and Richter, C., (1956). Earthquake magnitude, intensity, energy, and acceleration. Bull. Seis. Soc. Am., 46, 105−145.

Hammond, J., Kendall, J., Angus, D., and Wookey, J., (2010). Interpreting spatial variations in anisotropy : insights into the Main Ethiopian Rift from SKS waveform modelling. 1701−1712. https://doi.org/10.1111/j.1365-246X.2010.04587.x.

Hanks, C., and Kanamori, H., (1979). A moment magnitude scale. J. Geoph. Res., 84, 2348−2350.

Havskov, J., Bormann, P., and Schweitzer, J., (2002). Earthquake location. In: P. Bormann (Ed.) New manual of seismological observatory practice. GeoForschungsZentrum, Potsdam.

Havskov, J. and Ottemoller, L., (2015). SEISAN: The Earthquake Analysis Software. Inst. Solid Earth Phys, Univ. Bergen.

Hayward, N., and Ebinger, C., (1996). Variations in the along-axis segmentation of the Afar Rift system. Tect., 15(2), 244−257. https://doi.org/10.1029/95TC02292.

Henderson, J., Main, I., (1992). A simple fracture-mechanical model for the evolution of seismicity, Geoph. Res. Lett., 19, 365−368.

Hendrie, D., Kusznir, N., Morley, C., and Ebinger, C., (1994). Cenozoic extension in northern Kenya : a quantitative model of rift basin development in the Turkana region. 236, 409−438.

Hingee, M., Tkali, H., Fichtner, A., and Sambridge, M., (2011). Seismic moment tensor inversion using a 3-D structural model: Applications for the Australian region. Geoph. J. Inter., 184(2), 949−964. https://doi.org/10.1111/j.1365-246X.2010.04897.x.

Hofstetter, R., and Beyth, M., (2003). The afar depression: Interpretation of the 1960−2000 earthquakes. Geoph. J. Inter., 155(2), 715−732. https://doi.org/10.1046/j.1365-246X.2003.02080.x.

Hopper, J., ad Buck, W., (1996). extension and passive margin formation . Straining Region. 101.

Huismans, R., and Beaumont, C., (2011). Depth-dependent extension, two-stage breakup and cratonic underplating at rifted margins. Nature, 473(7345), 74−78. https://doi.org/10.1038/nature09988.

Ichinose, G., Roman-Nieves., J., Kraft, G., (2014). Moment Tensor Inversion Toolkit (MTINV) Documentation, Manual and Tutorial.Version 3.0.3.

Iranga, M., (1992). Seismicity of Tanzania: distribution in time, space, magnitude, and strain release. Tect., 209(1−4), 313−320. https://doi.org/10.1016/0040-1951(92)90040-D.

Isola, I., Mazzarini, F., Bonini, M., Corti, G., (2014). Spatial variability of volcanic features in early-stage rift settings: The case of the Tanzania Divergence, East African rift system. Terra Nova, 26(6), 461−468. https://doi.org/10.1111/ter.12121.

Jackson, J., Austrheim, H., McKenzie, D., and Priestley, K., (2004). Metastability, mechanical strength, and the support of mountain belts. Geology, 32(7), 625−628. https://doi.org/10.1130/G20397.1.

Jackson, J., and Blenkinsop, T., (1993). The Malawi earthquake of March 10, 1989: Deep faulting within the East African Rift System. Tect., 12, 1131−1139.

Jost, L., Herrmann, R., (1989). A students guide to and review of moment tensors. Seismol Res Lett 60:37−57.

Julian, B., Miller, D., and Foulger, G., (1998). NON-DOUBLE-COUPLE EARTHQUAKES. (98), 525−549.

Kanamori, H., (1977). The energy release in great earthquakes. J. Geoph. Res., 82, 2981−2987.

Karpin, T., and Thurber, C., (1987). The relationship between earthquake swarms and magma transport: Kilauea volcano, Hawaii. Pure and Appl. Geoph., 125(6), 971−991. https://doi.org/10.1007/BF00879363.

Kebede, F., (1989). Seismotectonics of the East African rift system north of 12S to southern Red Sea. Seismological Dept., Uppsala Univ., Report No. 1−89, pp. 34.

Kebede, F., Kim, W., and Kulhánek, O., (1989). Dynamic source parameters of the March-May 1969 Serdo earthquake sequence in Central Afar, Ethiopia, deduced from teleseismic body waves. J. Geoph. Res., 94, 5603−5614.

Kebede F., and Kulhánek, O., (1991). Recent seismicity of the East African rift system and its implication , Phys. Earth planet Inter. 68259273.

Kebede, F., and Kulhánek, O., (1994). Spatial and temporal variations in b-values along the East African rift system and the southern Red Sea. Phys. Earth Pla. Inter., 83, 249−264.

Keir, D., Ebinger, C., Stuart, G., Daly, E., and Ayele, A., (2006a). Strain accommodation by magmatism and faulting as rifting proceeds to breakup: Seismicity of the northern Ethiopian Rift. J. Geoph. Res., 111, B05314, doi:1029/2005JB 003748.

Keir, D., Stuart, G., Jackson, A., and Ayele, A., (2006b). Local earthquake magnitude scale and seismicity rate for the Ethiopian rift. Bull. Seis. Soc. Amr., 96, 1−10.

Keir, D., Bastow, I., Whaler, K., Daly, E., Cornwell, D., Hautot, S., (2009). Lower crustal earthquakes near the Ethiopian rift induced by magmatic processes. Geochem, Geoph. Geos., 10(6), 1−10. https://doi.org/10.1029/2009GC002382.

Kendall, J., Stuart, G., Ebinger, C., Bastow, I., and Keir, D., (2005). Magma-assisted rifting in Ethiopia Magma-assisted rifting in Ethiopia. https://doi.org/10.1038/nature03161.

Keranen, K., Klemperer, S., Gloaguen, R. and EAGLE working group.,(2004). Three- dimensional imaging of a protoridge axis in the Main Ethiopian Rift. Geol., 39, 949−952.

Keranen, K., Klemperer, S., Julia, J., Lawrence, F., and Nyblade, A., (2009). Low lower crustal velocity across Ethiopia: Is the Main Ethiopian Rift a narrow rift in a hot craton? Geochem. Geoph. Geosy., 10, Q0AB01, doi:10.1029/2008GC002293.

Key, R., and Neil, A., (2000). The 1998 Edition of the National Geological Map of Botswana. J. Afr. Earth Sci. 30(3):427−51.

Khoza, D., Jones, A., Mullera, M., Evans, R., Webb, S., Miensopust, M., and the SAMTEX Team., (2013). Tectonic Model of the Limpopo Belt Derived from Magnetotelluric Data. Precambrian Research 226:143−56.

Kieffer, B., Arndt, N., Pecher, A., Yirgu, G., Ayalew, D., and Meugniot, C., (2004). Flood and Shield Basalts from Ethiopia : Magmas from the African Superswell. https://doi.org/10.1093/petrology/egg112.

Kikuchi, M., and Kanamori, H., (1991). Inversion of complex body waves - III. Bull. Seism. Soc. Amer. 81(6), 2335−2350.

Kim, S., Kraeva, N., Chen, Y., (2000). Source parameter determination of regionaleartquakes in the Far East using moment tensor inversion of single-station data. Tect., 317(1−2), 125−136. https://doi.org/10.1016/S0040-1951(99)00274-7.

Kim, S., Nyblade, A., Baag, C., (2009). Crustal velocity structure of the Rukwa Rift in the western branch of the east african Rift system. South Afr. J. Geol., 112(3−4), 251−260.

https://doi.org/10.2113/gssajg.112.3-4.251.

Kinabo, B., (2007). Incipient Continental Rifting: Insights from the Okavango Rift Zone, Northwestern Botswana. 97.

Kinabo, B., Hogan, J., Atekwana, E., Abdelsalam, M., and Modisi, M., (2008). Fault Growth and Propagation during Incipient Continental Rifting : Insights from a Combined Aeromagnetic and Shuttle Radar Topography Mission Digital Elevation Model Investigation of the Okavango Rift Zone , Northwest Botswana. 27:1−16.

Knopoff, L., Randall, M., (1970). The compensated linear-vector dipole: a possible mechanism for deep earthquakes. J. Geoph. Res., 75:4957−963.

Kogan, L., Fisseha, S., Bendick, R., Reilinger, R., McClusky, S., King, R., and Solomon, T., (2012). Lithospheric strength and strain localization in continental extension from observations of the East African Rift. J. Geoph. Res., 117, B03402. https://doi.org/10.1029/2011JB008516.

Kuge, K,, Lay, T., (1994). Data-dependent non-double-couple components of shallow earthquake source mechanisms: effects of waveform inversion instability. Geoph. Res. Letters, 21:9−12.

Langston, C., Nyblade, A., and Owens, T., (2002). Regional wave propagation in Tanzania, East Africa. J. Geoph, Res., 107(B1), ESE 1−1−ESE 1−18. https://doi.org/10.1029/2001jb000167.

Lapins, S., Kendall, M., Ayele, A., Wilks, M., Nowacki, A., Cashman, K., (2020). Lower Crustal Seismicity on the Eastern Border Faults of the Main Ethiopian Rift. J. Amer. Res., 125, 8. https://doi.org/10.1029/2020JB020030.

Larson, E., Ekström, G., (2006). Global Models of Surface Wave Group Velocity. Pure and Applied Geophysics, 158(8), 1377−1399. https://doi.org/10.1007/pl00001226.7.

Lay, T., and Wallace, T., (1995). Modern global seismology. Academic Press San Diego, California.

Le Gall, B., Gernigon, L., Rolet, J., Ebinger, C., Gloaguen, R., Nilsen, O., Mruma, A.,

(2004). Neogene-Holocene rift propagation in central Tanzania: Morphostructural and aeromagnetic evidence from the Kilombero area. Bull. Geol. Soc. Amer., 116(3−4), 490−510. https://doi.org/10.1130/B25202.1.

Le Gall, B., Nonnotte, P., Rolet, J., Benoit, M., Guillou, H., Mousseau-Nonnotte, M., Deverchre, J., (2008). Rift propagation at craton margin. Distribution of faulting and volcanism in the North Tanzanian Divergence (East Africa) during Neogene times. Tect., 448(1−4), 1−19. https://doi.org/10.1016/j.tecto.2007.11.005.

Leseane, K., Atekwana, E., Mickus, K., Abdelsalam, M., Shemang, E., and Atekwana, E., (2015). J. Geoph. Res., 1210−28.

Lienert, B., Havskov, J., (1995). A computer program for locating earthquakes both locally and globally. Seis. Res. Letters, 66(5), 26−36. https://doi.org/10.1785/gssrl.66.5.26.

Lindenfeld, M., R*ü*mpker, G., (2011). Detection of mantle earthquakes beneath the East African Rift. Geoph. J. Inter., 186(1), 1−5. https://doi.org/10.1111/j.1365−246X.2011.05048.x.

Lindenfeld, M., R*ü*mpker, G., Batte, A., andSchumann, A., (2012). Seismicity at the Rwenzori Mountains, East African Rift: earthquake distribution, magnitudes and source mechanisms. Solid Earth Discussions, 4(1), 565−598. https://doi.org/10.5194/sed-4-565-2012.

Lindenfeld, M., Rmpker, G., Link, K., Koehn, D., and Batte, A., (2012). Fluid-triggered earthquake swarms in the Rwenzori region, East African Rift-Evidence for rift initiation. Tect., 566−567, 95−104. https://doi.org/10.1016/j.tecto.2012.07.0102.

Maasha, N., and Molnar, P., (1972). Earthquake fault parameters and tectonics in Africa. J. Geoph. Res., 77(29), 5731−5743. https://doi.org/10.1029/jb077i029p05731.

Maasha, N., (1975). The seismicity and tectonics of Uganda. Tectonophysics, 27(4), 381−393. https://doi.org/10.1016/0040-1951(75)90005-0.

Macheyeki, A., Delvaux, D., Batist, M., Mruma, A., (2008). Fault kinematics and tectonic stress in the seismically active Manyara−Dodoma Rift segment in Central Tanzania -Implications for

the East African Rift. J. Afr. Earth Sci., 51(4), 163−188. https://doi.org/10.1016/j.jafrearsci.2008.01.007.

Maggi, A., Jackson, J., McKenzie, D., and Priestley, K., (2000). Earthquake Focal Depths, Effective Elastic Thickness, and the Strength of the Continental Lithosphere. Geol., 28(6):495−98.

Makris, J., and Ginzburg, A., (1987). The Afar Depression: transition between continental riftingand sea-floor spreading. Tect., 141(1−3), 199−214. https://doi.org/10.1016/0040-1951(87)90186-7.

Makris, J., Henke, C., Egloff, F., and Akamaluk, T., (1991). The gravity field of the Red Sea and East Africa. Tect., 198: 369−381.

Mammo, T., (2013). Crustal Structure of the Flood Basalt Province of Ethiopia from Constrained 3-D Gravity Inversion. Pure and Appl. Geoph., 170(12), 2185−2206. doi:10.1007/s00024-013-0663-0.

Mana, S., Furman, T., Carr, M., Mollel, G., Mortlock, R., Feigenson, M., Swisher, C., (2012). Geochronology and geochemistry of the Essimingor volcano: Melting of metasomatized lithospheric mantle beneath the North Tanzanian Divergence zone (East African Rift). Lithos., 155, 310−325. https://doi.org/10.1016/j.lithos.2012.09.009.

Mana, S., Furman, T., Turrin, B., Feigenson, M., Swisher, C., (2015). Magmatic activity across the East African North Tanzanian Divergence Zone. J. Geol. Soci., 172(May), 368−389. https://doi.org/10.1144/jgs2014-072.

Manighetti, I., Tapponnier, P., Courtillot, V., Gruszow, S., and Gillot, P., (1997). Propagation of rifting along the Arabia-Somalia Plate Boundary: The Gulfs of Aden and Tadjoura. J. Geoph. Res., 102(B2), 2681−2710. https://doi.org/10.1029/96jb01185.

Manighetti, I., Tapponnier, P., Gillot, P., Jacques, E., Courtillot, V., Armijo, R., King, G., (1998). Propagation of rifting along the Arabia-Somalia Plate Boundary: Into Afar. J. Geoph. Res., 103(B3), 4947−4974. https://doi.org/10.1029/97jb02758.

Marty, B., and Carignan, J., (2003). Stability of the Upper Nile drainage network (Ethiopia) deduced from (U Th) He thermochronometry: implications for uplift and erosion of the Afar plume dome. 215. doi.org/10.1016/S0012-821X(03)00457-6.

Materna, K., Wei, Sh., Wang, X., Heng, L., Wang, T., Chen, W., Salman, R., and B*ü*rgmann, R., (2019). Source Characteristics of the 2017 M w 6.4 Moijabana, Botswana Earthquake, a Rare Lower-Crustal Event within an Ancient Zone of Weakness. Earth and Plan. Sci. Letters, 506:348−59.

Mayeda, K., and Walter, W., (1996). Moment, energy, stress drop, and source spectra of western United States earthquakes from regional coda envelopes. https://doi.org/10.1029/96JB00112.

McCourt, S., Kampunzu, A., Bagai, Z., and Armstrong, A., (2004). The Crustal Architecture of Archaean Terranes in Northeastern Botswana. South African J. Geol., 107(1−2):147−58.

McCourt, S., Armstrong, R., Jelsma, H., and Mapeo, R., (2013). New U-Pb SHRIMP Ages from the Lubango Region, SW Angola: Insights into the Palaeoproterozoic Evolution of the Angolan Shield, Southern Congo Craton, Africa. J. Geol. Soci. 170(2):353−63.

Meghraoui, M., and Pondrelli, S., (2012). Active faulting and transpressiontectonics along the plate boundary in North Africa, Annals of Geophy., 55, pp. 5; doi: 10.4401/ag-4970.

Menke, W., 1989. Geophysical data analysis: Discrete inverse theory. Geophy. series, 45.

Midzi, V., Saunders, I., Manzunzu, B., Kwadiba, M., Jele, V., Mantsha, R., Marimira, K., Mulabisana, T., Ntibinyane, O., Pule, T., Rathod, G., Sitali, M., Tabane, L., van Aswegen, G., and Zulu, B., (2018). T he 03 April 2017 Botswana M6.5 Earthquake: Preliminary Results. J. Afr. Earth Sci. 143(April 2017):187−94.

Modisi, M., (2000). Fault system at the southeastern boundary of the Okavango Rift, Botswana. J. Afr. Earth Sci., 30(3), 569−578. https://doi.org/10.1016/S0899-5362(00)00039-7.

Mogi, K., (1967). Earthquakes and fractures. Tect., 5(1), 35−55. https://doi.org/10.1016/0040-1951(67)90043-1.

Mohr, P. A., (1967). The Ethiopian Rift system. Bull. Geoph. Obser. Addis Ababa 11, 1−65.

Mohr, P., (1971). SURFACE STRUCTURE AND PLATE TECTONICS OF AFAR. In EAST AFRICAN RIFTS: Developments in Geot., 7). https://doi.org/10.1016/B978- 0-444-41087-0.50006-3.

Mohr, P., (1983). Volcanotectonic aspects of the Ethiopian Rift evolution. Bull. Centre Recherches Elf Aquitaine Exploration Production 7, 175−189.

Moore, J., and Davidson, A., (1978). Rift structure in southern Ethiopia. Tect., 46(1− 2), 159−173. https://doi.org/10.1016/0040-1951(78)90111-7.

Moorkamp, M., Fishwick, S., Walker, R., and Jones, A., (2019). Geophysical Evidence for Crustal and Mantle Weak Zones Controlling Intra-Plate Seismicity the 2017 Botswana Earthquake Sequence. Earth and Plan. Sci. Letters, 506:175−83.

Mosley, K., Atekwana, E., Abdelsalam, M., Shemang, E., Atekwana, E., Mickus, K., Moidaki, M., Modisi, M., and Molwalefhe, L., (2012). Geometry and Faults Tectonic Activity of the Okavango Rift Zone , Botswana : Evidence from Magnetotelluric and Electrical Resistivity Tomography Imaging. J. Afr. Earth Sci., 65:61−71.

Motae, T., (1910). The Rukwa earthquake of. Earthquake.

Mougenot, D., Recq, M., Virlogeux, P., Lepvrier, C., (1986). Seaward extension of the East African Rift. Nature, 321(6070), 599−603. https://doi.org/10.1038/321599a0.

Moussa, H., (2008). Spectral P-wave magnitudes, magnitude spectra and other source parameters for the 1990 southern Sudan and the 2005 Lake Tanganyika earthquakes.J. Afr. Earth Sci., 52(3), 89−96.

Mulibo, G., and Nyblade, A., (2009). The 1994-1995 manyaraand KwaMtoro earthquake swarms: Variation in the depth extent of seismicity in northern Tanzania. South African J. Geol., 112(3−4), 387−404. https://doi.org/10.2113/gssajg.112.3-4.387 https://doi.org/10.1016/j.tecto.2016.02.009.

Mulibo, G., and Nyblade, A., (2016). The seismotectonics of Southeastern Tanzania: Implications for the propagation of the eastern branch of the East African Rift. Tect., 674, 20−30.

Mulibo, G., (2019). Investigation of macroseismic intensity of the Mw5.9 September 10, 2016 Kagera earthquake: Implications for site effect amplification. J. Afr. Earth Sci., 159(July), 1−11. https://doi.org/10.1016/j.jafrearsci.2019.103568.

Noh, M., (2019). Assessment of the completeness of earthquake catalogs. Geos. J., 23(2), 253−263. https://doi.org/10.1007/s12303- 018-0028-x.

Nthaba, B., Simon, R., and Ogubazghi, G., (2018). Seismicity Study of Botswana from 1966 to 2012. Inter. J. Geos. 09(12):707−18.

Nyblade, and Brazier A., (2002). Precambrian lithospheric controls on the development of the East African Rift system. Geol., 30, 755−758.

Nyblade, A., and Langston, C., (2002). Broadband Seismic experiments probe in East African rift. Eos Trans. AGU, 83, 405−410.

Nyblade, A., Langston, C., (1995). East African earthquakes below 20 km depth and their implications for crustal structure. Geoph. J. Inter., 121(1), 49−62. https: doi.org/10.1111/j.1365-246X.1995.tb03510.x.

Nyblade, A., Birt, C., Langston, C., Owens, T., Last, R., (1996). Seismic experiment reveals rifting of craton in Tanzania. Eos, 77(51). https://doi.org/10.1029/96EO00339.

O′Donnell, J., Adams, A., Nyblade, A., Mulibo, G., and Tugume, F., (2013). The uppermost mantle shear wave velocity structure of eastern Africa from Rayleigh wave tomography: Constraints on rift evolution. Geoph. J. Inter., 194(2), 961−978. https://doi.org/10.1093/gji/ggt135.

Ottemöller, L., Voss, P., Havskov, J., (2015). The SEISAN Earthquake Analysis Software.

Pagli, C., Wang, H., Wright, T., Calais, E., and Lewi, E., (2010). Current plate boundary deformation of the Afar rift from a 3-D velocity field inversion of InSAR and GPS. J. Geoph. Res., 119, 8562.

Peccerillo, A., Barberio, M., Yirgu, G., Ayalew, D., Barbieri, M., Wu, T., (2012). Relationships between mafic and peralkaline silicic magmatism in continental rift settings: a petrological, geochemical and isotopic study of the Gedemsa volcano, central Ethiopian Rift. J. Petrology 44, 2,003−2,032.

Perez-Gussiny, M., Morgan, J., Reston, T., and Ranero, C., (2006). The rift to drift transition at non-volcanic margins: Insights from numerical modelling. Earth and Plan. Sci. Letters, 244(1−2), 458−473. https://doi.org/10.1016/j.epsl.2006.01.059.

Pizzi, A., Coltorti, M., Abebe, B., Disperati, L., Sacchi, G., Salvini, R., (2006). The Wonji fault belt (Main Ethiopian Rift): structural and geomorphological constraints and GPS monitoring. 191−207.

Plasman, M., Tiberi, C., Ebinger, C., Gautier, S., Albaric, J., Peyrat, S., Gama, R., (2017). Lithospheric low-velocity zones associated with a magmatic segment of the Tanzanian Rift, East Africa. Geoph. J. Inter., 210(1), 465−481. https://doi.org/10.1093/gji/ggx177.

Ranganai, R., Kampunzu, A., Atekwana, E., Paya, B., King, J., Koosimile, D., and Stettler, E., (2002). Gravity Evidence for a Larger Limpopo Belt in Southern Africa and Geodynamic Implications. Geoph. J. Inter. 149(3).

Republic, C., (2015). Moment Tensors : Decomposition and Visualization. (2), 116. https://doi.org/10.1007/978-3-642-36197-5.

Ricard, Y., and Froidevaux, C., (1986). Stretching instabilities and lithospheric boudinage. J. Geoph. Res,, 91(B8), 8314. https://doi.org/10.1029/jb091ib08p08314.

Richter, C., (1935). An instrumental earthquake magnitude scale. Bull. Seis. Soci. Amer., 25(1), 1−32. Retrieved from https://pubs.geoscienceworld.org/ssa/bssa/article-abstract/25/1/1/115102.

Ring, U., (1994). The influence of preexisting structure on the evolution of the Cenozoic Malawi rift (East African rift system). Tect., 13, 313−326.

Ritsema, J., Lay, T., (1995). Long-period regional wave moment tensor inversion for earthquakes in the western United States. J. Geoph. Res., 100(B6), 9853−9864. https://doi.org/10.1029/95JB00238.

Roberts, E., Stevens, N., Connor, P., Dirks, P., Gottfried, M., Clyde, W., Hemming, S., (2012). Initiation of the western branch of the East African Rift coeval with the eastern branch. Nature Geos., 5(4), 289−294. https://doi.org/10.1038/ngeo1432.

Roering, C., Van Reenen, D., Smit, C., Barton, J., De Beer, Jr., and De Wit, M., (2000) Tectonic Model for the Evolution of the Limpopo Belt. 55(1992):539−52.

Rooney, T., Hanan, B., Graham, D., Furman, T., Blichert-Toft, J., Schilling, J., (2012). Upper mantle pollution during Afar plumecontinental rift interaction. J. Petrology 53, 365−389.

Rosendahl, B., (1987). Architecture of continentalrifts with spec ial reference to east Africa, Annu.Rev. Earth Planet. Sci.,15, 445 − 503.

Sandri, L., and Marzocchi, W., (2007). A technical note on the bias in the estimation of the b-value and its uncertainty through the least squares technique. Annals of Geoph., 50(3), 329−339. https://doi.org/10.4401/ag-4422.

Saria, E., Calais, E., Altamimi, Z., Willis, P., Farah, H., (2013). A new velocity field for Africa from combined GPS and DORIS space geodetic Solutions: Contribution to the definition of the African reference frame (AFREF). J. Geoph. Res., 118(4), 1677−1697. https://doi.org/10.1002/jgrb.50137.

Saria, E., Calais, E., Stamps, D., Delvaux, D., Hartnady, C., (2014). Journal of Geophysical Research : Solid Earth Present-day kinematics of the East African Rift. J. Geoph. Res., 119(4), 1−17. https://doi.org/10.1002/2013JB010901.

Scholz, C., (1968). The frequency-magnitude relation of microfracturing in r ock and its relation to earthquakes. Bull. Seis. Soc. Amr., 58: 399−415.

Scholz, C., and Koczynski, T., (2007). Evidence for Incipient Rifting in Southern Africa Evidence

for Incipient Rifting in Southern Africa.44(1):135−144, DOI: 10.1111/j.1365-246X.1976.tb00278.x.

Seno, T., and Saito, A., (1994). Recent East African earthquakes in the lower crust. Earth Plan. Sci. Letters, 121, 125−136, doi:10.1016/0012821X(94)900361.

Shah, E., (1986). Seismicity of Kenya. Ph.D. Thesis , Seismol.Dept., Uppsala University and Dept. of Physics, University of Kenya, 282 pp.

Shi, Y., Bolt, B., (1982). The standard error of the magnitude-frequency b value. Bull. seis. Soc. Amr., 72, 1677−1687.

Shudofsky, G., (1985). Source mechanisms and focal depths of East African earthquakes using Rayleighwave inversion and bodywave modelling. Geophysical Journal of the Royal Astronomical Society, 83(3), 563−614. https://doi.org/10.1111/j.1365-246X.1985.tb04328.x.

Shudofsky, G., Cloetingh, S., Stein, S., Wortel, R., (1987). Unusually deep earthquakes in East Africa: Constraints on the thermomechanical structure of a continental rift system. Geoph. Res. Letters, 14, 7. https://doi.org/10.1029/GL014i007p00741.

Singletary, S., Hanson, H., Martin, M., Crowley, J., Bowring, S., Key, R., Ramokate, L., Direng, B., and Krol, M., (2003). Geochronology of Basement Rocks in the Kalahari Desert, Botswana, and Implications for Regional Proterozoic Tectonics. Precambrian Res., 121(1−2):47−71.

Sipkin, S., (1986). Interpretation of non-double-couple earthquake mechanisms derived from moment tensor inversion (USA). J. Geoph. Res., 91(B1), 531−547. https://doi.org/10.1029/JB091 iB01p00531.

Smith, M., and Mosley, P., (1993). data from granulites in northern Tanzania P-T-t. 12(2), 591−606.

Snoke, J., Munsey, J., Teague, A., Bollinger, G., (1984). A programme for focal mechanism determination by combined use of polarity and SV-P amplitude ratio data. Earthquake Note., 55, pp.15

Snoke, J., (2003). FOCMEC: focal mechanism determinations. In: Lee, W.H.K., Kanamori, H., Jennings, P., Kisslinger, C., (Eds.), International Handbook of Earthquake and Engineering Seismology. Academic Press, San Diego, USA (Chapter 85.12). (1000 pp.).

Sokos, E., and Zahradnik, J., (2008). ISOLA a Fortran code and a Matlab GUI to perform multiple-point source inversion of seismic data. Computers and Geos., 34(8), 967− 977. https://doi.org/10.1016/j.cageo.2007.07.005.

Stamps, D., Calais, E., Saria, E., Hartnady, C., Nocquet, J., Ebinger, C., Fernandes, R., (2008). A kinematic model for the East African Rift. Geoph. Res. Letters, 35(5), 16.

Stamps, D., Flesch, D., Calais, E., and Ghosh, A., (2014). Journal of Geophysical Research : Solid Earth Current Kinematics and Dynamics of Africa and the East. 1−26.

Stamps, D., Saria, E., Kreemer, C., (2018). A Geodetic Strain Rate Model for the East African Rift System. Scientific Rep., 8(1), 1−8. http://dx.doi.org/10.1038/s41598-017-19097-w.

Stein, S., and Wysession, M., (2003). An Introduction to Seismology, Earthquakes, and Earth Structure.

Sykes, L., and Landisman, M., (1964). The seismicity of East Africa, the Gulf of Aden and the Arabian and the Red Sea, Bull. seis. Soc., Amr., 54, 1927−1940.

Tedla, G., Meijde, M., Nyblade, A., and Van der Meer, F., (2011). A Crustal Thickness Map of Africa Derived from a Global Gravity Field Model Using Euler Deconvolution. Geoph. J. Inter., 187(1):1−9.

Tesfaye, S., Harding, D., and Kusky, T., (2003). Early continental breakup boundary and migration of the Afar triple junction, Ethiopia. Geol. Society of Amer. Bull., 115(9), 1053−1067. https://doi.org/10.1130/B25149.1.

Tesfaye, S., and Harding, D., (2004). Early continental breakup boundary and migration of the Afar triple junction , Ethiopia. https://doi.org/10.1130/B25149.1.

Tiberi, C., Ebinger, C., Ballu, V., Stuart, G., and Oluma, B., (2005). Inverse models of gravity data from the Red Sea-Aden-East African rifts triple junction zone. Geoph. J. Inter., 163(2), 775−787. https://doi.org/10.1111/j.1365-246X.2005.02736.xs.

Tongue, J., Maguire, P., and Young, P., (1992). Seismicity distribution from temporary earthquake recording networks in Kenya. Tect., 204(1−2), 71−79. https://doi.org/10.1016/0040-1951(92)90270-G.

Twesigomwe, E., (1997). Probabilistic seismic hazard assessment of Uganda. J. Afr. Earth Sci., 24, 183−195.

Twesigomwe, E., (1997). Seismic hazards in Uganda. J. Afr. Earth Sci., 24, 1−2, 183-195.

Vavryuk, V., (2004). Inversion for anisotropy from non-double-couple components of moment tensors. J. Geoph. Res., 109:B07306. doi:10.1029/2003JB002926.

Vavryuk, V., Bohnhoff, M., Jechumtlov, Z., Kol, P., len J., (2008). Non-double-couple mechanisms of micro-earthquakes induced during the 2000 injection experiment at the KTB site, Germany: a result of tensile faulting or anisotropy of a rock?, Tect., 456, 74−93, doi:10.1016/j.tecto.2007.08.019.

Vavryuk, V., (2011). Tensile earthquakes: Theory, modeling, and inversion. J. Geoph. Res., 116(12). https://doi.org/10.1029/2011JB008770.

Vavryuk, V., (2015). Moment Tensors: Decomposition and Visualization. DOI 10.1007/978-3-642-36197-$5_2$88 − 1.

Weeraratne, D., Forsyth, D., Fischer, K., Nyblade, A., (2003). Evidence for an upper mantle plume beneath the Tanzanian craton from Rayleigh wave tomography. J. Geoph. Res.108(B9). https://doi.org/10.1029/2002JB002273.

Weichert, D., (1980). Estimation of the earthquake recurrence parameters for unequal observation periods for different magnitudes, Bull. seis. Soc. Amr., 70, 1337−1346.

Weinstein, A., Oliva, S., Ebinger, C., Roecker, S., Tiberi, C., Aman, M., Fischer, T., (2017). Fault-magma interactions during early continental rifting: Seismicity of the Magadi- Natron-Manyara basins, Africa. Geoch. Geoph. Geosy., 18(10), 3662− 3686. https://doi.org/10.1002/2017GC007027.

Wiemer, S., and Wyss, M., (1997). Mapping the frequency-magnitude distribution in asperities: An improved technique to calculate recurrence times? J. Geoph. Res., 102(B7), 15115−15128. https://doi.org/10.1029/97jb00726.

White, R., and McKenzie, D., (1989). Magmatism at rift zones: the generation of volcanic continental margins and flood basalts. J. Geoph. Res., 94(B6), 7685−7729. https://doi.org/10.1029/JB094iB06p07685.

Wilks, M., Kendall, J., Nowacki, A., Biggs, J., Wookey, J., Birhanu, Y., Bedada, T., (2017). Seismicity associated with magmatism, faulting and hydrothermal circulation at Aluto Volcano, Main Ethiopian Rift. J. Volcanology and Geothermal Res., 340, 52−67. https://doi.org/10.1016/j.jvolgeores.2017.04.003.

Woessner, J., and Wiemer, S., (2005). Assessing the quality of earthquake catalogues: Estimating the magnitude of completeness and its uncertainty. Bull. Seis. Soc. Amer., 95(2), 684−698. https://doi.org/10.1785/0120040007.

Woessner, J., Hardebeck, J., and Hauksson, E., (2010). What is an instrumental seismicity catalog. Community Online Resource for Statistical Seismicity Analysis. 1−14. https://doi.org/10.5078/corssa-38784307.

Wohlenberg, J., (1969). Remarks on the seismicity of East Africa between 4°N−12°S and 23°E−40°E. Tect., 8:567−577.

Woldegabriel, G., Aronson, J., and Walter, R., (1990). Geological Society of America Bulletin Main Ethiopia Rift Geology, geochronology, and rift basin development in the central sector of the. 102, 439−458. https://doi.org/10.1130/0016- 7606(1990)102¡0439:GGARBD¿2.3.CO;2.

Woldegabriel, G., Heiken, G., White, T., Hart, W., and Renne, P., (2000). Volcanism, tectonism, sedimentation, and the paleoanthropological record in the Ethiopian Rift System. https://doi.org /10.1130/0-8137-2345-0.83.

Wolfenden, E., Ebinger, C., Yirgu, G., Deino, A., and Ayalew, D., (2004). Evolution of the northern Main Ethiopian rift : birth of a triple junction. 224, 213−228. https://doi.org/10.1016/ j.epsl.2004.04.022.

Wolfenden, E., Ebinger, C., Yirgu, G., Renne, P., and Kelley, S., (2005). Evolution of a volcanic rifted margin: Southern Red Sea, Ethiopia. Bull. Geol. Soci. Amer., 117(7−8), 846−864. https://doi.org/10.1130/B25516.1

Yang, Z., and Chen, W., (2008). Mozambique earthquake sequence of 2006: High-angle normal faulting in southern Africa. J. Geoph. Res., 113(B12). https://doi.org/10.1029/2007jb005419.

Yang, Z., and Chen, W., (2010). Earthquakes along the East African Rift System: A multiscale, system-wide perspective. J. Geoph. Res., 115(12), 1−31. https://doi.org/10.1029/2009JB006779.

Youssof, M., Thybo, H., Artemieva, I., and Levander, A., (2013). Moho Depth and Crustal Composition in Southern Africa. Tect., 609:267−87.

Yu, Y., Gao, S., Moidaki, M., Reed, C., and Liu, K., (2015). Seismic Anisotropy beneath the Incipient Okavango Rift: Implications for Rifting Initiation. Earth and Plan. Sci. Letters, 430:1−8.

Yu, Y., Liu, K., Huang, Z., Zhao, D., Reed, C., Moidaki, M., Lei, J., and Gao, S., (2016). Mantle Structure beneath the Incipient Okavango Rift Zone in Southern Africa Zambia Namibia. 13(1):1−10.

Zahradnk, J., Serpetsidaki, A., Sokos, E., and Tselentis, G., (2005). Iterative deconvolution of regional waveforms and a double-event interpretation of the 2003 Lefkada earthquake, Greece. Bull. Seis. Soci. Amer., 95(1), 159−172. https://doi.org/10.1785/0120040035.

Zahradnik, J., Gallovic, F., Sokos, E., Serpetsidaki, A., and Tselentis, A., (2008). Quick fault-plane identification by a geometrical method: Application to the Mw 6.2 Leonidio Earthquake, 6 January 2008, Greece. Seis. Res. Letters, 79(5), 653−662. https://doi.org/10.1785/gssrl.79.5.653.

Zahradnk, J., Fojtkov, L., Carvalho, J., Barros, L., Sokos, E., Jansk, J., (2015). Compromising polarity and waveform constraints in focal-mechanism solutions; the Mara Rosa 2010 Mw 4 central Brazil earthquake revisited. J. South American Earth Sci., 63, 323−333. https://doi.org/10.1016/j.jsames.2015.08.011.

Zhao, M., Langston, C., Nyblade, A., Owens, T., (1997). Lower-crustal rifting in the Rukwa Graben, East Africa. Geoph. J. Inter., 129(2), 412−420. https://doi.org/10.1111/j.1365-246X.1997.tb01592.x.

Zwaan, F., Corti, G., Sani, F., Keir, D., Muluneh, A., Illsley-Kemp, F., Papini, M., (2020). Structural Analysis of the Western Afar Margin, East Africa: Evidence for Multiphase Rotational Rifting. 39, 7. https://doi.org/10.1029/2019TC006043.

Appendix

7.1 Appendix A: Full moment tensor inversion results

Table 6.1: Earthquakes source parameters obtained from full moment tensor inversion in both time and frequency domains which are computed in this study. Results of focal mechanisms are shown on Figure 2.1 under chapter two of this thesis. Date, time and locations are taken from the International Seismological Centre (ISC) catalog.
Date - Date of the event (year/month/day)
Or. Time - Event origin time in GMT (Hour:Minute:Second)
Lat. - Latitude of the earthquake epicenter in degree
Long. - Longitude of the earthquake epicenter in degree
Str.- Strike angle in degrees
Di.- Dip angle in degrees
Ra.- Rake angle in degrees
Dep.- Depth in km
Mw- Moment magnitude
M0- Scalar moment

Date	*Or.Time*	*Lat.*	*Long.*	*Str.*	*Dip.*	*Ra.*	*Dep.*	Mw	$M0$
2013/07/03	19:21:46	1.57	30.88	259,359	74,58	-33,-161	29.1	5.7	4.67E+17
2015/08/07	01:25:02	-2.02	28.71	46,200	41,52	-70,-07	10.5	5.7	5.38E+17
2016/02/04	12:43:57	-1.57	28.4	86,273	67,23	-93,-84	6.9	4.9	2.87E+16
2016/07/13	03:01:14	-5.5	35.96	38,158	55,54	-45,-135	4.8	5.1	6.28E+16
2017/01/27	16:29:20	7.61	38.79	56,148	62,85	-6,-152	9.7	5.0	4.81E+16
2017/02/24	00:32:18	-8.31	29.86	83,236	31,62	-67,-163	33.9	5.9	8.24E+17

7.2 Appendix B: Global Centroid Moment Tensor (GCMT) results

Table 6.2: Earthquakes source parameters compiled from GCMT across the EARS. Results of focal mechanisms are shown on Figure 2.1 of this thesis. Date and locations are taken from the

International Seismological Centre (ISC) catalog.
Date - Date of the event (year/month/day), Lat.- Latitude of the earthquake epicenter in degree, Long. - Longitude of the earthquake epicenter in degree, Str.- Strike angle in degrees, Di.- Dip angle in degrees, Ra.- Rake angle in degrees, Dep.- Depth in km, Mw- Moment magnitude

Date	*Lat.*	*Long.*	*Str.*	*Dip.*	*Ra.*	*Dep.*	*Mw*
2003/06/14	-5.71	35.97	184,340	66,26	-80,-112	15.0	5.0
2007/07/26	-2.79	35.7	88,233	51,45	-66,-116	17.0	5.2
2010/04/08	-4.18	35.193	263,355	60,88	-2,-150	25.3	5.1
2010/06/13	-0.15	34.51	29,238	72,21	-100,-62	12.0	5.0
2010/08/03	-9.5	39.0649	142,313	49,41	-84,-96	10.0	5.3
2010/10/14	-10.35	42.84	97,290	44,47	-99,-84	53.2	5.2
2010/10/23	4.82	36.08	23,203	55,35	-90,-90	21.0	5.0
2010/11/14	12.02	43.93	93,292	48,44	-103,-76	12.0	5.1
2010/12/19	7.49	37.80	22,166	47,49	-64,-115	12.5	5.2
2011/03/15	1.89	31.02	54,240	34,56	-95,-87	22.5	5.0
2011/03/19	6.81	38.62	17,223	51,42	-108,-70	12.0	5.0
2011/06/12	13.58	41.8	127,280	39,54	-69,-106	12.0	5.4
2011/08/08	9.93	43.21	8,278	69,90	-180,-21	24.5	5.0
2011/09/08	-16.16	42.20	191,291	70,64	-27,-158	25.9	5.2
2011/09/09	-12.18	44.77	164,327	51,31	-76,-107	27.1	5.0
2011/12/03	4.75	36.73	5,242	51,56	-134,-50	12.0	5.1
2012/01/22	3.66	36.091	12,170	51,41	-76,-106	12.0	5.1
2012/12/24	-3.8	28.04	195,355	55,37	-78,-107	23.4	5.0
2013/07/02	1.70	30.83	30,260	50,53	-128,-54	23.3	5.0
2013/12/01	-0.89	26.92	75,326	55,65	-148,-40	26.0	5.0
2014/11/11	-4.84	29.15	16,154	38,60	-55,-114	19.3	5.0
2014/12/31	-9.73	33.79	195,246	46,48	-68,-111	12.0	5.2
2015/05/30	11.97	43.15	110,251	40,57	-58,-114	18.8	5.0
2015/07/15	-15.58	41.15	14,109	67,79	-12,-156	28.9	5.1
2015/08/07	-2.11	28.76	50,204	50,43	-72,-110	31.1	5.5
2015/09/08	-6.99	39.87	171,326	29,64	-67,-102	20.0	5.0
2016/04/12	-10.64	41.45	19,156	54,45	-62,-123	23.0	5.1
2016/09/22	-21.29	33.38	181,339	54,38	-76,-108	12.0	5.6

7.3 Appendix C: Waveform modelling and depth phase analysis results

Table 6.3: Earthquakes source parameters from waveform modelling and depth phase analysis taken from literature. Results of focal mechanisms are shown on Figure 2.1 of this thesis. The final column refers to works in which the modelling and depth phase anaysis results are published on: Craig et al., 2011; Bra., Brazier et al., 2005; Fo.,Ja., Foster and Jackson, 1998; Ja.,Bl., Jackson and Blenkinsop, 1993; Se.,Sa, Seno and Saito, 1994; Shu., Shudofsky, 1985; Ya.,Ch., Yang and Chen, 2010;
Date - Date of the event (year/month/day), Or. Time - Event origin time in GMT (Hour:Minute) Lat. - Latitude of the earthquake epicenter in degree, Long. - Longitude of the earthquake epicenter in degree, Str.- Strike angle in degrees, Di.- Dip angle in degrees, Ra.- Rake in degrees, Dep.- Depth in km, Mw- Moment magnitude, Lit.- Literature.

Date	*Or.Time*	*Lat.*	*Long.*	*Str.*	*Dip.*	*Ra.*	*Dep.*	*Mw*	*Lit.*
1996/03/29	09:15	11.93	41.21	32.05	74.0	-20.0	9.0	6.2	Fo.,Ja.
1969/04/05	02:18	11.95	41.33	320.0	66.0	-51.0	5.0	6.2	Fo.,Ja.
1976/09/19	14:59	-11.05	32.90	349.0	42.0	-123.0	29.0	5.6	Fo.,Ja.
1977/12/01	23:20	-4.76	34.98	168.0	56.0	-51.0	12.0	5.4	Shu.
1982/12/13	09:12	14.68	44.23	272.0	67.0	-139.0	6.0	5.8	Se.,Sa.
983/09/30	18:58	11.78	43.40	58.0	87.0	-160.0	5.0	5.6	Fo.,Ja.
1984/08/25	20:37	-8.76	32.63	81.0	65.0	-123.0	26.0	5.3	Fo.,Ja.
1987/10/25	16:46	5.49	36.83	177.0	57.0	-127.0	14.0	6.1	Fo.,Ja.
1989/002/09	23:48	-8.6	29.82	172.0	37.0	-105.0	25.0	5.2	Ya.,Ch.
1989/03/10	21:49	-13.71	34.49	154.0	34.0	-92.0	32.0	6.1	Ja.,Bl.
1989/08/20	11:16	11.74	41.95	302.0	46.0	-76.0	5.0	6.4	Cra.
1990/07/27	20:41	5.07	32.18	335.0	52.0	-120.0	35.0	4.8	Ya.,Ch.
1994/04/24	02:57	11.57	43.0	127.0	36.0	-71.0	4.0	5.5	Cra.
1994/04/24	09:52	-9.05	30.47	340.0	61.0	-100.0	32.0	5.1	Ya.,Ch.
1995/07/22	13:31	-13.98	34.84	315.0	50.0	-105.0	44.0	4.9	Ya.,Ch.
1995/08/10	00:41	-15.57	41.53	308.0	34.0	-120.0	20.0	5.2	Cra.
2005/09/24	19:24	12.44	40.54	296.0	83.0	-144.0	5.0	5.6	Cra.
2006/02/22	22:19	-21.3	33.61	160.0	72.0	-71.0	9.0	5.6	Cra.
1994/09/30	01:36	-5.92	29.89	335.0	36.0	-01.0	11.0	4.5	Bra.
1994/11/16	01:08	-9.42	33.51	301.0	64.0	-11.0	33.51	4.5	Bra.